Day 1

10h30 - Session 1: Cosmic discordance

1. The Hubble tension — Constança Freire

2. The local void — Duarte Santos

3. Cosmic chronometers and spatial curvature — Miguel Martins

14h00 - Session 2: Dark and Baryonic matter

4. Dark matter particles — Filipe Correia

5. Hydrodynamic simulations — Duarte Almeida

6. CDM problems — André Cipriano

7. Intensity Mapping — Lara Piscarreta

Day 2

11h00 - Session 3: Beyond ΛCDM

8. Quintessence — José Ferreira

9. Modified gravity parameterisations — Maria Gonçalves

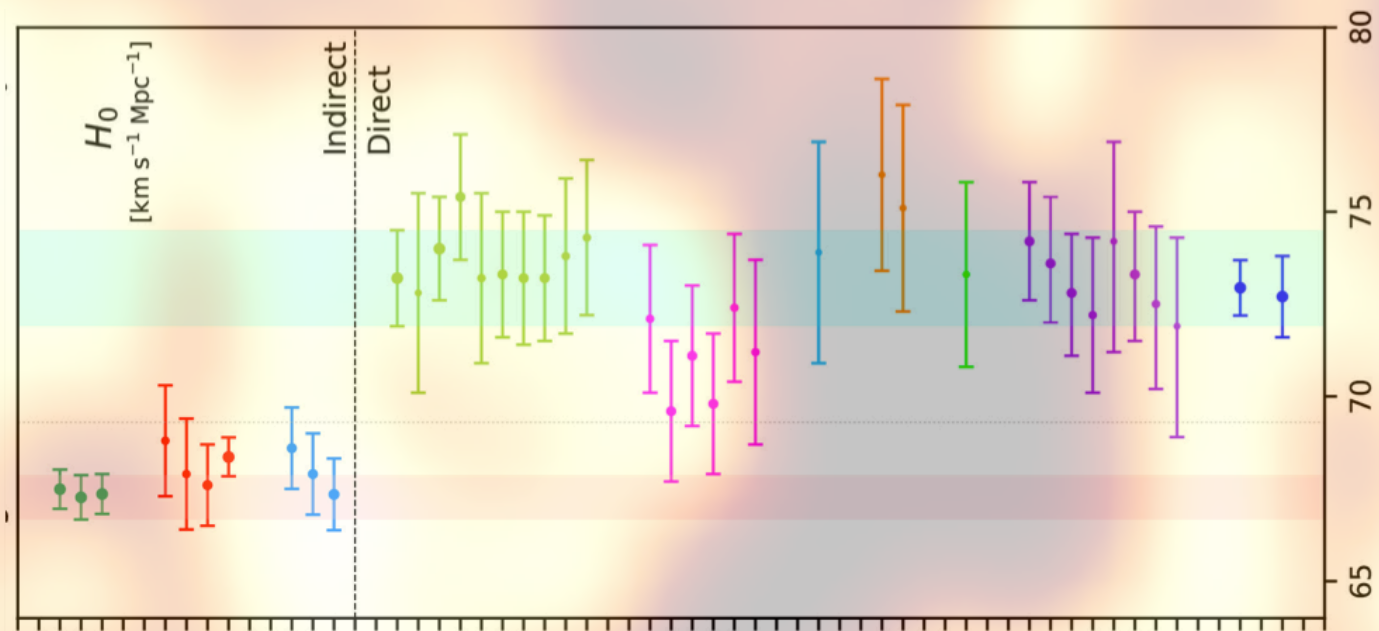10. Neutrinos — Gonçalo Guerra ~~CANCELLED~~

14h00 - Session 4: Structure formation

11. Boltzmann equation — Miguel Pinto

12. Perturbation theory — Ricardo Cipriano

13. N-body dark matter simulations — Diogo Calado

14. Weak lensing theory — Iu "Anthony" Chitou
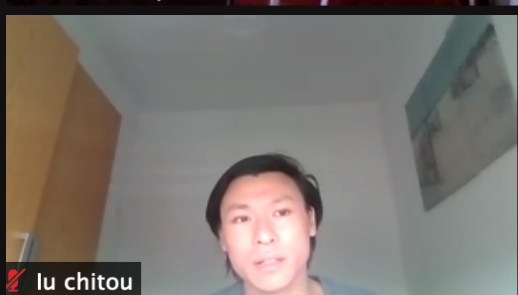
I. Cosmic discordance

Hubble Tension

MSc Astrophysics and Cosmology
Physical Cosmology
Professor: Ismael Tereno

Constança Freire
Nº 49543
2020/2021

Index

- Describing the Hubble Tension
  - Early type measurements
  - Late type measurements
- Relation with sound horizon
  - Early time solutions as a way to solve the tension

Describing the Hubble Tension

Early and Late type measurements

The Hubble Tension

- Not all datasets are consistent: Combined with direct measurements of H_0, joint constraints can be quite different;
- By combining the usual cosmological probes - lower value of H_0;
- Direct measurements of H_0 - higher value of H_0;

Both with small uncertainties - two inconsistent values.

$$H_0 \equiv a^{-1}\frac{da}{dt}$$

The Hubble Tension

"The Hubble constant tension appears to manifest as a difference between its value predicted via the use of measurements in concert with Early Universe physics (described by ΛCDM) and the value measured in the Late Universe (with or without the use of the late-time behavior of ΛCDM)"

E. Di Valentino et al (2021)

$$H_0 \equiv a^{-1}\frac{da}{dt}$$

Early Type

- ΛCDM model predictions
- Plank measurements of the CMB
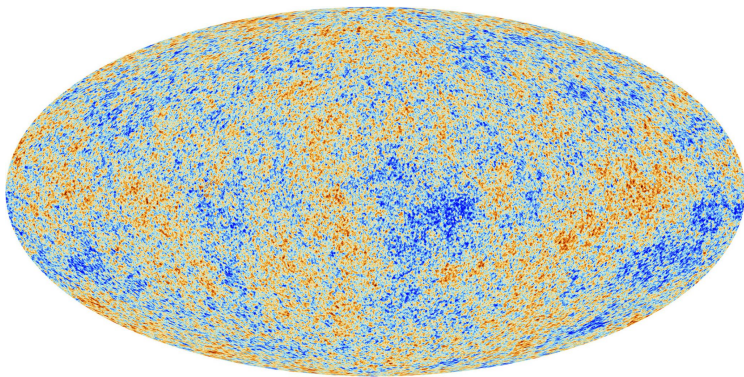
Late Type

- Empirical, direct measurements of the the distance-redshift relation by building a "distance ladder"
- Use geometry to calibrate the luminosities of specific star types which can be seen at great distances where their redshifts measure cosmic expansion.

Early Type Measurements

CMB with Planck
Balkenhol et al. (2021), Planck 2018+SPT+ACT : 67.49 ± 0.53
Pogosian et al. (2020), eBOSS+Planck $\Omega_m H^2$: 69.6 ± 1.8
Aghanim et al. (2020), Planck 2018: 67.27 ± 0.60
Aghanim et al. (2020), Planck 2018+CMB lensing: 67.36 ± 0.54
Ade et al. (2016), Planck 2015, $H_0 = 67.27 \pm 0.66$

CMB without Planck
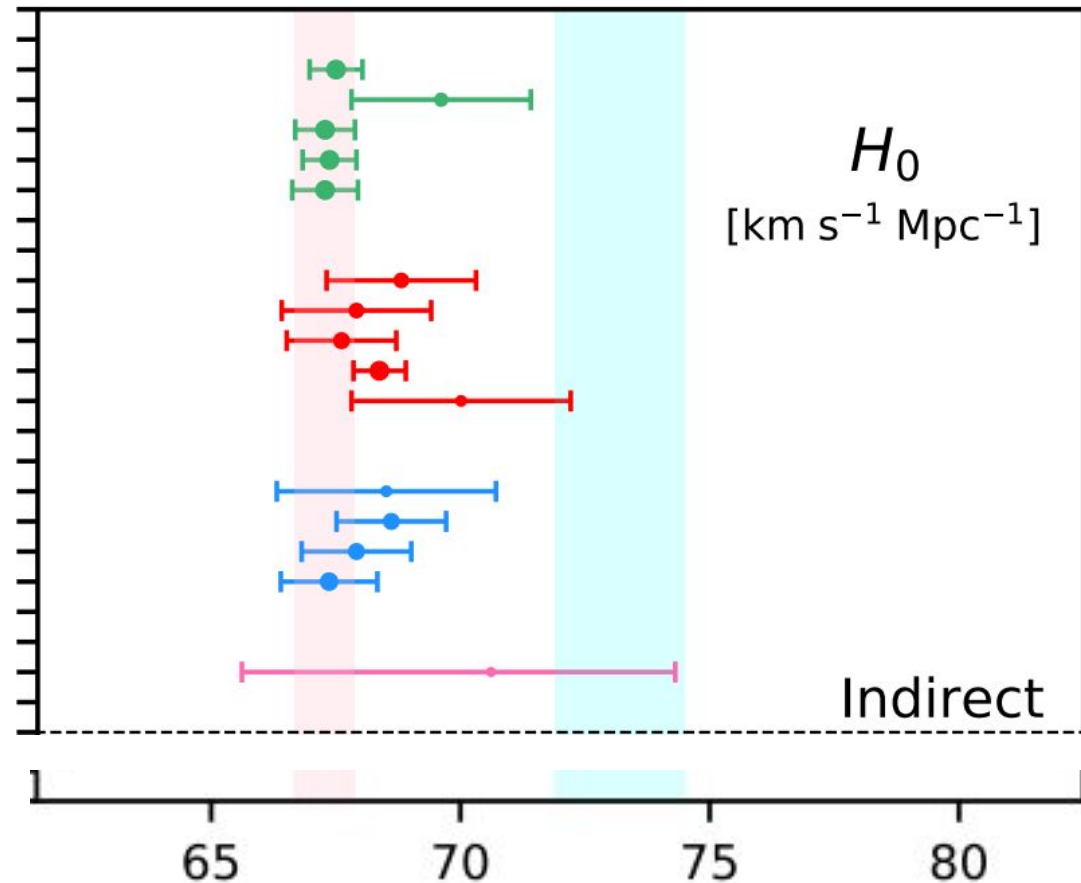Dutcher et al. (2021), SPT: 68.8 ± 1.5
Aiola et al. (2020), ACT: 67.9 ± 1.5
Aiola et al. (2020), WMAP9+ACT: 67.6 ± 1.1
Zhang, Huang (2019), WMAP9+BAO: $68.36^{+0.53}_{-0.52}$
Hinshaw et al. (2013), WMAP9: 70.0 ± 2.2

No CMB, with BBN
D'Amico et al. (2020), BOSS DR12+BBN: 68.5 ± 2.2
Philcox et al. (2020), P_ℓ+BAO+BBN: 68.6 ± 1.1
Ivanov et al. (2020), BOSS+BBN: 67.9 ± 1.1
Alam et al. (2020), BOSS+eBOSS+BBN: 67.35 ± 0.97

$P_l(k)$ + CMB lensing
Philcox et al. (2020), $P_l(k)$+CMB lensing: $70.6^{+3.7}_{-5.0}$

H_0
[km s^{-1} Mpc^{-1}]

Indirect

65   70   75   80

Early Type Measurements

CMB – Systematics in Planck?

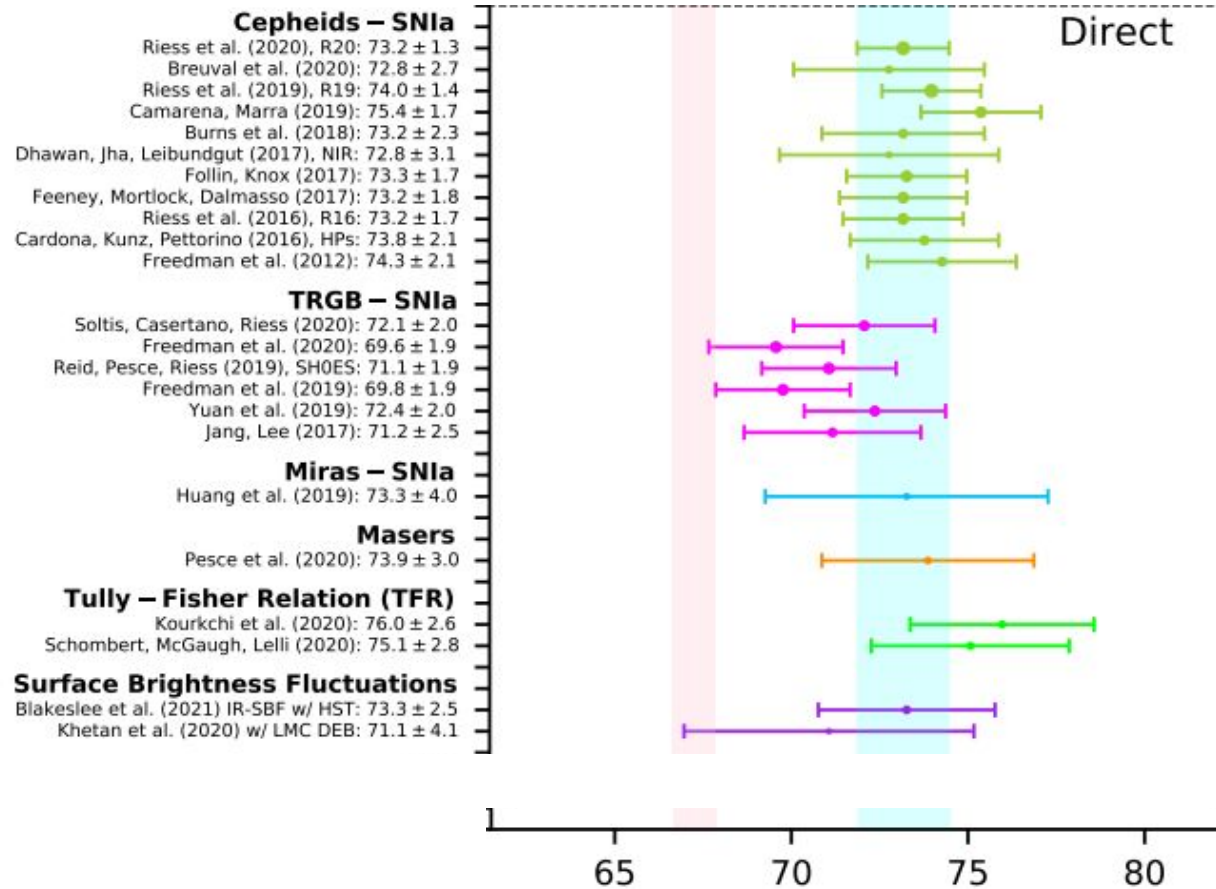- Two different likelihood pipelines - that consider different sky masks and chunks of data
  - Differ at most by 0.1σ for the Hubble constant
- A_{lens} anomaly
  - If not due to new physics, the A_{lens} anomaly is probably due to a small but still undetected systematic error in the Planck data
  - Helps reduce the tension: A_{lens} is included in the analysis, H_0 are indeed slightly shifted towards higher values

Early Type Measurements

CMB – Systematics in Planck?
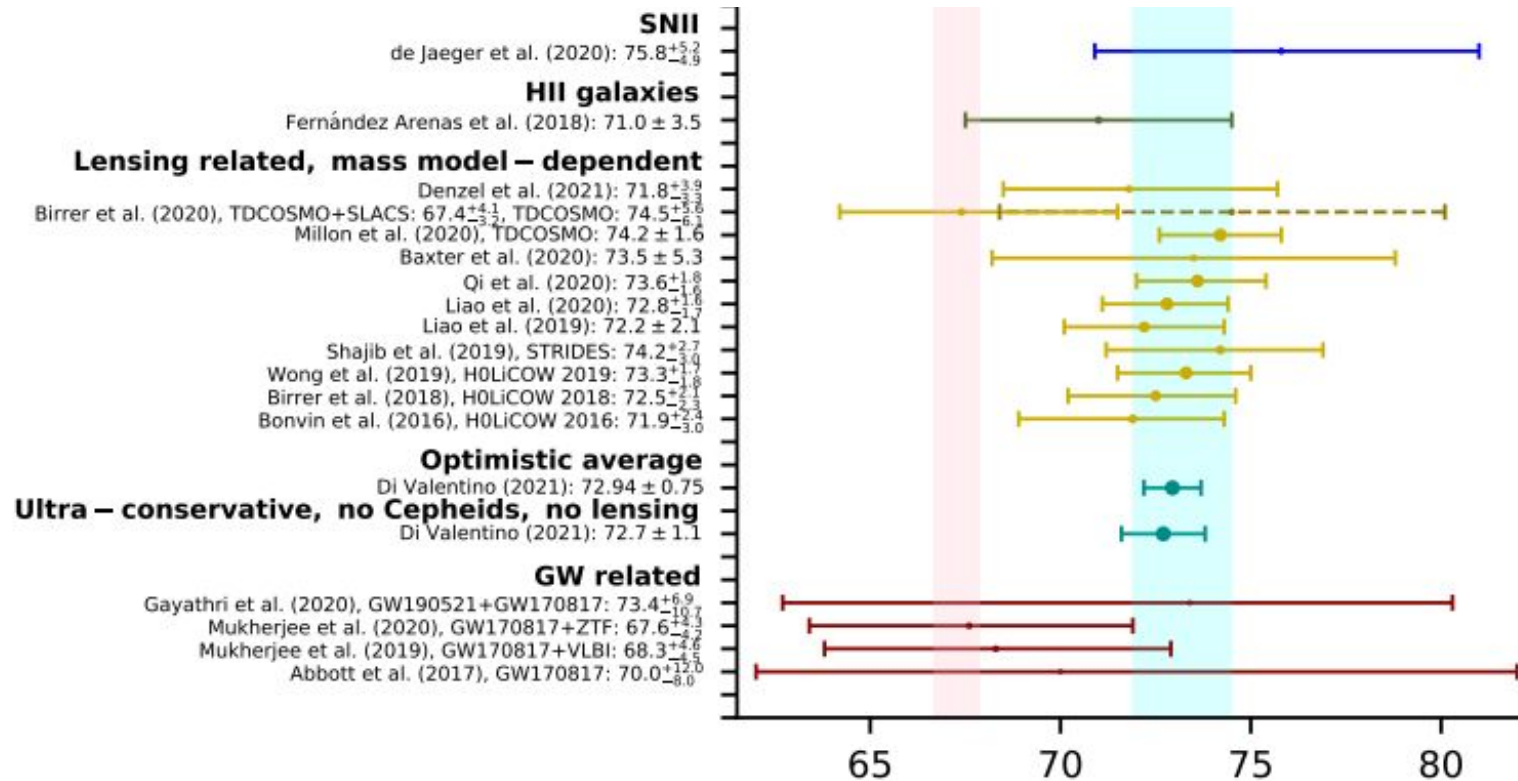
- Systematics in the Planck data could certainly be present and are actually suggested by the A_{lens} anomaly
- No indication for a systematic that could increase the mean value of the Hubble constant from Planck by significantly more than 1 km s−1 Mpc−1 under the ΛCDM assumption.
- The Hubble tension, even if weakened in statistical significance, would probably remain.

Late Type Measurements
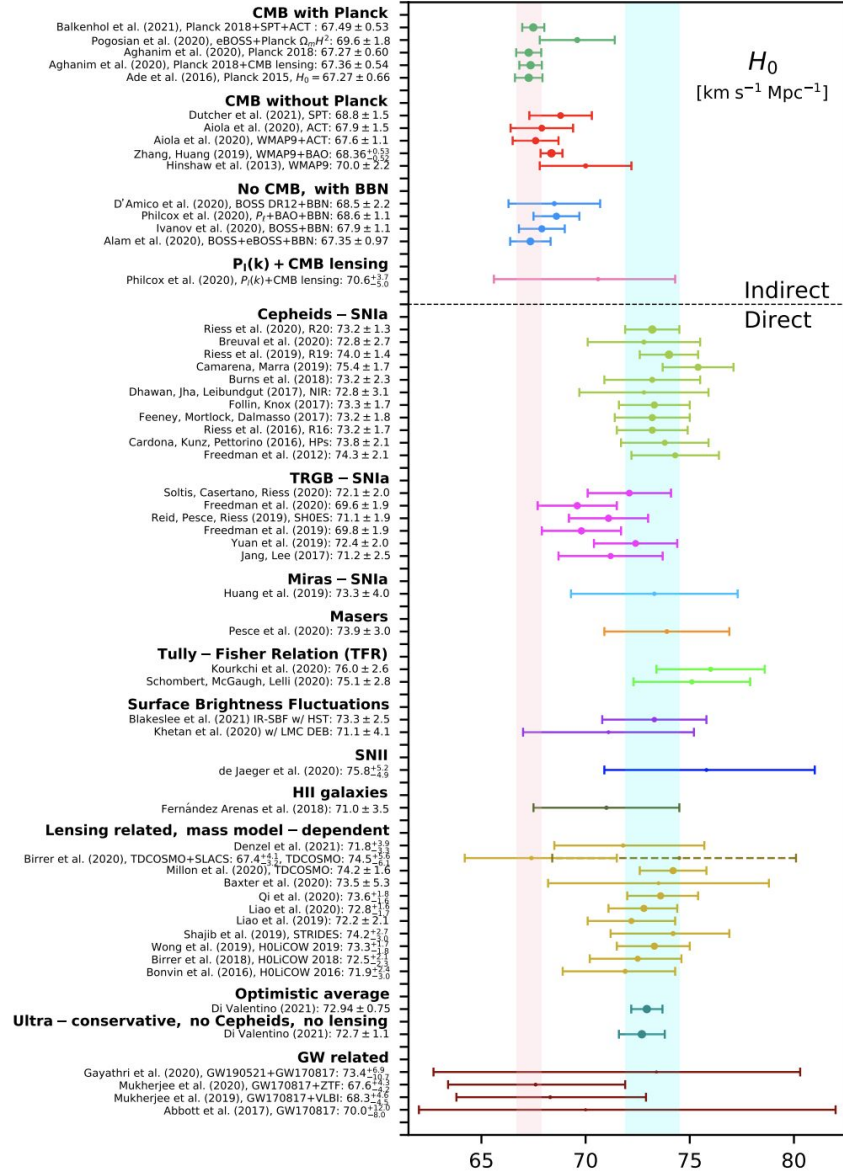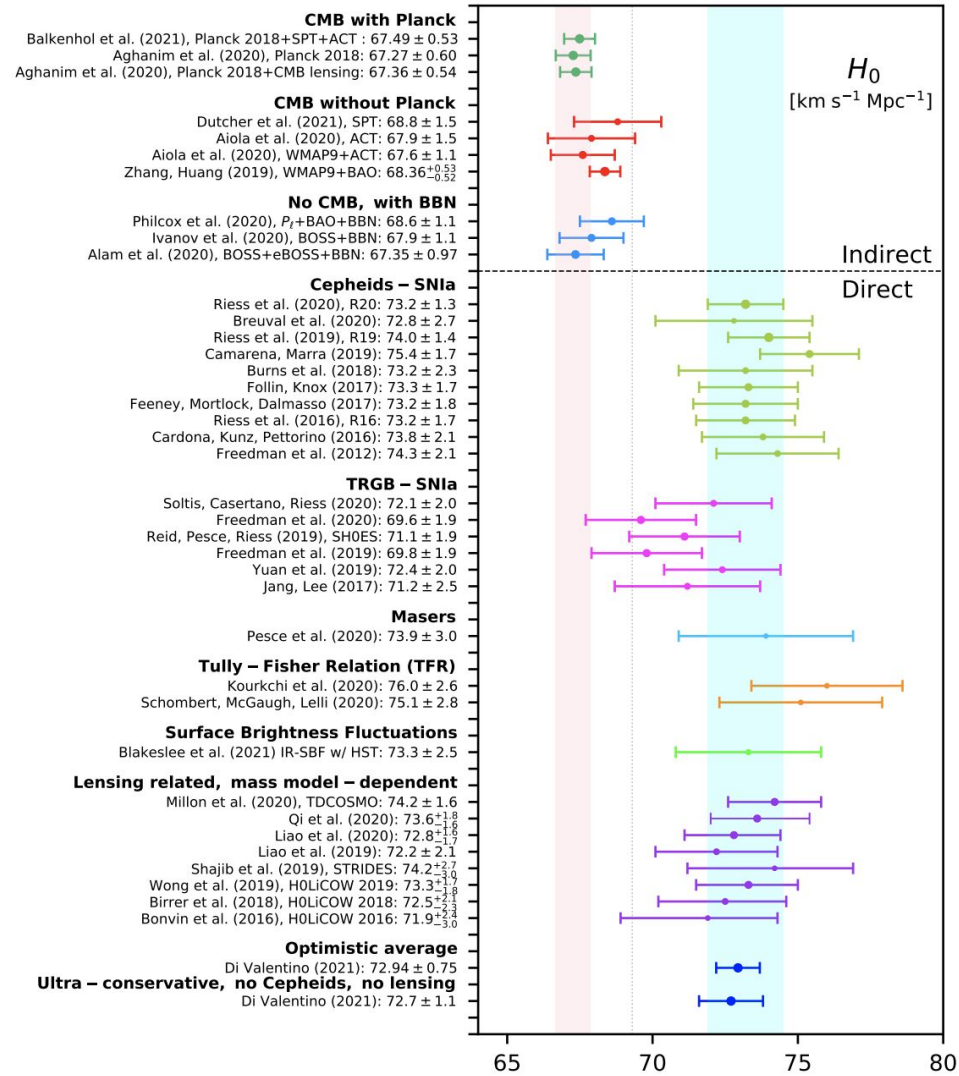

Cepheids – SNIa
Riess et al. (2020), R20: 73.2 ± 1.3
Breuval et al. (2020): 72.8 ± 2.7
Riess et al. (2019), R19: 74.0 ± 1.4
Camarena, Marra (2019): 75.4 ± 1.7
Burns et al. (2018): 73.2 ± 2.3
Dhawan, Jha, Leibundgut (2017), NIR: 72.8 ± 3.1
Follin, Knox (2017): 73.3 ± 1.7
Feeney, Mortlock, Dalmasso (2017): 73.2 ± 1.8
Riess et al. (2016), R16: 73.2 ± 1.7
Cardona, Kunz, Pettorino (2016), HPs: 73.8 ± 2.1
Freedman et al. (2012): 74.3 ± 2.1

TRGB – SNIa
Soltis, Casertano, Riess (2020): 72.1 ± 2.0
Freedman et al. (2020): 69.6 ± 1.9
Reid, Pesce, Riess (2019), SH0ES: 71.1 ± 1.9
Freedman et al. (2019): 69.8 ± 1.9
Yuan et al. (2019): 72.4 ± 2.0
Jang, Lee (2017): 71.2 ± 2.5

Miras – SNIa
Huang et al. (2019): 73.3 ± 4.0

Masers
Pesce et al. (2020): 73.9 ± 3.0

Tully – Fisher Relation (TFR)
Kourkchi et al. (2020): 76.0 ± 2.6
Schombert, McGaugh, Lelli (2020): 75.1 ± 2.8

Surface Brightness Fluctuations
Blakeslee et al. (2021) IR-SBF w/ HST: 73.3 ± 2.5
Khetan et al. (2020) w/ LMC DEB: 71.1 ± 4.1

Direct

65 70 75 80

Late Type Measurements

CMB with Planck
Balkenhol et al. (2021), Planck 2018+SPT+ACT : 67.49 ± 0.53
Pogosian et al. (2020), eBOSS+Planck $\Omega_m H^2$: 69.6 ± 1.8
Aghanim et al. (2020), Planck 2018: 67.27 ± 0.60
Aghanim et al. (2020), Planck 2018+CMB lensing: 67.36 ± 0.54
Ade et al. (2016), Planck 2015, $H_0 = 67.27 \pm 0.66$

CMB without Planck
Dutcher et al. (2021), SPT: 68.8 ± 1.5
Aiola et al. (2020), ACT: 67.9 ± 1.5
Aiola et al. (2020), WMAP9+ACT: 67.6 ± 1.1
Zhang, Huang (2019), WMAP9+BAO: $68.36^{+0.53}_{-0.52}$
Hinshaw et al. (2013), WMAP9: 70.0 ± 2.2

No CMB, with BBN
D'Amico et al. (2020), BOSS DR12+BBN: 68.5 ± 2.2
Philcox et al. (2020), P_l+BAO+BBN: 68.6 ± 1.1
Ivanov et al. (2020), BOSS+BBN: 67.9 ± 1.1
Alam et al. (2020), BOSS+eBOSS+BBN: 67.35 ± 0.97

$P_l(k)$ + CMB lensing
Philcox et al. (2020), $P_l(k)$+CMB lensing: $70.6^{+3.7}_{-5.0}$

Indirect

- -

Direct

Cepheids − SNIa
Riess et al. (2020), R20: 73.2 ± 1.3
Breuval et al. (2020): 72.8 ± 2.7
Riess et al. (2019), R19: 74.0 ± 1.4
Camarena, Marra (2019): 75.4 ± 1.7
Burns et al. (2018): 73.2 ± 2.3
Dhawan, Jha, Leibundgut (2017), NIR: 72.8 ± 3.1
Follin, Knox (2017): 73.3 ± 1.7
Feeney, Mortlock, Dalmasso (2017): 73.2 ± 1.8
Riess et al. (2016), R16: 73.2 ± 1.7
Cardona, Kunz, Pettorino (2016), HPs: 73.8 ± 2.1
Freedman et al. (2012): 74.3 ± 2.1

TRGB − SNIa
Soltis, Casertano, Riess (2020): 72.1 ± 2.0
Freedman et al. (2020): 69.6 ± 1.9
Reid, Pesce, Riess (2019), SH0ES: 71.1 ± 1.9
Freedman et al. (2019): 69.8 ± 1.9
Yuan et al. (2019): 72.4 ± 2.0
Jang, Lee (2017): 71.2 ± 2.5

Miras − SNIa
Huang et al. (2019): 73.3 ± 4.0

Masers
Pesce et al. (2020): 73.9 ± 3.0

Tully − Fisher Relation (TFR)
Kourkchi et al. (2020): 76.0 ± 2.6
Schombert, McGaugh, Lelli (2020): 75.1 ± 2.8

Surface Brightness Fluctuations
Blakeslee et al. (2021) IR-SBF w/ HST: 73.3 ± 2.5
Khetan et al. (2020) w/ LMC DEB: 71.1 ± 4.1

SNII
de Jaeger et al. (2020): $75.8^{+5.2}_{-4.9}$

HII galaxies
Fernández Arenas et al. (2018): 71.0 ± 3.5

Lensing related, mass model − dependent
Denzel et al. (2021): $71.8^{+3.9}_{-3.3}$
Birrer et al. (2020), TDCOSMO+SLACS: $67.4^{+4.1}_{-3.2}$, TDCOSMO: $74.5^{+5.6}_{-6.1}$
Millon et al. (2020), TDCOSMO: 74.2 ± 1.6
Baxter et al. (2020): 73.5 ± 5.3
Qi et al. (2020): $73.6^{+1.8}_{-1.6}$
Liao et al. (2020): $72.8^{+1.6}_{-1.7}$
Liao et al. (2019): 72.2 ± 2.1
Shajib et al. (2019), STRIDES: $74.2^{+2.7}_{-3.0}$
Wong et al. (2019), H0LiCOW 2019: $73.3^{+1.7}_{-1.8}$
Birrer et al. (2018), H0LiCOW 2018: $72.5^{+2.1}_{-2.3}$
Bonvin et al. (2016), H0LiCOW 2016: $71.9^{+2.4}_{-3.0}$

Optimistic average
Di Valentino (2021): 72.94 ± 0.75
Ultra − conservative, no Cepheids, no lensing
Di Valentino (2021): 72.7 ± 1.1

GW related
Gayathri et al. (2020), GW190521+GW170817: $73.4^{+6.9}_{-10.7}$
Mukherjee et al. (2020), GW170817+ZTF: $67.6^{+4.3}_{-4.2}$
Mukherjee et al. (2019), GW170817+VLBI: $68.3^{+4.6}_{-4.5}$
Abbott et al. (2017), GW170817: $70.0^{+12.0}_{-8.0}$

H_0
[km s^{-1} Mpc^{-1}]

65   70   75   80

High Precision Measures of H_0

CMB with Planck
Balkenhol et al. (2021), Planck 2018+SPT+ACT : 67.49 ± 0.53
Aghanim et al. (2020), Planck 2018: 67.27 ± 0.60
Aghanim et al. (2020), Planck 2018+CMB lensing: 67.36 ± 0.54

CMB without Planck
Dutcher et al. (2021), SPT: 68.8 ± 1.5
Aiola et al. (2020), ACT: 67.9 ± 1.5
Aiola et al. (2020), WMAP9+ACT: 67.6 ± 1.1
Zhang, Huang (2019), WMAP9+BAO: $68.36^{+0.53}_{-0.52}$

No CMB, with BBN
Philcox et al. (2020), P_ℓ+BAO+BBN: 68.6 ± 1.1
Ivanov et al. (2020), BOSS+BBN: 67.9 ± 1.1
Alam et al. (2020), BOSS+eBOSS+BBN: 67.35 ± 0.97

Indirect

Direct

Cepheids − SNIa
Riess et al. (2020), R20: 73.2 ± 1.3
Breuval et al. (2020): 72.8 ± 2.7
Riess et al. (2019), R19: 74.0 ± 1.4
Camarena, Marra (2019): 75.4 ± 1.7
Burns et al. (2018): 73.2 ± 2.3
Follin, Knox (2017): 73.3 ± 1.7
Feeney, Mortlock, Dalmasso (2017): 73.2 ± 1.8
Riess et al. (2016), R16: 73.2 ± 1.7
Cardona, Kunz, Pettorino (2016): 73.8 ± 2.1
Freedman et al. (2012): 74.3 ± 2.1

TRGB − SNIa
Soltis, Casertano, Riess (2020): 72.1 ± 2.0
Freedman et al. (2020): 69.6 ± 1.9
Reid, Pesce, Riess (2019), SH0ES: 71.1 ± 1.9
Freedman et al. (2019): 69.8 ± 1.9
Yuan et al. (2019): 72.4 ± 2.0
Jang, Lee (2017): 71.2 ± 2.5

Masers
Pesce et al. (2020): 73.9 ± 3.0

Tully − Fisher Relation (TFR)
Kourkchi et al. (2020): 76.0 ± 2.6
Schombert, McGaugh, Lelli (2020): 75.1 ± 2.8

Surface Brightness Fluctuations
Blakeslee et al. (2021) IR-SBF w/ HST: 73.3 ± 2.5

Lensing related, mass model − dependent
Millon et al. (2020), TDCOSMO: 74.2 ± 1.6
Qi et al. (2020): $73.6^{+1.8}_{-1.6}$
Liao et al. (2020): $72.8^{+1.6}_{-1.7}$
Liao et al. (2019): 72.2 ± 2.1
Shajib et al. (2019), STRIDES: $74.2^{+2.7}_{-3.0}$
Wong et al. (2019), H0LiCOW 2019: $73.3^{+1.7}_{-1.8}$
Birrer et al. (2018), H0LiCOW 2018: $72.5^{+2.1}_{-2.3}$
Bonvin et al. (2016), H0LiCOW 2016: $71.9^{+2.4}_{-3.0}$

Optimistic average
Di Valentino (2021): 72.94 ± 0.75
Ultra − conservative, no Cepheids, no lensing
Di Valentino (2021): 72.7 ± 1.1

H_0
[km s^{-1} Mpc^{-1}]

65   70   75   80

Relation with the Sound Horizon

Early time solutions as a way to solve the tension

Two classes of models in order to solve the Hubble Tension

$$\theta_{\star} \equiv \frac{r_{\star}}{D(z_{\star})}$$

1. Introduces modifications at late times while still preserving the integrated distance D
2. Modification at early times, aim to reduce the numerator - modify the sound horizon at recombination.

15
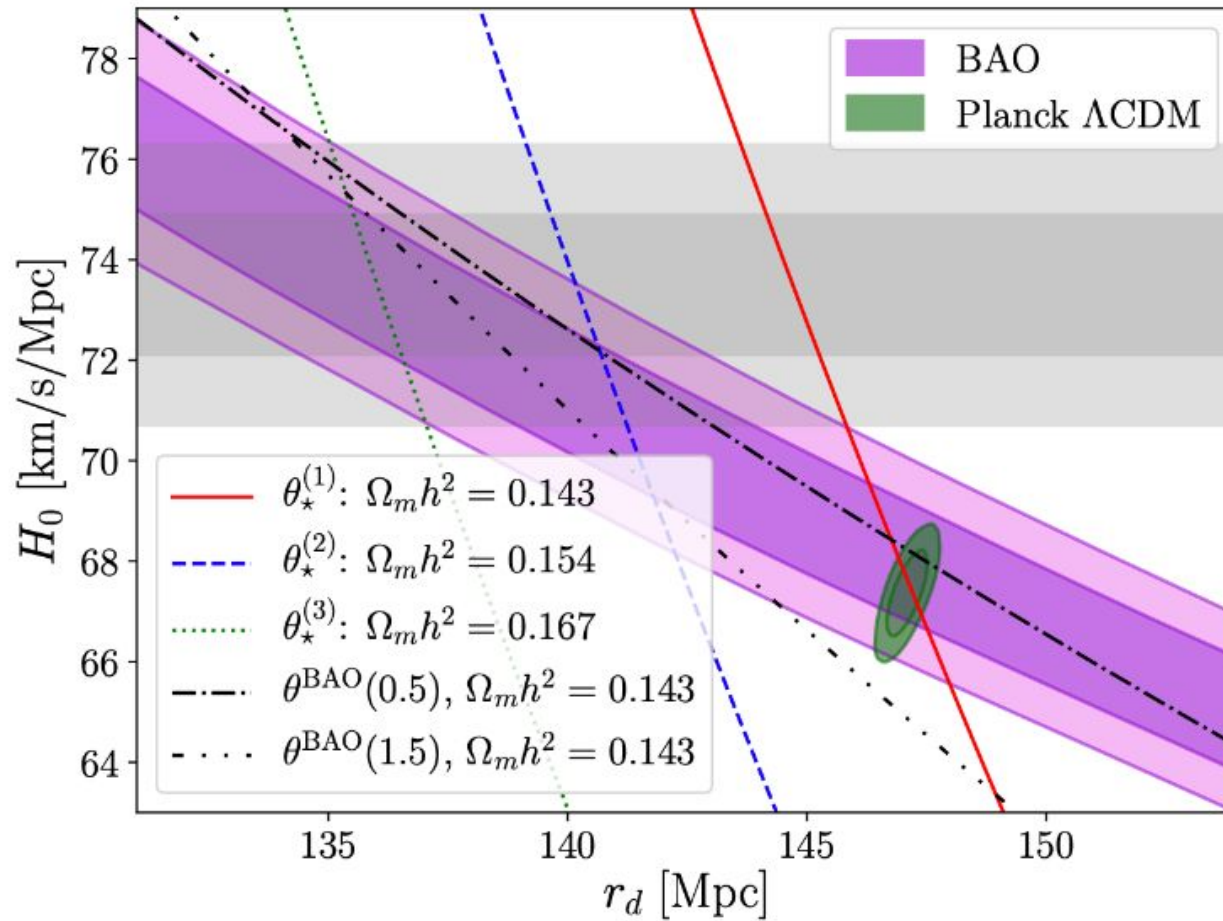
Planck best fit values of $\Omega_m h^2 = 0.143 \pm 0.001$

$$S_8 \equiv \sigma_8 (\Omega_m/0.3)^{0.5}$$

■ (red)	ΛCDM
▲ (green)	Early Dark Energy (EDE) model I [14]
▼ (blue)	EDE model II [14]
◆ (cyan)	evolving scalar fields I [15]
● (olive)	evolving scalar fields II [15]
△ (green)	a new EDE model [18]
■ (black)	interacting neutrino cosmology I [19]
● (red)	interacting neutrino cosmology II [19]
○ (red)	neutrino sector radiation [22]
★ (blue)	ultralight scalar decay [24]
◄ (magenta)	decaying dark matter (DM) I [25]
► (green)	decaying DM II [25]
□ (open)	DM - dark radiation interaction [26]
✳ (blue)	swampland & fading DM [29]
+ (green)	primordial magnetic fields I [30]
✕ (teal)	primordial magnetic fields II [30]
⬟ (purple)	non-standard recombination I [31]
● (dark red)	non-standard recombination II [31]
■ (orange)	early recombination [33]

Conclusion

- The case for an observational difference between the Early and Late Universe appears strong, is hard to dismiss, and demands a hypothesis with enough rigor to explain multiple observations–whether these invoke new physics, unexpected large-scale structures or multiple, unrelated errors.
- Any model which tries to reconcile the CMB inferred value of H0 with that measured by SH0ES by only reducing the sound horizon automatically runs into tension with either the BAO or the galaxy WL data

References

- E. Di Valentino et al (2021) - Sections 2 and 3: https://arxiv.org/pdf/2103.01183.pdf
- K. Jedamzik et al (2020): https://arxiv.org/pdf/2010.04158.pdf

The Local Void

TRYING TO SOLVE THE HUBBLE TENSION

Duarte Muñoz Santos

Physical Cosmology

Table of contents

Introduction

Hubble Tension

The Hubble tension describes the difference between the Hubble constant with "early" and "late" type measurements, which has been quantified to be

$$\frac{(H_{\text{late}} - H_{\text{early}})}{H_{\text{early}}} = 9\% \approx 6 \text{ km s}^{-1} \text{ Mpc}^{-1}$$

Hubble Tension

High Precision Measures of H_0

CMB with Planck
Balkenhol et al. (2021), Planck 2018+SPT+ACT : 67.49 ± 0.53
Aghanim et al. (2020), Planck 2018: 67.27 ± 0.60
Aghanim et al. (2020), Planck 2018+CMB lensing: 67.36 ± 0.54

CMB without Planck
Dutcher et al. (2021), SPT: 68.8 ± 1.5
Aiola et al. (2020), ACT: 67.9 ± 1.5
Aiola et al. (2020), WMAP9+ACT: 67.6 ± 1.1
Zhang, Huang (2019), WMAP9+BAO: $68.36^{+0.53}_{-0.52}$

No CMB, with BBN
Philcox et al. (2020), P_ℓ+BAO+BBN: 68.6 ± 1.1
Ivanov et al. (2020), BOSS+BBN: 67.9 ± 1.1
Alam et al. (2020), BOSS+eBOSS+BBN: 67.35 ± 0.97

Indirect

Direct

Cepheids − SNIa
Riess et al. (2020), R20: 73.2 ± 1.3
Breuval et al. (2020): 72.8 ± 2.7
Riess et al. (2019), R19: 74.0 ± 1.4
Camarena, Marra (2019): 75.4 ± 1.7
Burns et al. (2018): 73.2 ± 2.3
Follin, Knox (2017): 73.3 ± 1.7
Feeney, Mortlock, Dalmasso (2017): 73.2 ± 1.8
Riess et al. (2016), R16: 73.2 ± 1.7
Cardona, Kunz, Pettorino (2016): 73.8 ± 2.1
Freedman et al. (2012): 74.3 ± 2.1

TRGB − SNIa
Soltis, Casertano, Riess (2020): 72.1 ± 2.0
Freedman et al. (2020): 69.6 ± 1.9
Reid, Pesce, Riess (2019), SH0ES: 71.1 ± 1.9
Freedman et al. (2019): 69.8 ± 1.9
Yuan et al. (2019): 72.4 ± 2.0
Jang, Lee (2017): 71.2 ± 2.5

Masers
Pesce et al. (2020): 73.9 ± 3.0

Tully − Fisher Relation (TFR)
Kourkchi et al. (2020): 76.0 ± 2.6
Schombert, McGaugh, Lelli (2020): 75.1 ± 2.8

Surface Brightness Fluctuations
Blakeslee et al. (2021) IR-SBF w/ HST: 73.3 ± 2.5

Lensing related, mass model − dependent
Millon et al. (2020), TDCOSMO: 74.2 ± 1.6
Qi et al. (2020): $73.6^{+1.8}_{-1.6}$
Liao et al. (2020): $72.8^{+1.6}_{-1.7}$
Liao et al. (2019): 72.2 ± 2.1
Shajib et al. (2019), STRIDES: $74.2^{+2.7}_{-3.0}$
Wong et al. (2019), H0LiCOW 2019: $73.3^{+1.7}_{-1.8}$
Birrer et al. (2018), H0LiCOW 2018: $72.5^{+2.1}_{-2.3}$
Bonvin et al. (2016), H0LiCOW 2016: $71.9^{+2.4}_{-3.0}$

Optimistic average
Di Valentino (2021): 72.94 ± 0.75
Ultra − conservative, no Cepheids, no lensing
Di Valentino (2021): 72.7 ± 1.1

Credit: *Di Valentino et al. (2021)*

4
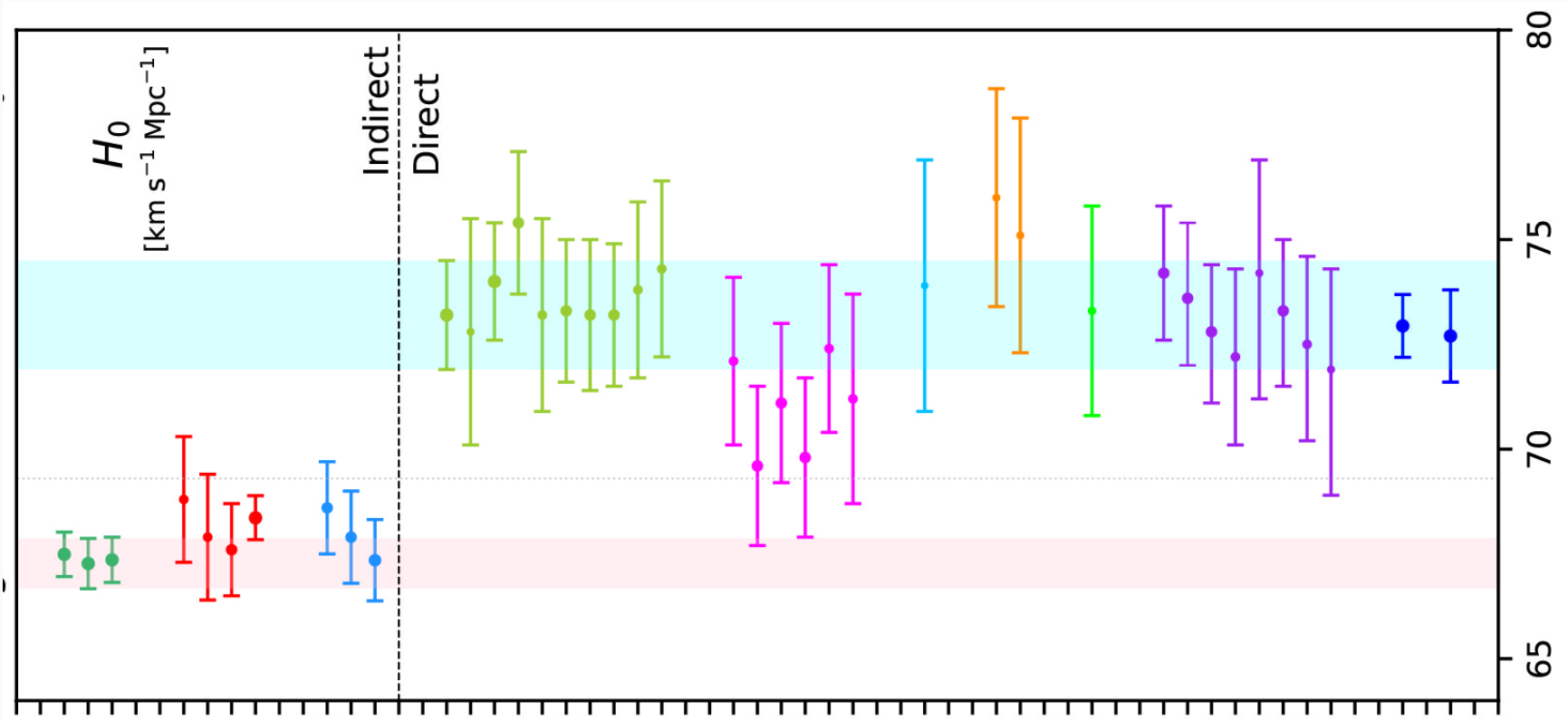
Hubble Tension

Adapted from *Di Valentino et al. (2021)*

Possible Solutions

Several suggestions have been proposed to try to solve the Hubble tension, such as

Possible Solutions

Several suggestions have been proposed to try to solve the Hubble tension, such as

- An underdense local Universe;

Possible Solutions

Several suggestions have been proposed to try to solve the Hubble tension, such as

- An underdense local Universe;

- Adding extra dark energy components;

Possible Solutions

Several suggestions have been proposed to try to solve the Hubble tension, such as

- An underdense local Universe;

- Adding extra dark energy components;

- Modifying the ΛCDM model with, for example, Modified Gravity;

Possible Solutions

Several suggestions have been proposed to try to solve the Hubble tension, such as

- An underdense local Universe;

- Adding extra dark energy components;

- Modifying the ΛCDM model with, for example, Modified Gravity;

- Many, many more...

Possible Solutions

Several suggestions have been proposed to try to solve the Hubble tension, such as

- **An underdense local Universe**;

- Adding extra dark energy components;

- Modifying the ΛCDM model with, for example, Modified Gravity;

- Many, many more...

Local Void

In an underdense local Universe, nearby galaxies will tend to have positive peculiar velocities, which will bias the "late" type Hubble constant to higher values than it should have.

Local Void

In an underdense local Universe, nearby galaxies will tend to have positive peculiar velocities, which will bias the "late" type Hubble constant to higher values than it should have.

I am going to explore, via 2 simulations, whether this local void is a feasible enough explanation to show why the "late" and "early" type Hubble constants have such different values.

Simulation by Wu & Huterer (2017)

Data and Procedings

Instead of using local density perturbations, Wu & Huterer opted to use non-uniform spatial distributions of Supernovae (SNe) from the data of the paper by Riess et al. (2016), or R16.

From the absolute magnitude of the SNe, we can get the Hubble constant with the following equation

$$\log_{10} H_0^{\text{loc}} = \frac{M_x^0}{5} + a_x + 5$$

To quantify the difference between the Hubble constant measured and one where we're considering a local void, then we have that

$$\Delta H_0^{\text{loc}} = (H_0^{\text{loc}} \ln 10)\Delta a_x = \frac{1}{N} \sum_{i=1}^{N} \frac{v_{r,i}}{r_i}$$

Data and Procedings

This difference in the Hubble constant can also be written in a different way, where we have

$$\Delta H_0^{\text{loc}} = \sum_{i=1}^{N} \frac{v_{r,i}}{\sigma_i^2 \cdot r_i} \cdot \left(\sum_{i=1}^{N} \frac{1}{\sigma_i^2} \right)^{-1}$$

The SNe were chosen to be in the redshift range of $0.023 < z < 0.15$, since at redshift $z = 0.023$ the effects of peculiar velocities on SNe are small.

Data and Proceedings

Credit: *Wu & Huterer (2017)*
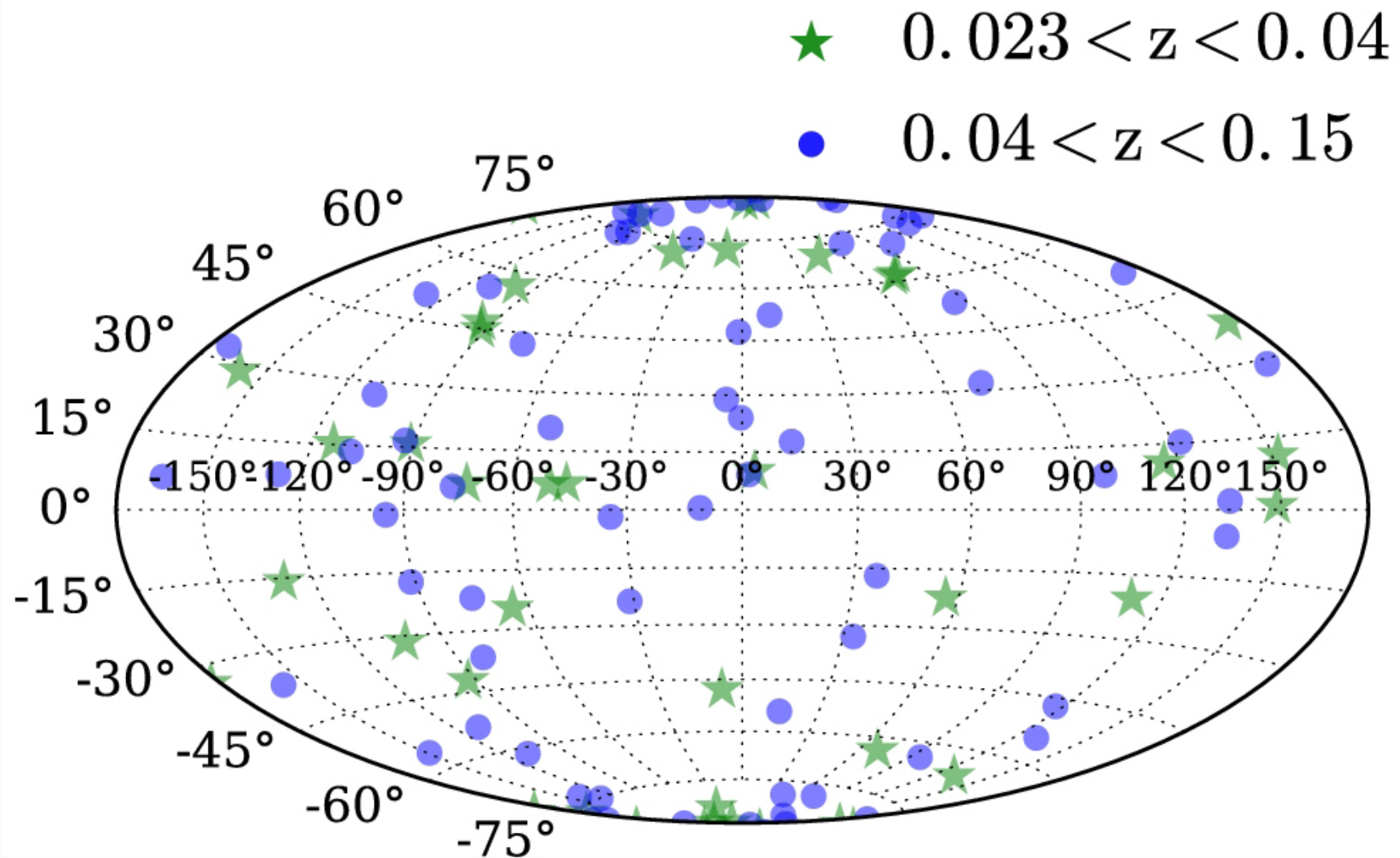
Credit: *Wu & Huterer (2017)*

Results

At worst, the value of ΔH_0^{loc} is smaller than 0.01 km s^{-1} Mpc^{-1}, with a $\sigma = 0.12$ km s^{-1} Mpc^{-1}. At best, considering the most underdense region, $\Delta H_0^{\text{loc}} = 0.65 \pm 0.13$ km s^{-1} Mpc^{-1}.

Source of Scatter	No Weighting	Weighted by $n^{\text{SN}}(z)/n^{\text{halo}}(z)$
Cumulative σ	0.12	0.38

Source of Scatter	Rotations, no Weighting	Weighted by mag error
Cumulative σ	0.42	0.31
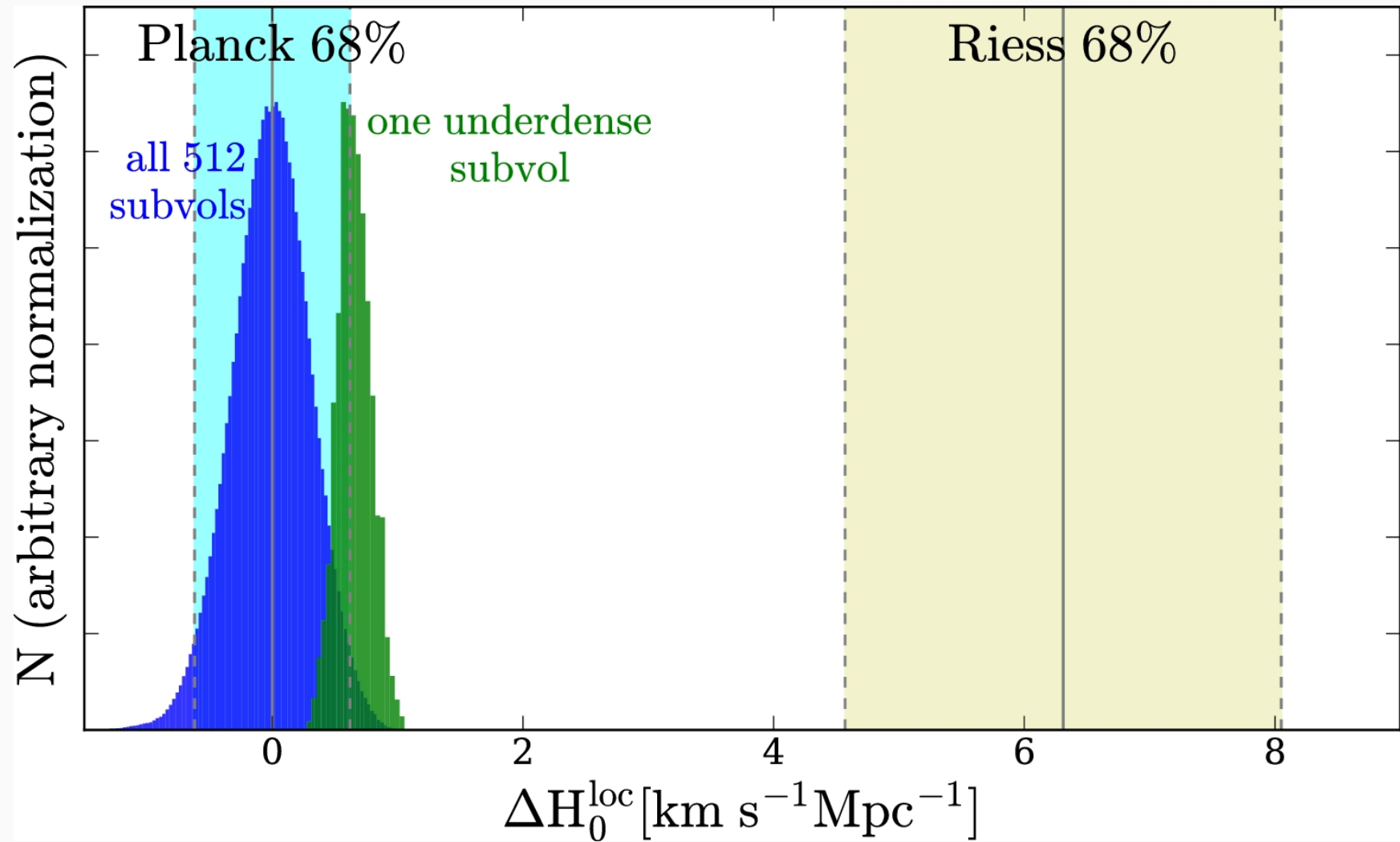
Results

Credit: *Wu & Huterer (2017)*

Results

We define the density of a medium as $\delta = \dfrac{(\rho - \bar{\rho})}{\rho}$

Results

We define the density of a medium as $\delta = \dfrac{(\rho - \overline{\rho})}{\rho}$
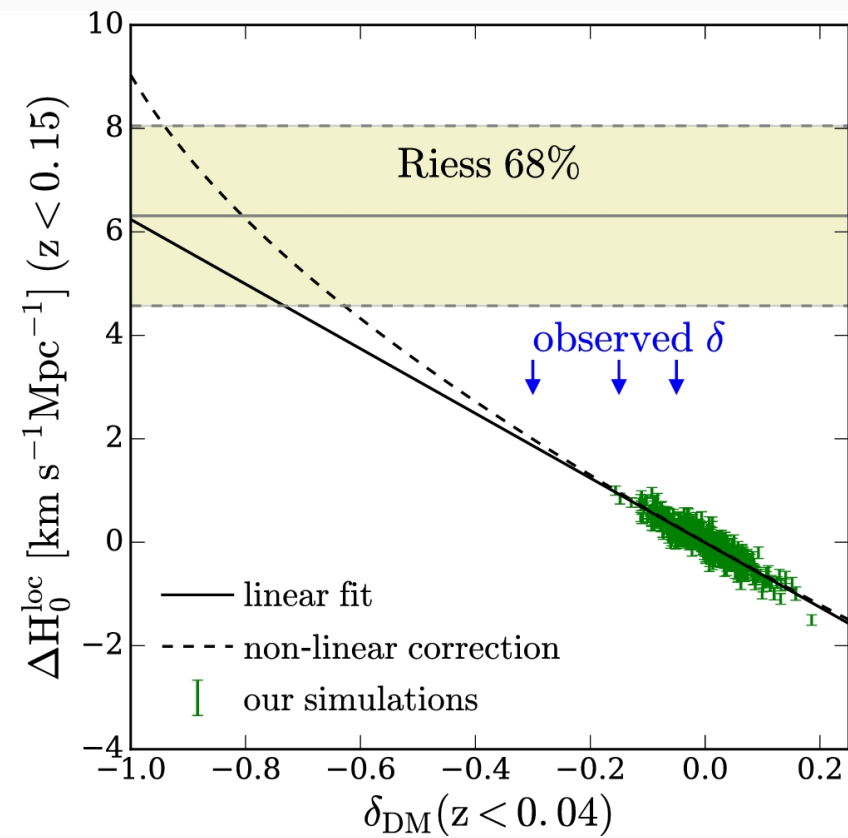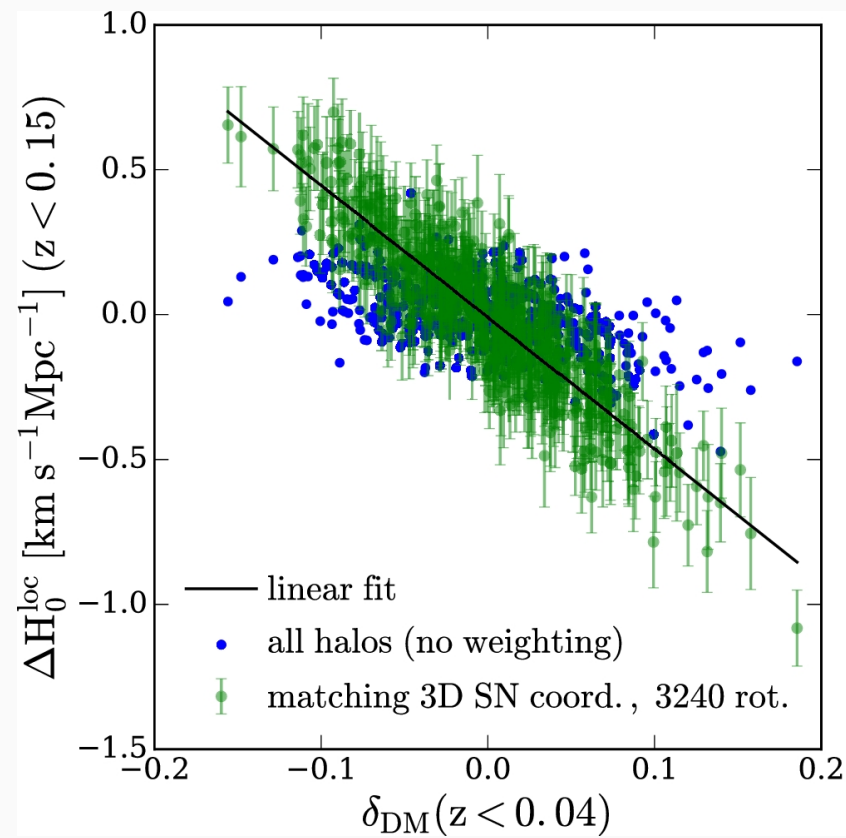
Credit: *Wu & Huterer (2017)*

Simulation by Kenworthy et al. (2019)

Key Differences

In terms of data, Kenworthy et al. decided to use several SNe data from Pantheon, Foundation and Carnegie Supernova Project (CSP), to attempt to cover as much of the sky as possible, instead of focusing on the inhomogenous distribution of SNe across the sky.

To calculate the difference in the local measurement of the Hubble constant, they start off with the same equation as Wu & Huterer

$$\log_{10} H_0^{\text{loc}} = \frac{M_B^0}{5} + a_B + 5$$

Instead of focusing on ΔH_0^{loc}, however, they focus on Δa_B, looking for evidences in variation of this value with redshift in regards of the outflow surrounding an isotropic void.

Results

From the data that was mentioned previously, the authors applied their results of Δa_B between two redshift ranges: $0.023 < z < 0.15$ and $0.01 < z < 0.15$, as they argue that at $z = 0.01$ the Hubble constant will be further constrained than at $z = 0.023$. This also takes into account two models for the local void - one where it ends at $z = 0.05$ (the Whitbourn & Shanks (2014), or WS14, model) and another at $z = 0.07$ (the KBC model).

z range	Field	Δa_B ($z_v = 0.07$)	Δa_B ($z_v = 0.05$)
$0.023 < z < 0.15$	Whole Sky	0.0013 ± 0.0040	0.0010 ± 0.0036
$0.01 < z < 0.15$	Whole Sky	0.0006 ± 0.0036	0.0002 ± 0.0034
$0.01 < z < 0.15$	KBC Fields	-0.0031 ± 0.0043	-
$0.01 < z < 0.15$	WS14 Fields	-	0.0040 ± 0.0045

None of these models are significantly different from the FLRW model.
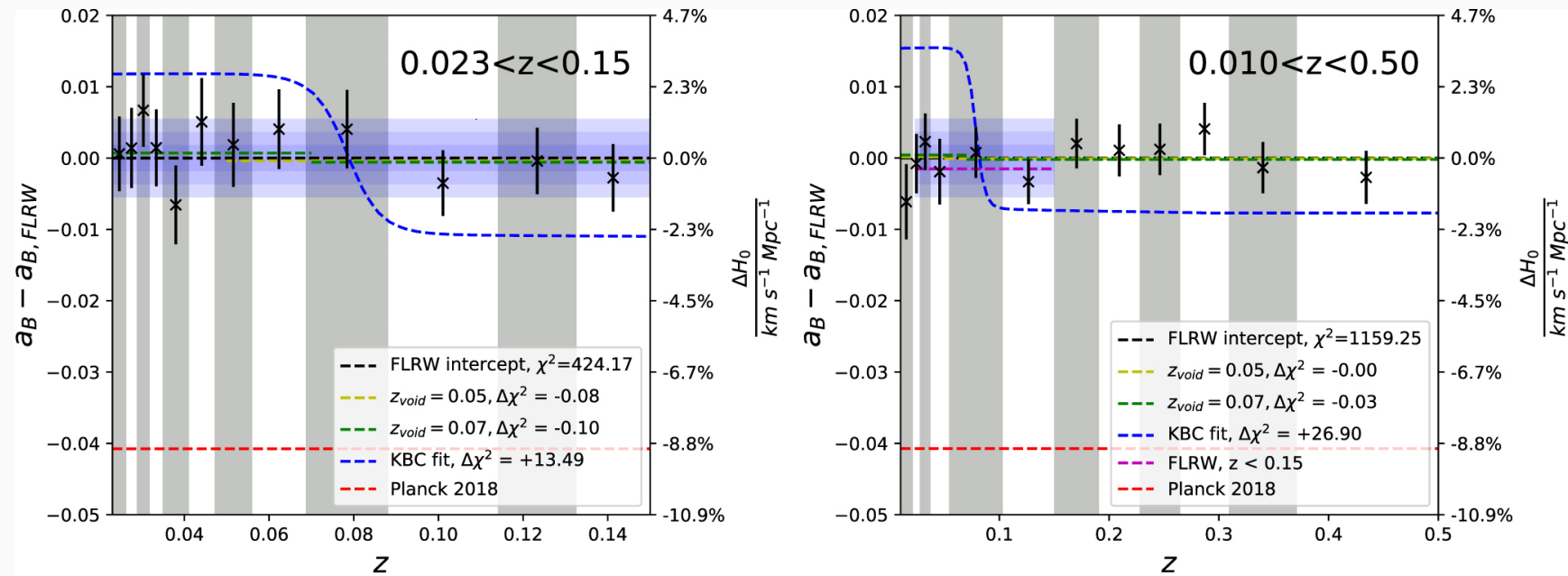
Credit: *Kenworthy et al. (2019)*

Results

Everything above assumes an isotropic void. However, if we consider anisotropies, then this might account for the high shift between the "late" and "early" type measurements of the Hubble constant. Matching the SNe data with the local void models proposed above we have the following

Credit: *Kenworthy et al. (2019)*
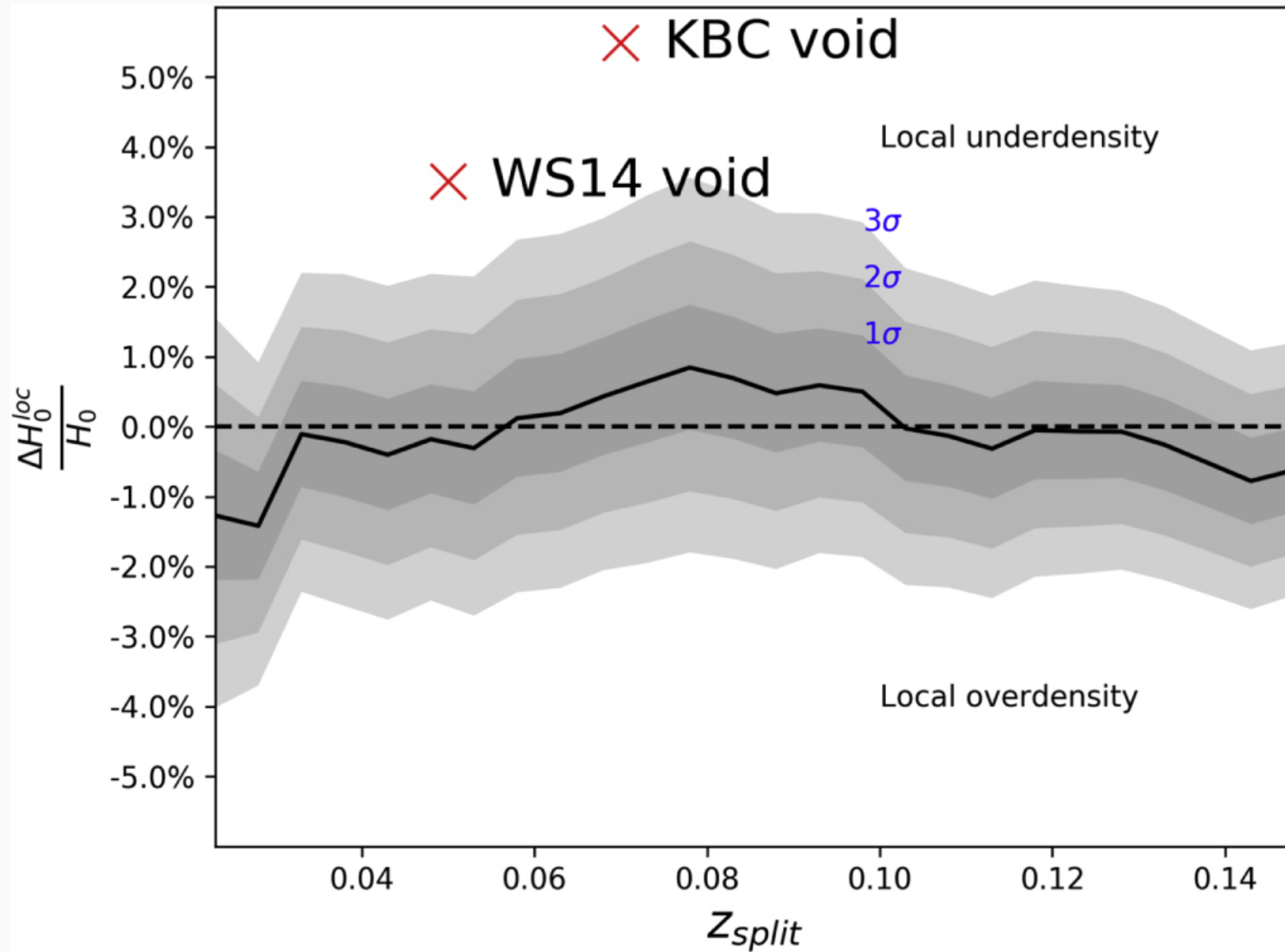
Credit: *Kenworthy et al. (2019)*

Overview

Summary

Overall, all the authors present reached the same conclusion: although there could exist a local underdensity, it isn't enough to explain the difference in values of the Hubble constant. Basing everything on two papers isn't very scientific, though, so, looking at the overview paper by Di Valentino et al. (2021), they point out a couple more references where the local void could explain the difference in the "late" and "early" type measurements.

Summary

We find that resolving the H_0 measurement discrepancy by postulating a local void requires an underdensity of $\delta \simeq -0.8$ with a radius of $120\, h^{-1}$Mpc, which is extremely unlikely in a ΛCDM universe. Existing direct observational constraints on the mass density at this scale, although highly uncertain, also exclude such a low density.

Nevertheless, the SN Ia data shows little evidence of a cosmic void *at any redshift*.

An underdense local Universe, corresponding to the simplest possibility for solving the Hubble constant tension for a sample-variance effect, has been definitely ruled out, because empirical and theoretical estimates of such fluctuations are a factor of ~ 20 too small. Such a void would need to extend to $z > 0.5$ or higher to not be apparent in the Hubble diagram of SNIa or BAO measurements.

Conclusion

Conclusion

No.

Conclusion

- Although it is the simpler explanation for the Hubble tension, the local void simply has too much damning evidence that tells us that it isn't a valid theory;

- Through simulations, observations and other methods, everything seems to point that this theory is wrong when it comes to the explanation of the Hubble tension;

- However, it has given us a better look at how the local Universe is distributed - although the theories wildly range from underdense to overdense, latest studies point towards a small underdensity.

References

Di Valentino, E. and 8 colleagues 2021. In the Realm of the Hubble tension − a Review of Solutions. arXiv e-prints.

Wu, H.-Y., Huterer, D. 2017. Sample variance in the local measurements of the Hubble constant. Monthly Notices of the Royal Astronomical Society 471, 4946–4955. doi:10.1093/mnras/stx1967

Kenworthy, W. D., Scolnic, D., Riess, A. 2019. The Local Perspective on the Hubble Tension: Local Structure Does Not Impact Measurement of the Hubble Constant. The Astrophysical Journal 875. doi:10.3847/1538-4357/ab0ebf

Cosmic Chronometers and Spatial Curvature

Miguel Martins

Cosmologia Física

Mestrado Integrado em Engenharia Física Tecnológica

Professor: Dr. Ismael Tereno

June 1, 2021

Hubble function

In the FRW background Universe, the Hubble function, $H(z)$, can be written as

$$H(z) = \frac{1}{a}\frac{\mathrm{d}a}{\mathrm{d}t} = -(z+1)\frac{1}{(1+z)^2}\frac{\mathrm{d}z}{\mathrm{d}t} = -\frac{1}{1+z}\frac{\mathrm{d}z}{\mathrm{d}t}. \tag{1}$$

Why is this expression useful?

- It is model independent;
- Allows the determination of $H(z)$ from knowledge of:
  - z: obtained with $< 0.1\%$ uncertainty in spectroscopic measurements of extragalactic objects;
  - $\mathrm{d}z$: obtained from two sufficiently close z values;
  - $\mathrm{d}t$: obtained from **cosmic chronometers**.

Cosmic Chronometers (CC)

Cosmic chronometers are passively evolving galaxies that:

- exhausted their fuel in a time scale (~ 0.3 Gyr) much shorter than their age;
- all their stars are about the same age;
- have a mass such that $\log_{10}(M/M_\odot) > 11$;
- were formed early at $z \sim 2 - 3$.

If two such galaxies formed at the same time t, but at different z values, we can measure their age difference Δt: small $\Delta t \implies \Delta t \approx \mathrm{d}t \implies$ can compute

$$\frac{\Delta z}{\Delta t} \to \frac{\mathrm{d}z}{\mathrm{d}t}.$$

Take home message:

Cosmic chronometers allow the determination of $H(z)$.

The curvature parameter Ω_K

In the FRW Universe, for a normalized spatial curvature K, the curvature parameter reads:

$$\Omega_K \equiv -\frac{K}{(H_0 a_0)^2}.$$

- $\Omega_K > 0 \implies K = -1 \implies$ open Universe;
- $\Omega_K = 0 \implies K = 0 \implies$ flat Universe;
- $\Omega_K < 0 \implies K = 1 \implies$ closed Universe;
- Ω_K quantifies the contribution of spatial curvature to the total energy density of the Universe.
- Ω_K influences the expansion history of the Universe via

$$H(z)^2 = H_0^2 \left[\Omega_m (1+z)^3 + \Omega_r (1+z)^4 + \Omega_\Lambda + \Omega_K (1+z)^2 \right].$$

The value of Ω_K

The current most widely accepted model of our Universe is the ΛCDM concordance model $\implies \Omega_K = 0$.
$\Omega_K = 0$ is predicted by **inflationary models** and several measurements have confirmed this value, such as:

- Baryon Acoustic Oscilations (BAO) distance and expansion rate;
- Full-Shape (FS) galaxy power spectra;
- Planck CMB lensing;
- local H_0 measurements;
- SNeIa distance moduli.
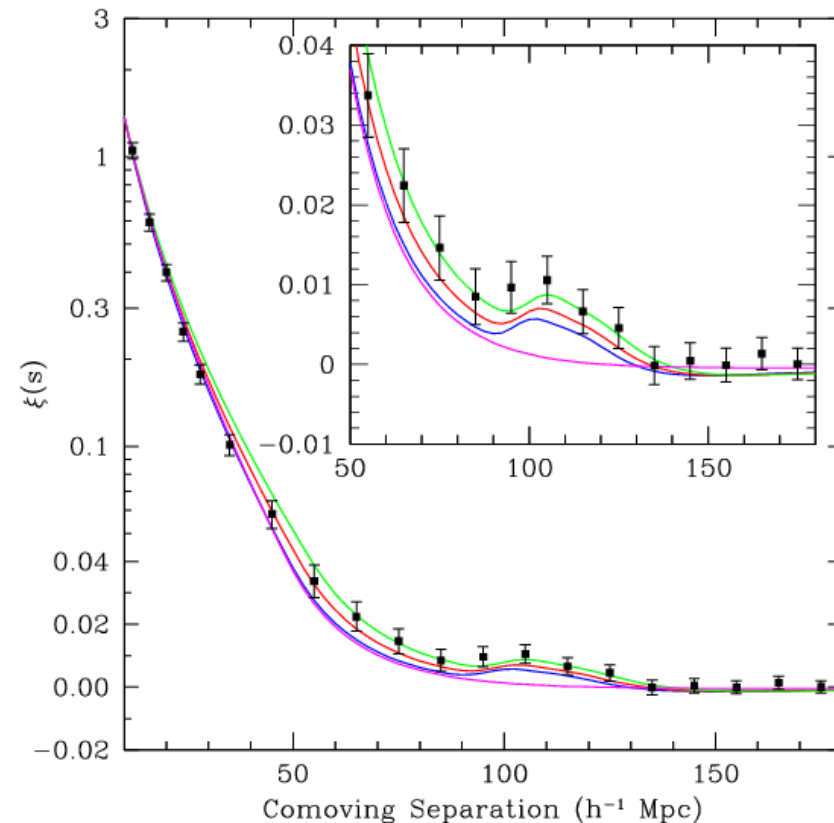
Curvature parameter: the tension awakens

CMB temperature and polarisation anisotropies from the Planck satellite 2018 data release (PL18) yielded

$$-0.095 < \Omega_K < -0.007 \text{ at } 95\% \text{ C.L.} \implies \text{ closed Universe,}$$

in conflict with the ΛCDM!
However, combined with other data sets (BAO, FS, ...) we can still get $\Omega_K = 0$!

Origin of the tension:

The tension arises when one assumes the Universe is closed $\implies$ PL18 results are incompatible with other data sets!

Why we can't jump to conclusions

One can not simply combine data sets!
First, we need to make sure the data sets are compatible.
Problem: Neither of data sets mentioned so far is compatible with the PL18 data set!
More caveats:

- $\Omega_K < 0$ is mostly driven by the **anomalous gravitational lensing** which smoothens high ℓ acoustic peaks of the CMB power spectrum;

- the constraining power of PL18 is limited by geometrical degeneracy (GD);

- the combination of PL18 with other data sets to break GD assumes a fiducial ΛCDM values $\implies$ possible erroneous interpretation of results.
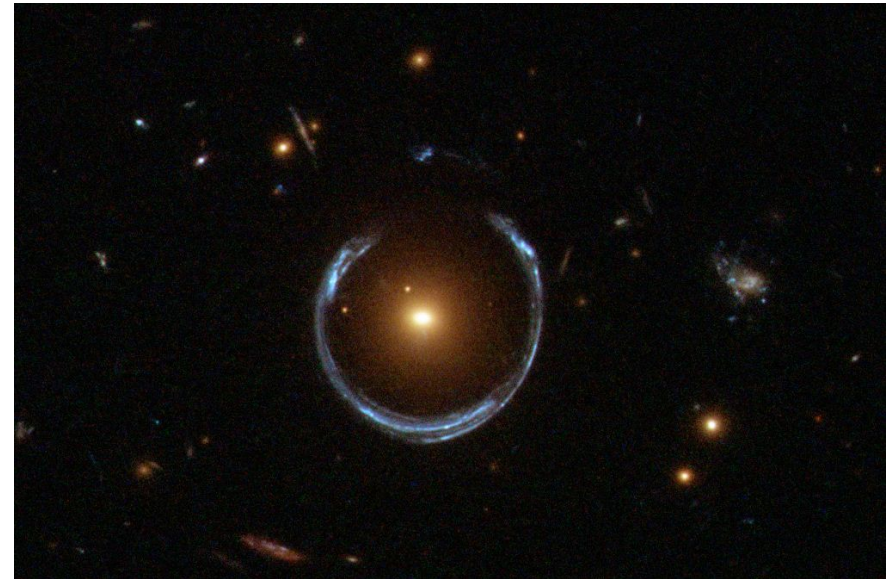
Anomalous gravitational lensing I

The anomalous gravitational effect:

- is quantified by the phenomenological parameter A_L;
- redistributes photons at the last scattering $\implies$ smoother low angular scale peaks;
- *is correlated with the curvature parameter* via

$$\Omega_m + \Omega_K = 1 - \Omega_r - \Omega_\Lambda.$$

So smaller $\Omega_K \implies$ larger $\Omega_m \implies$ stronger gravitational lensing

A_L has no physical meaning! It was introduced to:

- artificially re-scale high ℓ CMB peaks;
- account for possible systematics;
- test models of the Universe.

However PL18 arrived at

$$A_L = 1.15^{+0.13}_{-0.12}.$$

Anomalous gravitational lensing II
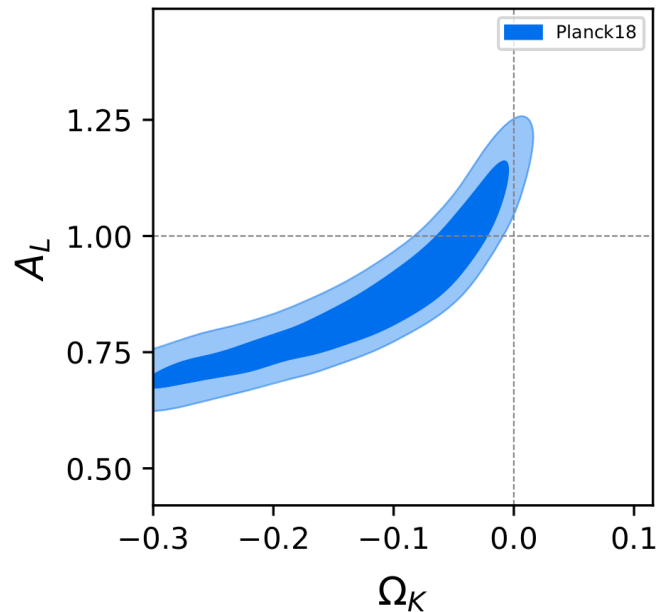
[DVMS19]
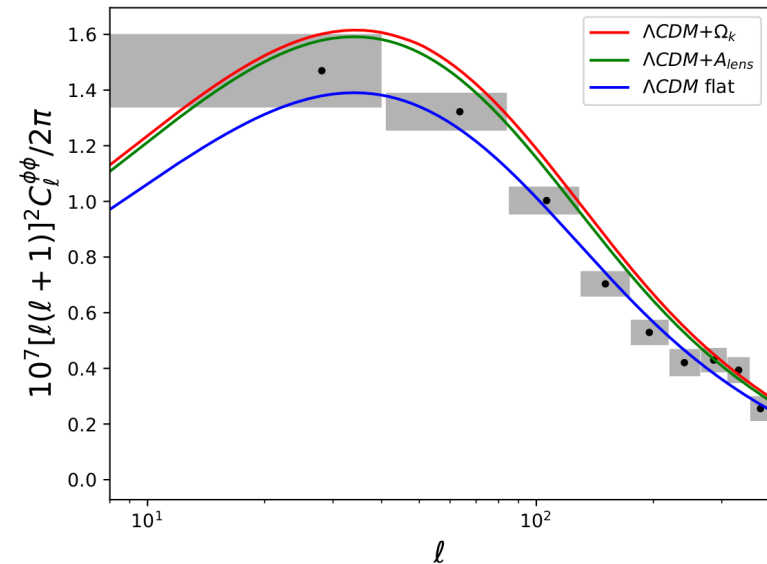
[DVMS19]

- $A_L - \Omega_K$ degeneracy stems from their correlation;
- flat Universe would require $A_L > 1$ (and is outside 68% C.L contour)!
- $\Omega_K < 0$ is a way to ensure $A_L = 1$ as expected!

Problem: Planck CMB lensing data favours ΛCMD model!

Conclusion:

$\Omega_K < 0$ fits PL18 data better due to smoother high ℓ peaks than expected.

Geometrical degeneracy

Let θ_s be the angular position of the first CMB peak. Then,

$$\ell_s = \frac{\pi}{\theta_s} = \pi \frac{d_M(z_{\text{dec}})}{r_s}.$$

- r_s is the comoving sound horizon scale;
- d_M is the comoving angular diameter distance at decoupling:

$$d_M(z) = \frac{c}{H_0 \sqrt{\Omega_K}} \sinh\left(H_0 \sqrt{\Omega_K} \int_0^z \frac{dz}{H(z)} \right).$$

Clearly, several combinations of Ω_K, Ω_m (via $H(z)$) and H_0 yield the same d_M $\implies$ same ℓ_s for fixed r_s (fixed by primitive Universe physics.) $\implies$ geometrical degeneracy.

Conclusion:

PL18 geometrical degeneracy might skew $P(\Omega_K)$ towards negative values $\implies$ it must be broken!

The ideal data set

One way to break the geometrical degeneracy is to introduce other data sets.
Problem: All data sets mentioned thus far are in tension with PL18 for a curved Universe $\implies$ cannot be safely combined.
The ideal data set should:

- break the geometrical degeneracy when combined with PL18;
- not be in strong tension with PL18 for a closed Universe;
- contain non to little amount of fiducial model assumptions.

Why cosmic chronometers offer the ideal data set

Question: Does the ideal data set exist?

Answer: Yes! Cosmic Chronometers (CC)!

The CC data set is a strong contender to a ideal one because:

- breaks the geometrical degeneracy through the computation of late time $H(z)$;

- is virtually independent of model assumptions;

- does not require any external calibration since they probe the $H(z)$ scale directly;

- Most importantly: *is mildly compatible* with PL18, as we will show.

Models and nomenclature

For the data sets we consider:

- CMB temperature and polarisation measurements of the Planck 2018 legacy release (PL18);
- 31 measurements of Cosmic Chronometers (CC) in the range $0.07 < z < 1.965$.

[PIa20]
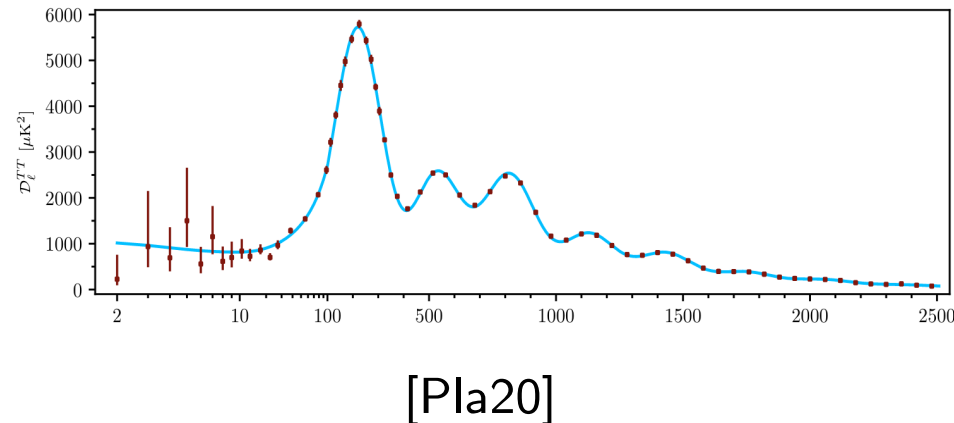
For the models we consider:

- $K\Lambda\text{CDM}$: ΛCDM (6 param.) $+ \Omega_K$ allowed to vary uniformly in $[-0.3, 0.3]$;
- $Kw\Lambda\text{CDM}$: $K\Lambda\text{CDM} + w_{\text{DE}}$ allowed to vary uniformly in $[-3, 1]$
- $M_\nu K\Lambda\text{CDM}$: $K\Lambda\text{CDM}$ but the sum of the neutrino masses, M_ν, is allowed to vary in $[0, 5]$ eV.

Some Bayesian inference definitions

The Bayes factor of $K\Lambda$CDM w.r.t ΛCDM reads, for a fixed data set:

$$B_{K0} = \frac{P(D|K\Lambda\text{CDM})}{P(D|\Lambda\text{CDM})} \frac{P(K\Lambda\text{CDM})}{P(\Lambda\text{CDM})}.$$

The best fit results in a larger posterior normalisation $\implies$

- $B_{K0} < 1 \implies \Lambda$CDM is preferred;
- $B_{K0} > 1 \implies K\Lambda$CDM is preferred;

For a parameter string θ, the deviance information criterion (DIC) reads:

$$\text{DIC} = 2\left\langle \chi^2(\theta) \right\rangle - \chi^2(\hat{\theta}).$$

For a fixed model, and two data sets:

$$\mathcal{I} = \exp\left[-\frac{\text{DIC}(D_1 \cup D_2) - \text{DIC}(D_1) - \text{DIC}(D_2)}{2} \right].$$

- $\ln \mathcal{I} < 0 \implies$ data sets are discordant;
- $\ln \mathcal{I} > 0 \implies$ data sets are concordant;

Results for the $K\Lambda$CDM model for PL18 and PL18+CC

Parameters	$K\Lambda$CDM	
	PL18	PL18+CC
Ω_K	$-0.044^{+0.018}_{-0.015}$	-0.0054 ± 0.0055
$H_0[\text{km s}^{-1}\text{Mpc}^{-1}]$	$54.36^{+3.25}_{-3.96}$	65.23 ± 2.14
Ω_m	$0.485^{+0.058}_{-0.068}$	0.336 ± 0.022

[VLM21]

- $\Omega_K < 0$ value for PL18 + geometrical degeneracy $\implies$ low H_0 and large Ω_m w.r.t ΛCDM;

- Strong tension between PL18 values and other late time measurements;

- CC breaks geometrical degeneracy:
  - flat Universe at 1σ;
  - values of H_0 and Ω_m compatible with PL18+BAO and PL18+FL galaxy power spectrum;

- Ω_k from PL18+CC has high uncertainty;

Posterior and contour plots for $K\Lambda$CDM model: PL18 and PL18+CC
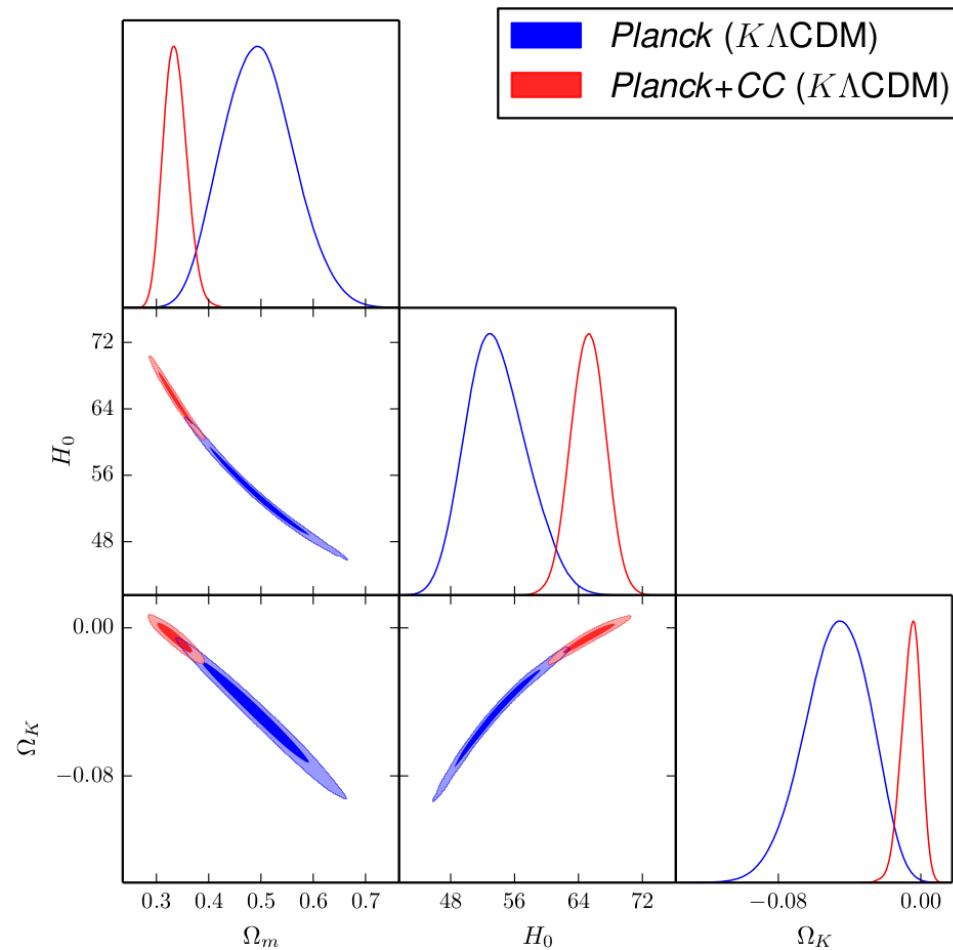
[VLM21]

- Broken geometric degeneracy $\implies$ narrower contours $\Omega_K - H_0$ and $\Omega_K - \Omega_m$ for PL18 + CC;

- Contour overlap of 95% C.L region $\implies$ not a strong tension between PL18 and PL18+CC even in curved Universe;

- PL18: Strong preference for $K\Lambda$CDM: $\ln B_{K0} = 2.5$

- PL18+CC: Strong preference for ΛCDM: $\ln B_{K0} = -3.4$.

Tension between PL18 and CC data sets

To quantify the concordance or discordance of PL18 and CC data sets we compute the factor $\mathcal{I}$:

$$\ln \mathcal{I}(\mathsf{PL18}, \mathsf{CC}) = -0.47$$

- The data sets have a mild disagreement;
- $\mathcal{I}$ value visually justified by disjoint 68% regions in the contour plots;
- Disagreement much milder w.r.t BAO and FS data sets

Conclusion:

Mild confidence in the combination of PL18 and CC data sets $\implies$ less tension for a curved Universe $\implies$ more confidence in the flat Universe result from PL18+CC.

Stability of Ω_K against a larger parameter space
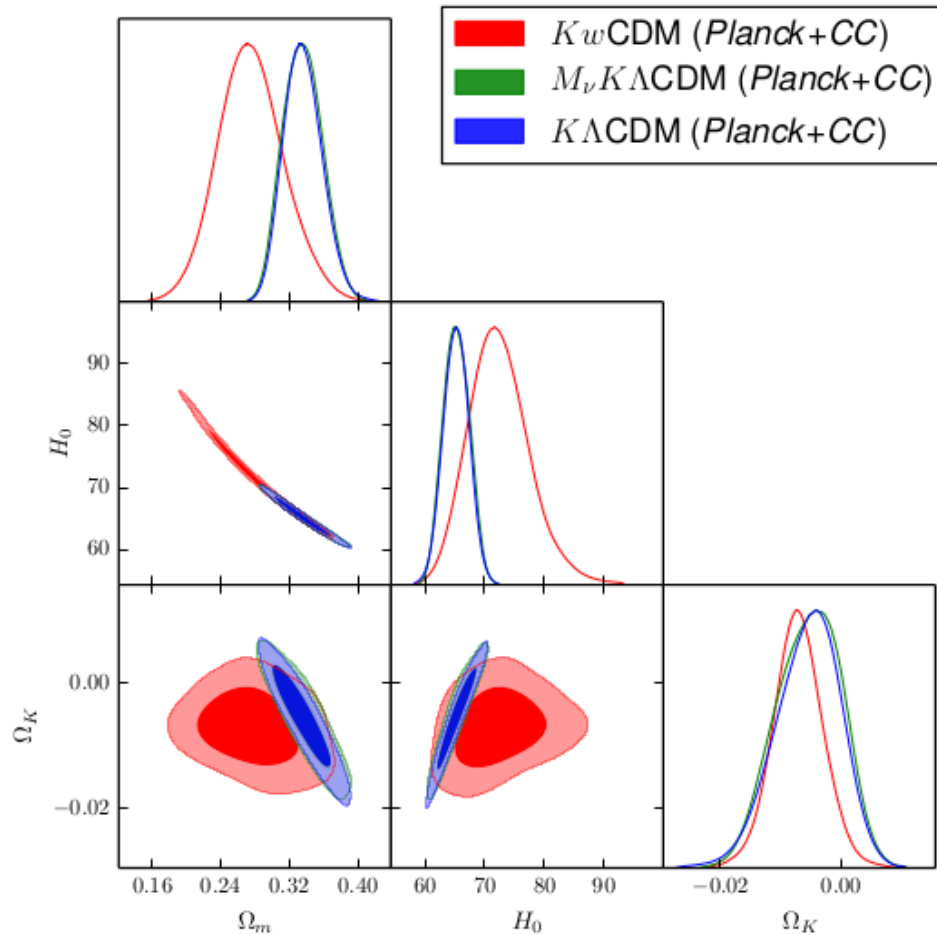
[VLM21]

- Increased parameter space $\implies$ test the stability of Ω_K of PL18+CC;

- Value of $\Omega_K = 0$ at $\leq 1.7\sigma$;

- Breaking geometrical degeneracy with CC $\implies$ stable spatially flat Universe against size of parameter space;

Conclusions

- Cosmic chronometers allow a model independent determination of $H(z)$;
- CC data set can be combined with PL18 data set, unlike BAO or FS;
- PL18+CC yield a spatially flat Universe

$$\Omega_K = -0.0054 \pm 0.0055.$$

- CC and PL18 are not is a strong tension $\implies$ solves curvature tension!
- PL18+CC determination is relativaly stable w.r.t increase in parameter space;
- Downside: CC data set renders a more imprecise determination of Ω_K;
- CC systematics have little impact on the above analysis;

References I

L. Amendola and S. Tsujikawa, *Dark energy: Theory and observations*, Cambridge University Press, 2010.

Eleonora Di Valentino, Alessandro Melchiorri, and Joseph Silk, *Planck evidence for a closed universe and a possible crisis for cosmology*, Nature Astronomy **4** (2019), no. 2, 196–203.

Vicente Estrada-Carpenter, Casey Papovich, Ivelina Momcheva, Gabriel Brammer, James Long, Ryan F. Quadri, Joanna Bridge, Mark Dickinson, Henry Ferguson, Steven Finkelstein, Mauro Giavalisco, Catherine M. Gosmeyer, Jennifer Lotz, Brett Salmon, Rosalind E. Skelton, Jonathan R. Trump, and Benjamin Weiner, *CLEAR. I. Ages and Metallicities of Quiescent Galaxies at 1.0 ¡ z ¡ 1.8 Derived from Deep Hubble Space Telescope Grism Data*, The Astrophysical Journal **870** (2019), no. 2, 133.

Planck Collaboration, *Planck 2018 results - i. overview and the cosmological legacy of planck*, A&A **641** (2020), A1.

Fabrizio Renzi, Eleonora Di Valentino, and Alessandro Melchiorri, *Cornering the planck alens tension with future cmb data*, Physical Review D **97** (2018), no. 12.

Sunny Vagnozzi, Abraham Loeb, and Michele Moresco, *Eppur è piatto? the cosmic chronometers take on spatial curvature and cosmic concordance*, The Astrophysical Journal **908** (2021), no. 1, 84.

II. Dark and baryonic matter
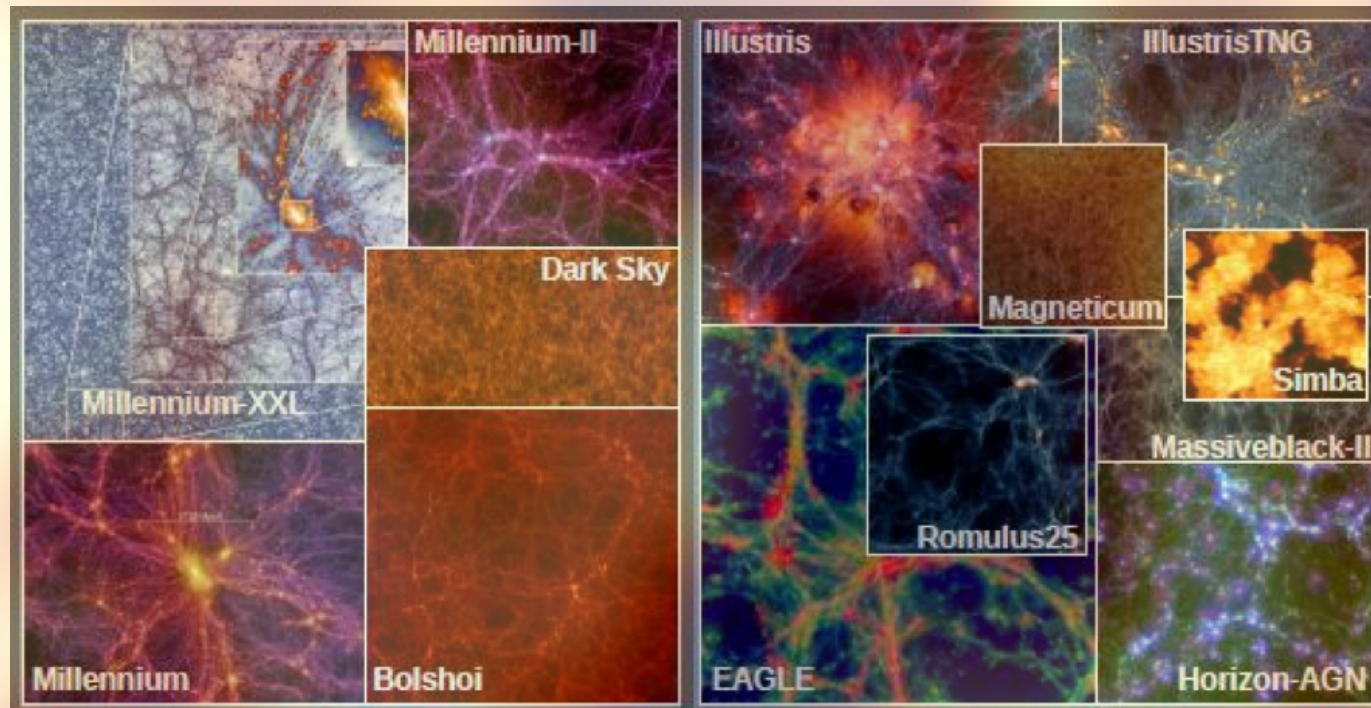
Dark Matter Particles

Physical Cosmology

Filipe Correia - 51120

June 2021

Introduction

Dark matter is one of the most important topics of research in Physics and our present knowledge comes from gravitational interactions detected in observations.

In this presentation, I will show a 2D parameter space which classifies different dark matter models in terms of their particle's interaction strength and the astrophysical scale on which new physics appear.

Thought Experiment

Considering a "dark matter scientist" who can only observe the "dark" sector of the Universe, the baryonic sector would be invisible to him.

Using the equivalent particle physics of dark matter would be extremely difficult but using astrophysics and cosmology would prove rather useful.

Introducing The Parameters

In order to organize these searches, it is useful to have a compact space in which to classify models both in terms of their observability in the sky and in the laboratory.

The dark matter models will be classified according to their interaction strength with the Standard Model (Λ^{-1}) and the cosmological scale at which it is expected to see a deviation from the Cold Dark Matter paradigm (M_{halo}).

Defining Λ^{-1}

The interaction strength with the Standard Model can be defined as

$$\Lambda^{-1} \equiv \frac{\lambda^2}{4\pi M}$$

where λ is the coupling constant, M the mass of the mediating particle and 4π is to account for phase space.

Larger values of Λ^{-1} correspond to stronger interactions with the Standard Model and smaller values correspond to dark matter models which are less coupled to visible matter.

Λ^{-1} For Different Models

Table: Values of Λ^{-1} for different dark matter models.

CDM	$\sim 10^{-19}$ GeV^{-1}
WIMPs	$\sim (6 - 40) \times 10^{-5}$ GeV^{-1}
TRDM	$\sim 5 \times 10^{-5}$ GeV^{-1}
Dark photons	$\sim 10^{-12} - 10^{-8}$ GeV^{-1}
ADM	$\gtrsim 5 \times 10^{-5}$ GeV^{-1}
Axions	$\sim 10^{-11} - 10^{-15}$ GeV^{-1}
FDM	$\sim 10^{-17} - 10^{-19}$ GeV^{-1}

Λ^{-1} For Different Models

Table: Values of Λ^{-1} for different dark matter models.

Sterile neutrinos	$\lesssim 10^{-7}$ GeV^{-1}
Gravitinos	$\lesssim 10^{-29} - 10^{-9}$ GeV^{-1}
PBHs	$\sim 10^{-19}$ GeV^{-1}

For baryons:

- proton-proton scattering - $\Lambda^{-1} \sim 10^4$ GeV^{-1}
- strong-force nucleon-nucleon scattering - $\Lambda^{-1} \sim$ GeV^{-1}
- weak-force nucleon-nucleon scattering - $\Lambda^{-1} \sim 10^{-4}$ GeV^{-1}

Dark Matter Primer

Considering models which are invisible to our particle detectors, it is possible to study them by their gravitational imprint on matter and light.

The fundamental macroscopic unit of dark matter is the halo, which is an overdensity that decoupled from the Hubble flow, collapsed and virialized into a gravitationally bound clump.

The halos are defined via their virial mass (M_{vir}), their virial radius (R_{vir}) and their virial velocity (v_{vir}).

Introducing M_{halo}

Dark matter can form gravitationally bound structures down to a mass of at least 10^8 $M_\odot$.

If there exist interactions either between dark matter particles or between dark matter and the Standard Model, then the number and structure of these halos can be modified.

Introducing M_{halo}

Deviations from the CDM model can be expressed in terms of the largest physical scale on which deviations from CDM appear noticeable.

This scale if often represented in terms of the halo mass, M_{halo}, which can be expressed in terms of a comoving wavenumber, k.

These deviations can be of two forms - primordial and evolutionary.

Primordial Deviations

Free-streaming out of small density perturbations by particles with semi-relativistic or relativistic momentum distribution can cause truncations in the matter power spectrum.

Interactions with the Standard Model can also lead to truncations with a structure of acoustic-type oscillations.

Primordial Deviations

Table: Values of M_{halo} for different dark matter models.

Thermal relics	$\sim 10^{-5}\ M_\odot - 10^{-2}\ M_\odot$
WIMPs (SUSY)	$\sim 10^{-8}\ M_\odot - 10^{-2}\ M_\odot$
WIMPs (KK)	$\sim 10^{-2}\ M_\odot - 10^{-1}\ M_\odot$
Dark photons	$\lesssim 10^{12}\ M_\odot$
ADM	$\lesssim 10^{-1}\ M_\odot$
Axions	$\sim 10^{-10}\ M_\odot - 10^{-13}\ M_\odot$
FDM	$\sim 10^{10}\ M_\odot (m_\chi / 10^{-22}\ \text{eV})^{-4/3}$

Primordial Deviations

Table: Values of M_{halo} for different dark matter models.

Sterile neutrinos	$10^{-6} - 10^{11}\ M_\odot$
Gravitinos	$10^{-17}\ M_\odot - 10^{13}\ M_\odot$
SIDM	$\lesssim 10^{11}\ M_\odot$
PBHs	$\approx 10^{-(17-16)}\ M_\odot, 10^{-(14-9)}\ M_\odot, 10^{0-3}\ M_\odot$

The growth of small halos at early times is suppressed by the flow of baryons with respect to dark matter. This happens on scales of $M_{\text{vir}} \sim 10^8\ M_\odot$.

Evolutionary Deviations

The structure of dark matter halos can also be altered by late-time effects.

Instead of time-dependent effects that result from primordial deviations, interactions or decays can cause evolutionary deviations.

For WIMPs and thermal relics, $\Gamma \sim 10^{-11}$ Gyr^{-1} which means that the relative evolution of WIMP-like thermal relic dark matter halos vs. pure CDM halos is completely negligible.

Evolutionary Deviations

Table: Values of M_{halo} for different dark matter models.

Axions	$\sim 10^{12}\ M_{\odot}$
FDM	$\sim 10^{8}\ M_{\odot} - 10^{10}\ M_{\odot}$
SIDM	$\lesssim 10^{15}\ M_{\odot}$
Baryons	$10^{8}\ M_{\odot} \lesssim M_{\text{halo}} \lesssim 10^{15}\ M_{\odot}$

The sterile neutrino lifetime is many orders of magnitude larger than the age of the Universe therefore they have negligible evolutionary deviations from CDM.

Combining Everything

By combining all of the information above, the 2D parameter space has the following plot
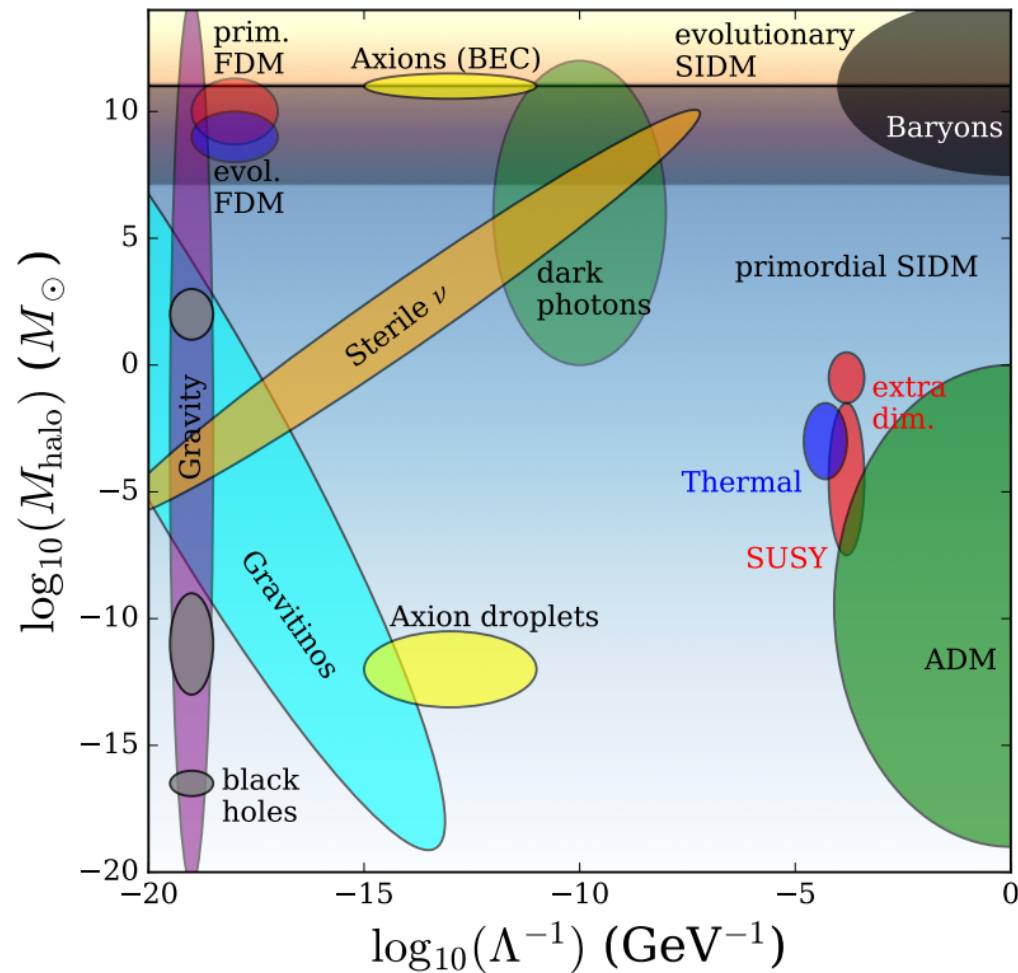
Conclusion

We still don't know a lot about dark matter but having a framework where interdisciplinary collaboration in dark matter physics is possible makes it easier to understand it.

With this new 2D parameter space, the bridge between particle physics and astronomy is made and a common language between these branches oh physics was created.

Hydrodynamical Simulations of galaxy formation

Ciências ULisboa

Duarte Almeida 49550

Physical Cosmology – Ismael Tereno

1st June 2021

Low-Resolution High-Resolution Super-Resolution
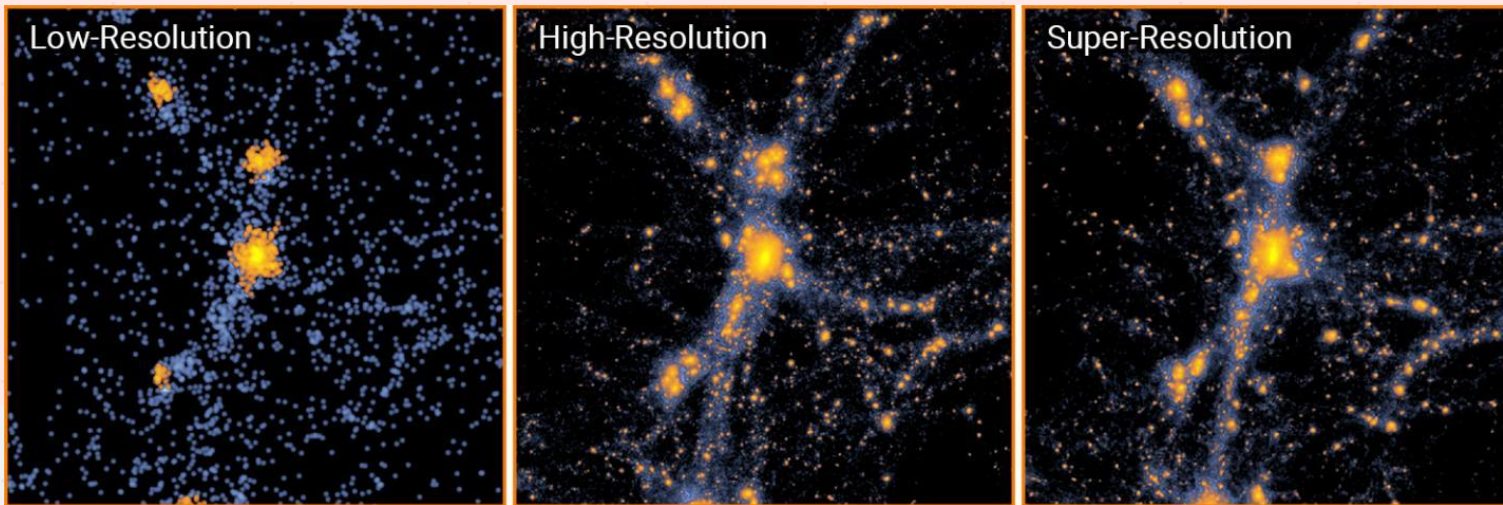
Credits: Y. Li et al./Proceedings of the National Academy of Sciences 2021

Topics:

- What are hydrodynamical simulations?
- What type of physical processes can be simulated?
- What is the impact of including baryonic effects in the matter power spectrum?

Hydrodynamical Simulations of galaxy formation

→ **Simulate a dynamical system of particles**, usually under the influence of physical forces.

Used to study processes of **non-linear structure formation** such as galaxy filaments and galaxy halos and to study the dynamical evolution of clusters.

Modern simulations model dark matter, dark energy, and ordinary matter in an expanding space-time starting from well-defined initial conditions.

31.25 Mpc/h
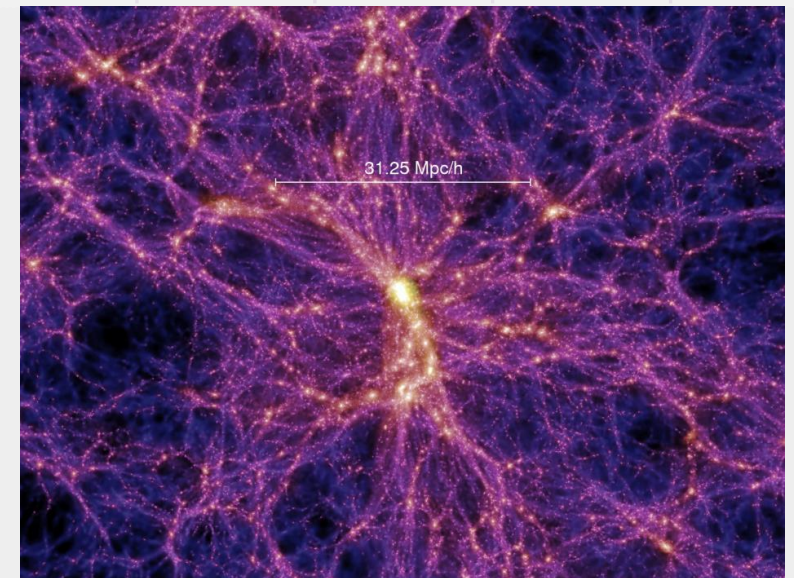
Springel et al. (2005)

Hydrodynamical Simulations of galaxy formation

N-body simulations consider **only dark-matter**.

Hydrodynamical simulations consider **dark matter plus baryons.**

Two types of simulations: "**zoom**" (more detail) and "**large volume**".

Mark Vogelsberger et al. (2019)

4
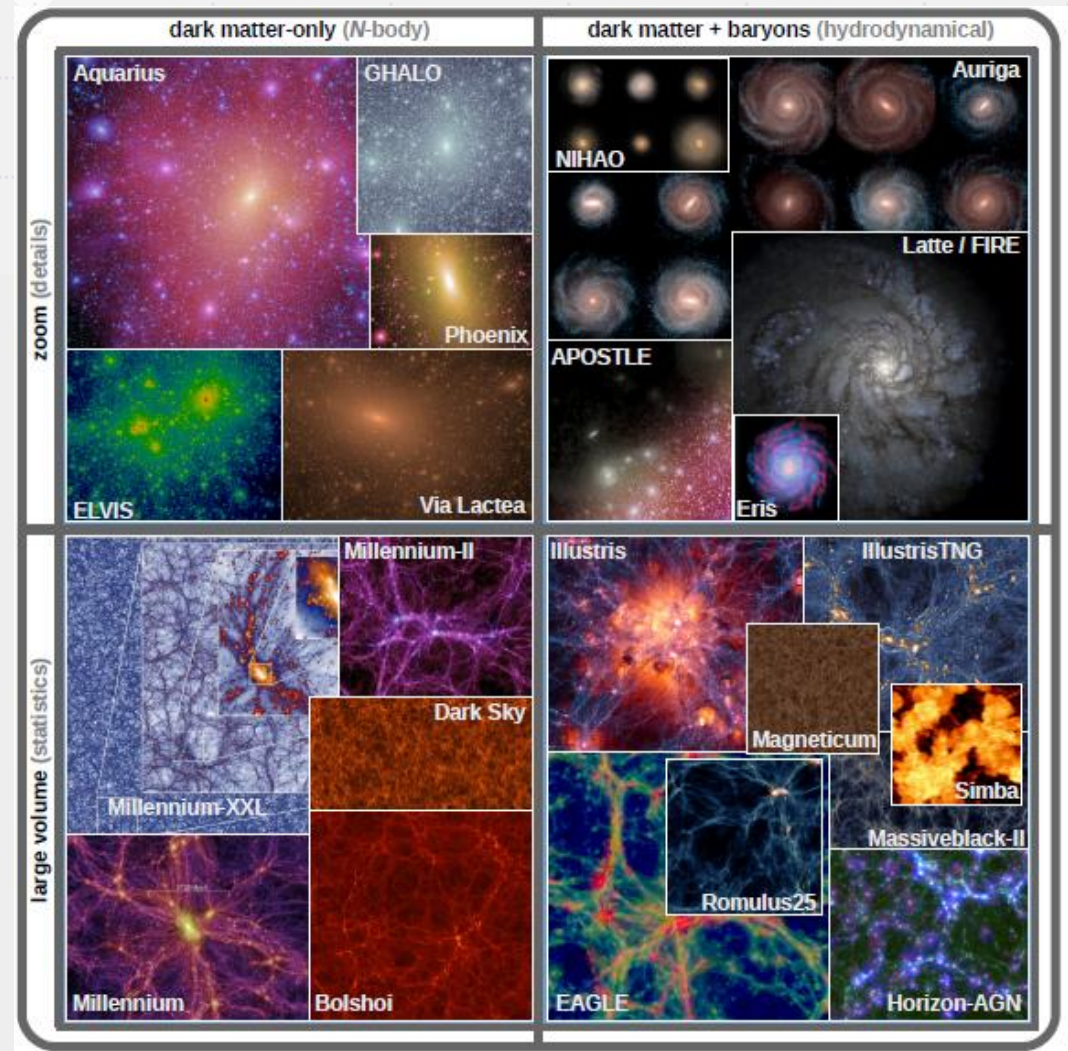
Hydrodynamical Simulations
of galaxy formation

Components of our simulation = cosmological model + specific initial conditions.

Cosmological model:

- **Cold dark matter**: negligible random motions when decoupled from other matter, and collisionless.

- **Dark energy**: drives the accelerated expansion of the Universe.

$\rightarrow$ **Concordance ΛCDM model**.

Initial conditions:

- Specify the perturbations imposed on top of a homogeneous expanding background (spatially flat FLRW space-time).
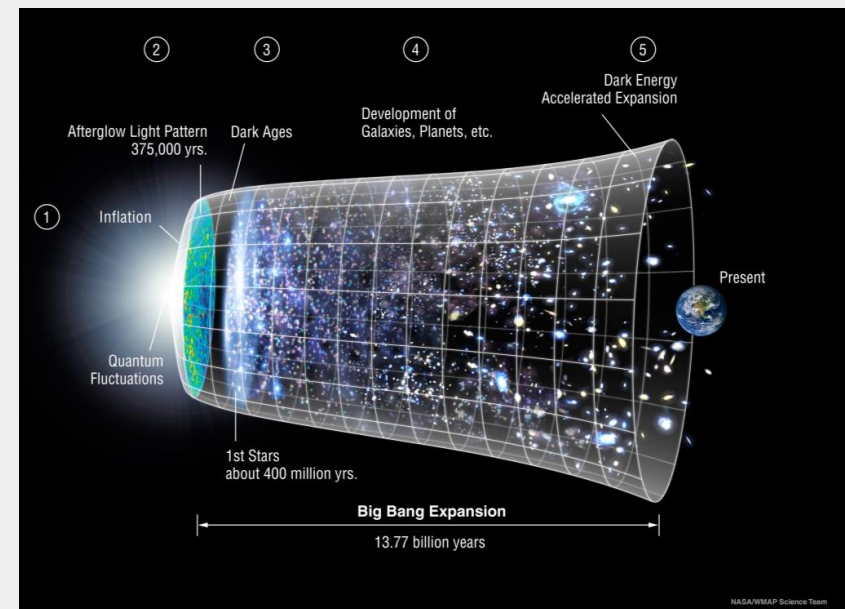
Credits: NASA/ LAMBDA Archive / WMAP Science Team

Hydrodynamical Simulations of galaxy formation

Dark matter follows the equations of collisionless gravitational dynamics that are solved through the N-body method.

Gas component of baryons is described through the equations of hydrodynamics that are solved with Lagrangian or Eulerian methods.

numerical discretization of matter components

Collisionless Gravitational Dynamics
- *N*-body methods based on integral Poisson's equation (e.g. tree, fast multipole)
- *N*-body methods based on differential Poisson's equation (e.g. particle-mesh, multigrid)
- *N*-body hybrid methods (e.g. TreePM)
- Beyond *N*-body methods (e.g. Lagrangian tesselation)

dark matter

Hydrodynamics
- Lagrangian methods (e.g. smoothed particle hydrodynamics)
- Eulerian methods (e.g. adaptive-mesh-refinement)
- Arbitrary Lagrangian-Eulerian methods (e.g. moving mesh)
- Mesh-free / mesh-based

gas

generating initial conditions

Volume — sample of galaxies ← linear perturbation theory → Zoom — individual galaxy

Gravity
- Newtonian gravity in an expanding background
- modified gravity as dark matter alternative
- modified gravity as dark energy alternative
- ...

Dark Matter
- cold dark matter
- warm dark matter
- self-interacting dark matter
- fuzzy dark matter
- ...

Dark Energy
- cosmological constant
- dynamical dark energy
- inhomogeneous dark energy
- coupled dark energy
- ...

Initial Conditions
- inflation generated initial perturbations on top of homogeneous Friedmann model
- ...

cosmological framework

Mark Vogelsberger et al. (2019)

6

Hydrodynamical Simulations of galaxy formation

Simulating baryons is crucial to make predictions for the visible Universe!

Mark Vogelsberger et al. (2019)

Initially, the baryon component is only made of gas (mostly H and He) but in high density regions, it will form stars → fraction of the available gas is converted to "star particles".

Gas is described as **ideal gas following Euler equations**.

Modeling cosmic gas

Eulerian formulation:

$$\frac{\partial \rho}{\partial t} + \nabla \cdot (\rho \mathbf{v}) = 0$$

$$\frac{\partial \rho \mathbf{v}}{\partial t} + \nabla \cdot (\rho \mathbf{v} \otimes \mathbf{v} + P\mathbb{1}) = 0$$

$$\frac{\partial \rho e}{\partial t} + \nabla \cdot (\rho e + P)\mathbf{v} = 0$$

Lagrangian formulation:

$$\frac{D\rho}{Dt} = -\rho \nabla \cdot \mathbf{v}$$

$$\frac{D\mathbf{v}}{Dt} = -\frac{1}{\rho} \nabla P$$

$$\frac{De}{Dt} = -\frac{1}{\rho} \nabla \cdot P\mathbf{v}$$

Arbitrary Lagrangian-Eulerian formulation:

$$\frac{d}{dt} \int_V \rho \, dV = -\int_S \rho(\mathbf{v} - \mathbf{w}) \cdot \mathbf{n} dS$$

$$\frac{d}{dt} \int_V \rho \mathbf{v} \, dV = -\int_S \rho \mathbf{v}(\mathbf{v} - \mathbf{w}) \cdot \mathbf{n} dS - \int_S P \mathbf{n} dS$$

$$\frac{d}{dt} \int_V \rho e \, dV = -\int_S \rho e(\mathbf{v} - \mathbf{w}) \cdot \mathbf{n} dS - \int_S P\mathbf{v} \cdot \mathbf{n} dS$$

Different forms of the hydrodynamical equations. $D/dt \equiv \partial/\partial t + \mathbf{v} \cdot \nabla$ denotes the Lagrangian derivative and $e = u + \mathbf{v}^2/2$ the total energy per unit mass. The equations are closed through $P = (\gamma - 1)\rho u$ with $\gamma = 5/3$. For the arbitrary Lagrangian-Eulerian formulation the grid moves with velocity $\mathbf{w}$ and cell volumes evolve as $dV/dt = \int_V (\nabla \cdot \mathbf{w}) \, dV$.

Focuses on specific locations in space through which the fluid flows as time passes.

Assumes an observer that follows an individual fluid parcel, with its own properties (like density), as it moves through space and time.

Hydrodynamical Simulations
of galaxy formation

The results from simulations can be directly confronted with observational data.

Early simulations successfully reproduced properties of the intergalactic medium but suffered from inconsistencies and only recently began to produce realistic galaxies.

- **Galaxy stellar mass function** - quantifies the comoving number density of galaxies as a function of galaxy stellar mass.

It requires a strong suppression of star formation at both the low and high mass ends → Including **supernova feedback** and **feedback from AGN** seems to provide better results.
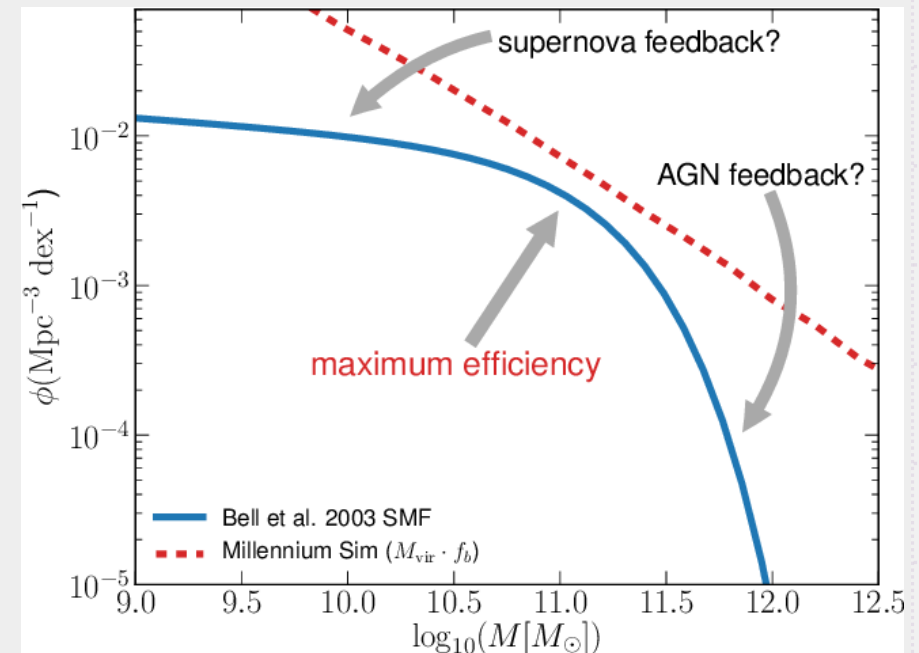
S. Mutch et al. (2013)

Hydrodynamical Simulations
of galaxy formation

- **Scaling relations**:

    Supermassive black hole mass-stellar velocity dispersion relation, the mass-metallicity relation and the color of galaxies as a function of galaxy stellar mass.

    For the **late-type galaxies** simulations struggled to form galaxies with extended and rotationally supported discs but the after introducing **stellar feedback** the star formation appears to be more efficiently regulated.

NGC 1566; ESA/Hubble & NASA

Hydrodynamical Simulations of galaxy formation
Impact of baryons in the matter power spectrum

Matter power spectrum, P(k), where k is the comoving wave number corresponding to a comoving spatial scale λ = 2π/k.

→ If we have a sufficiently accurate model, **we can infer the initial, linear power spectrum from the observed, non-linear one.**

OWLS project: large number of state-of-the-art hydrodynamical simulations to systematically study the effects of various baryonic processes on the matter power spectrum for k ∼ 0.1 − 500 h/Mpc.
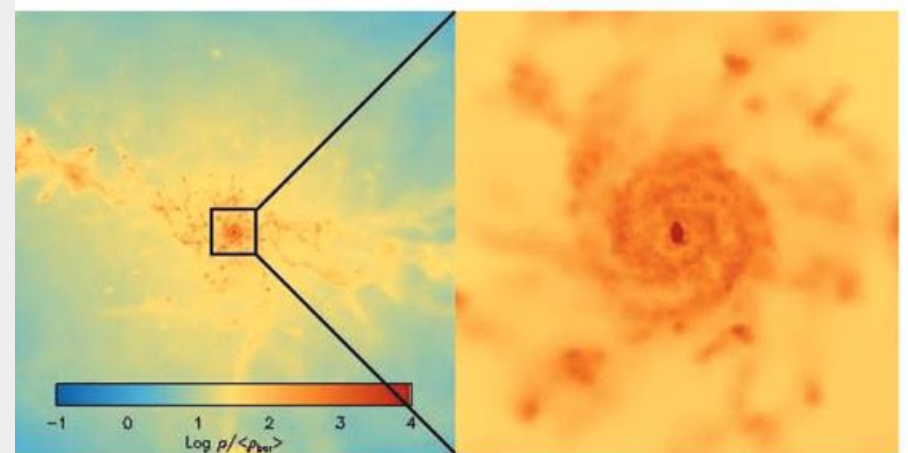
J. Schaye et al. (2009)

Hydrodynamical Simulations of galaxy formation
Impact of baryons in the matter power spectrum

Could provide sufficient energy to have a large effect on the matter power spectrum

Not realistic because the omitted processes exist, but they are valuable tools to investigate on what scales these processes affect the total matter power spectrum.

Simulation	Description
AGN	Includes AGN (in addition to SN feedback)
AGN_WMAP7	Same as AGN, but with a WMAP7 cosmology
DBLIMFV1618	Top-heavy IMF at high pressure, extra SN energy in wind velocity
DMONLY	No baryons, cold dark matter only
DMONLY_WMAP7	Same as DMONLY, but with a WMAP7 cosmology
MILL	Millennium simulation cosmology (i.e. WMAP1), $\eta = 4$ (twice the SN energy of REF)
NOSN	No SN energy feedback
NOSN_NOZCOOL	No SN energy feedback and cooling assumes primordial abundances
NOZCOOL	Cooling assumes primordial abundances
WDENS	Wind mass loading and velocity depend on gas density (SN energy as REF)
WML1V848	Wind mass loading $\eta = 1$, velocity $v_{\mathrm{w}} = 848\,\mathrm{km\,s^{-1}}$ (SN energy as REF)
WML4	Wind mass loading $\eta = 4$ (twice the SN energy of REF)

M. P. van Daalen et al. (2011)

Hydrodynamical Simulations of galaxy formation
Impact of baryons in the matter power spectrum

Reference simulation (REF) = SN feedback, radiative cooling and heating but doesn't have AGN.

The contribution of the baryons is significant, decreasing the power by more than 1% for $k \approx 0.8 - 5$ h/Mpc $\rightarrow$ **Gas pressure smooths the density field** relative to that expected from dark matter alone.

On scales with $k > 6$ h/Mpc the power in the reference simulation quickly rises far above that of the dark matter only simulation $\rightarrow$ **radiative cooling enables gas to cluster on smaller scales than the dark matter**.
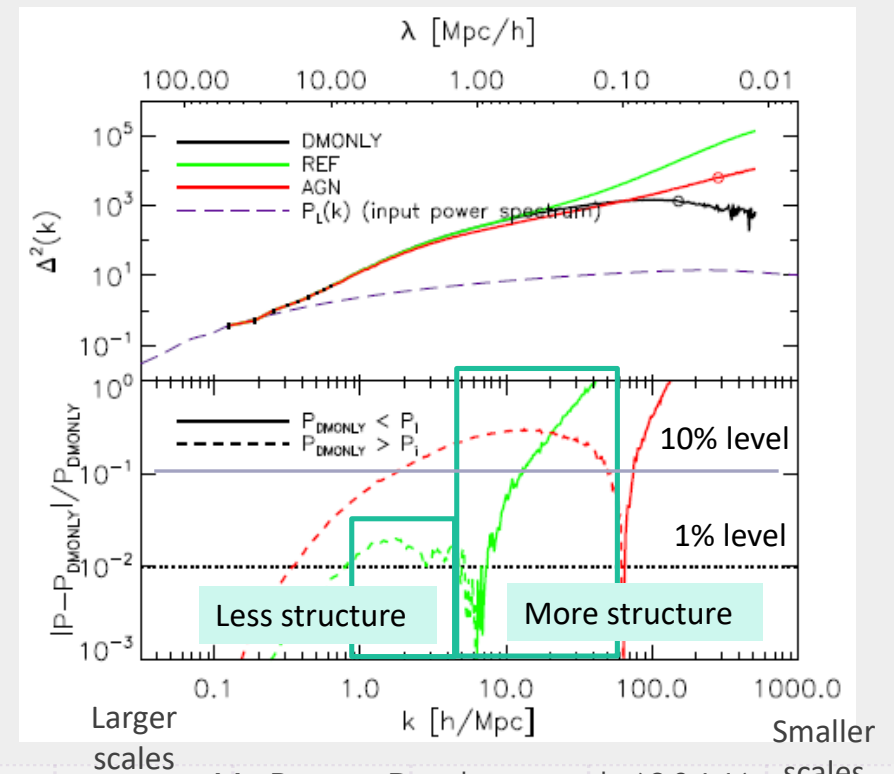
M. P. van Daalen et al. (2011)

12

Hydrodynamical Simulations of galaxy formation
Impact of baryons in the matter power spectrum

When AGN feedback is included, the results change drastically!
There is a reduction in power relative to DMONLY of 1% for k≈0.3 h/Mpc and it exceeds 10% for 2 < k < 50 h/Mpc.

→ **AGN feedback suppresses** the total matter power spectrum **on very large scales** and has tremendous effects!
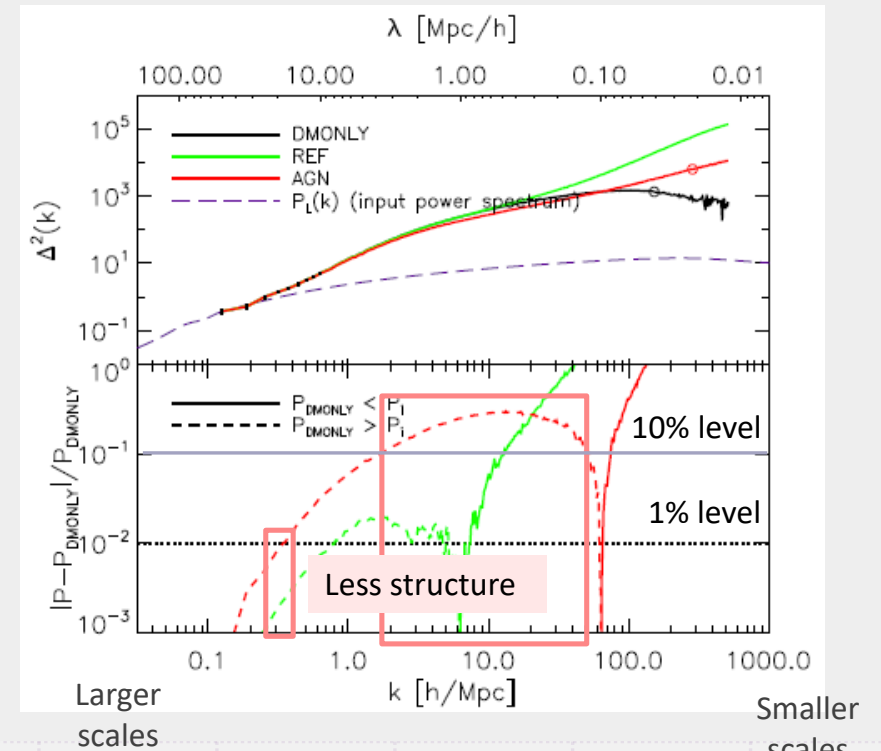
M. P. van Daalen et al. (2011)

Larger scales

Smaller scales

13

Hydrodynamical Simulations of galaxy formation
Impact of baryons in the matter power spectrum

SN feedback heats and ejects gas → should **decrease the small-scale power spectrum** → model without SN will have a higher power spectrum in smaller scales.

The power in NOSN is > 1% higher than in the reference simulation (that includes SN feedback) for k > 4 h/Mpc and the difference reach 10% at k ≈ 10 h/Mpc.
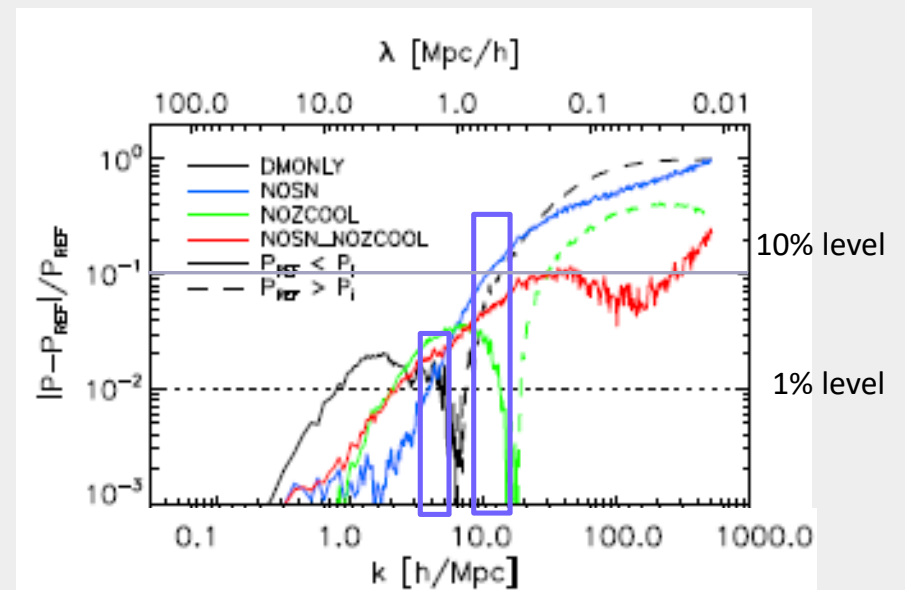
10% level

1% level

M. P. van Daalen et al. (2011)

Impact of baryons in the matter power spectrum

Turning off metal-line cooling should reduce the power on **small scales** because **less gas can cool down and accrete onto galaxies**.

Model NOZCOOL predicts 10 – 50% less power for k ≥ 30 h/Mpc.

However, the absence of metal-line cooling **increases the power** for λ ~ 1 h^{-1} Mpc because the **lower cooling rates force more gas to remain at large distances**.
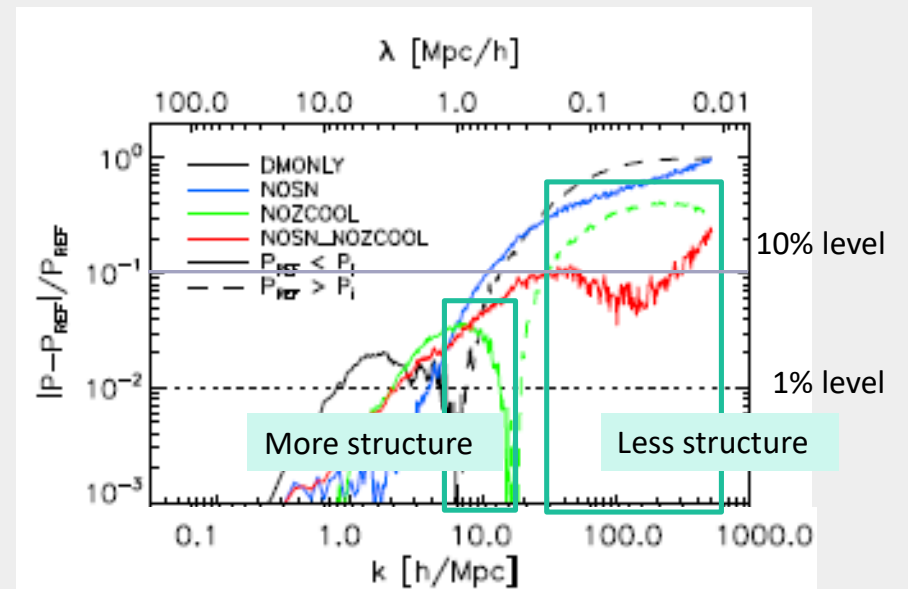
M. P. van Daalen et al. (2011)

Hydrodynamical Simulations of galaxy formation
Impact of baryons in the matter power spectrum

AGN feedback decreases the power by heating and ejecting gas.

With respect to the reference model, the power is decreased by more than 30% for k > 10 h/Mpc.

The reduction in power only falls below 1% for k < 0.4 h/Mpc.
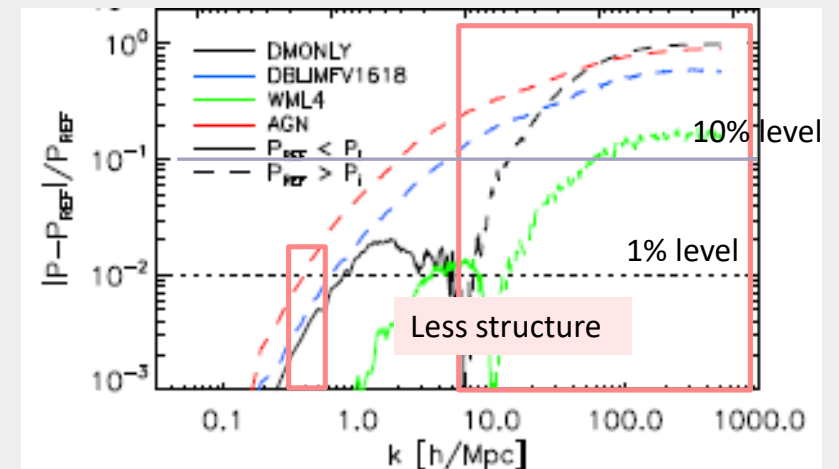
M. P. van Daalen et al. (2011)

Hydrodynamical Simulations of galaxy formation
Impact of baryons in the matter power spectrum

Even though **dark matter** is unable to cool through the emission of radiation, its distribution can still be altered by the inclusion of baryons due to **changes** in the **gravitational potential**.

Because the baryons can cool, they are able to collapse to very high densities, and in the process, they **steepen the potential wells** of virialized dark matter haloes, causing these to contract. The effect is larger closer to the centers of these haloes so smaller scales are more affected by this.
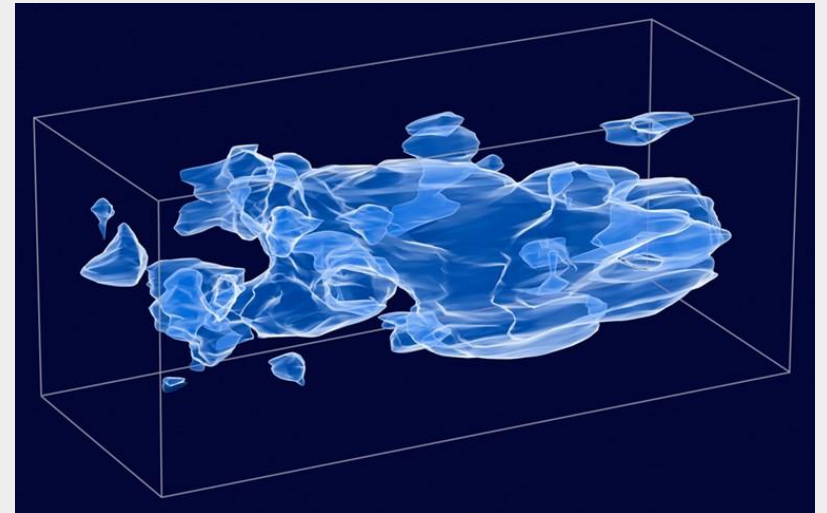
Three-dimensional distribution of dark matter in a patch of the universe. Credits: NASA / ESA / Caltech

Hydrodynamical Simulations
of galaxy formation – Conclusions

- Simulations have improved recently and will continue to improve, greatly because of our increasing knowledge of physical processes.

- Feedback effects modify the matter power spectrum by more than 1% and AGN feedback suppresses the total matter power spectrum on very large scales.
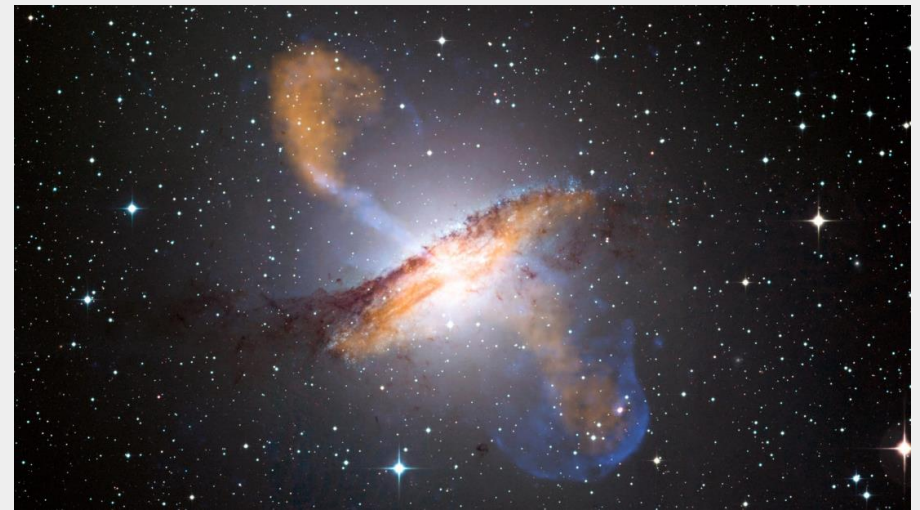
Credit: ESO/WFI (Optical); MPIfR/ESO/APEX/A.Weiss et al. (Submillimetre); NASA/CXC/CfA/R.Kraft et al. (X-ray)

Hydrodynamical Simulations
of galaxy formation

Thank you!

References:

1- M. Vogelsberger et al (2019) "Cosmological Simulations of Galaxy Formation"

2- M. van Daalen et al (2011) "The effects of galaxy formation on the matter power spectrum: A challenge for precision cosmology"

3- Michael Kuhlen et al. (2012) "Numerical simulations of the dark universe: State of the art and the next decade"

Cosmologia Física 2020/21

CDM Problems

André Cipriano 53761

Index

1. The cusp/core problem

2. The Missing Satellites problem

3. "Too Big To Fail"

4. The baryonic Tully-Fisher relation

5. Importance of baryons in each one of the problems

6. Overall and conclusions

1. Cusp/core problem

Earliest CDM simulations and calculations → dark matter halos should achieve extremely high densities at their centers.

CDM halos do not follow the scale-free $\rho \propto r^{-2}$ → NFW density profile

$$\rho(r) = \frac{\rho_s}{(r/r_s)\left(1 + r/r_s\right)^2}.$$

$\rho \propto r^{-1}$ fits CDM-only simulations quite well

Evidence: spiral galaxies with unusually diffuse disks (low baryon density) → should be dark matter dominated

Galaxies have rotation curves which rise linearly as a function of radius → halo core

- Shape of the density profile
- Mean density within some radius

Discrepancy between simulations and observations → **"cusp/core problem"**

1. Cusp/core problem
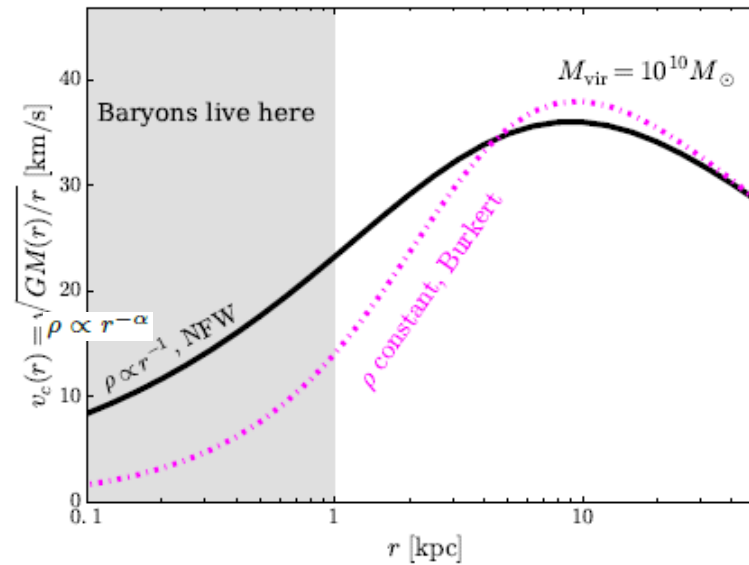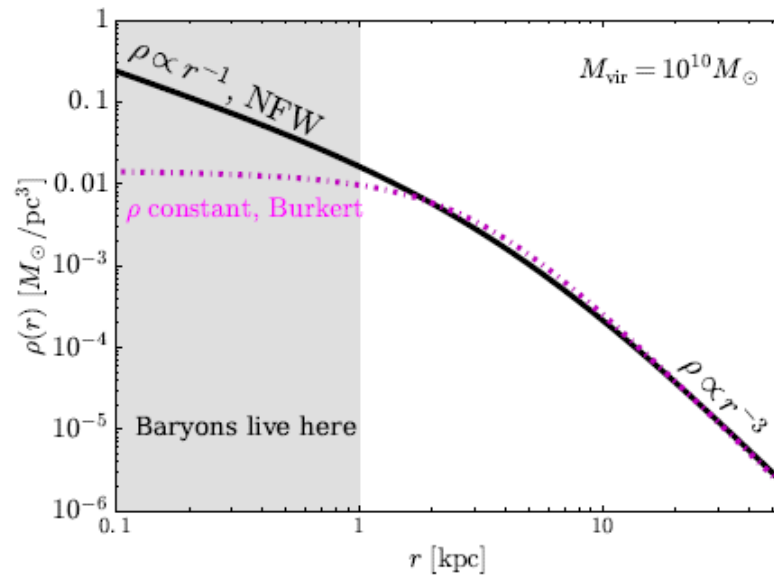
density profile $\rho \propto r^{-\alpha}$

$\alpha > 1$ – "cusped" profile

$\alpha = 1$ – NFW profile

$\alpha < 1$ – "cored" profile

- Comparison between NFW "cusped" profile and Burkert "cored" profile
- Burkert – good fit for both dwarf rotation curves and self-interacting dark matter halos

2. "Missing Satellites" problem

Arise from the non-smooth components

Hierarchical Universe →large objects grow by the accretion of smaller objects

Accretion incomplete → Due to satellite galaxies and unmixed stellar streams

MW like systems → Same substructure as galaxy clusters

Abundances → Cumulative number of subhalos of maximum velocity per unit host halo

Velocity function – Comparison between substructure and MW satellites → Significant mismatch

Vertical interpretation → Fewer large satellites than expected in CDM → **"Missing Satellites" problem**

How and why galaxies inhabit halos? At what scale halos remain totally dark? → Gravity

2. "Missing Satellites" problem
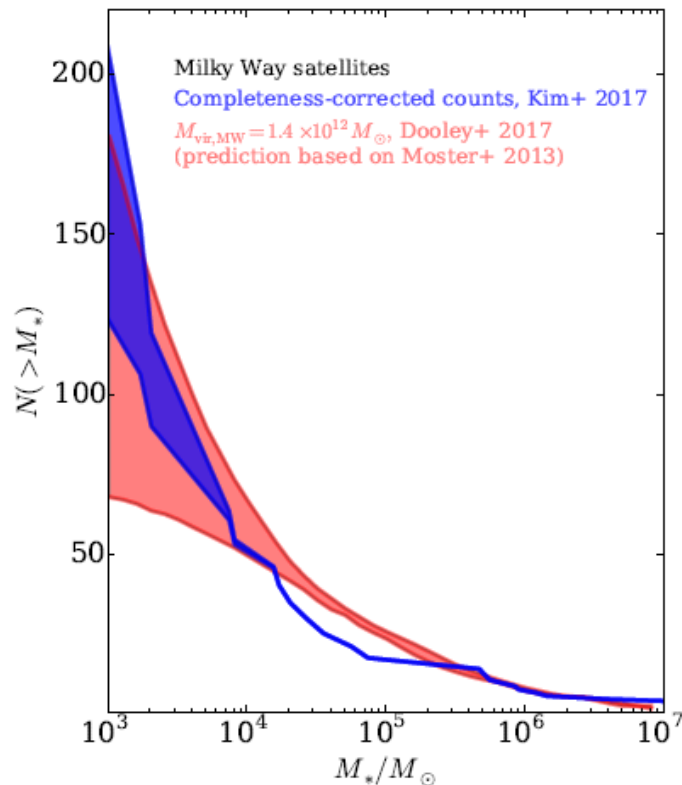
- Red region – counts using a SMHM relation applied to Monte Carlo realizations
- Early reionization suppression – bottom
- No reionization suppression – top
- Gap between satellite counts and analytic prescription → tidal disruption of cored satellite galaxies

3. "Too Big To Fail" problem

Alternative way to "missing satellites" problem → Comparison between observations and simulations of central densities of satellites → More precise measurements

Mismatch similar to "Missing Satellites" problem → Maximum velocity → More dense subhalos CDM prediction than dense satellites observation

Most massive subhalos in simulations → **"too big to fail"** to producing stars → Expected visible satellites **not** present in observations

TBTF → Central densities of classical dwarf satellites of MW as measured and in simulations

Degeneracy between velocity anisotropy of stellar orbits, mass profile of dark matter and stellar density profile → Can be break at half-light radius

3. "Too Big To Fail" problem
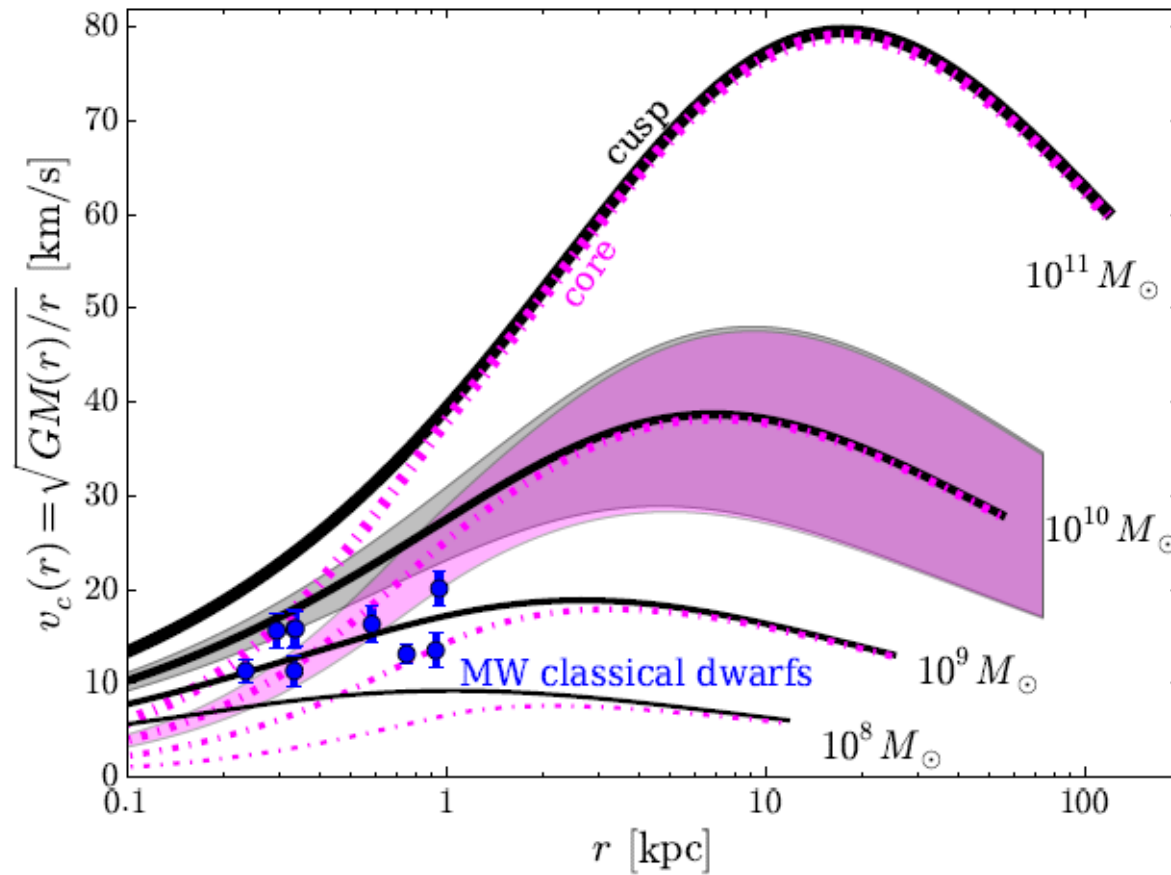
TBTF → grey shaded region does not overlap with the observed circular velocity values of the classical dwarfs.

4. The Baryonic Tully-Fisher (BTF) relation

Tully-Fisher relation → Power-law correlation between the intrinsic luminosity of spiral galaxies and spectroscopic rotation velocity

Tully-Fisher relation → Higher scatter for small galaxies → Gas-dominated

Cool Gas + Stars → Power-law correlation between the rotation velocity of galaxies and baryonic mass reappears → **Baryonic Tully-Fisher relation**

Tension with other measurements of the relation between the halo mass and baryonic mass of galaxies

Furthest measured point of the rotation curve is a good tracer of the halo potential → dwarf galaxies live in smaller halos than expected from SMHM

4. The Baryonic Tuller-Fisher (BTF) relation

5. Importance of Baryons

Baryons are relatively minor contributors in the energy budget of the Universe but they are dynamically important in the parts of the Universe where dark-matter-induced deviations from CDM might appear.

A true mapping between dark matter models and halo mass requires an accurate treatment of baryons.

5.1. Baryons – Cusp/Core Problem

Hydrodynamic simulations → Baryons aggravated the cusp/core problem

Baryons cooled efficiently in halos and dragged dark matter in as they deepened the gravitational potential wells → Halos appeared denser in hydrodynamic simulations

Insufficient spatial resolution → Energy and gas difficulties to leave the ISM → Very efficient Star Formation

Simulations at realistic scales → Energy and gas escaped from the ISM → Clumpy Star Formation → Dark Matter Halos → Less dense than CDM-only simulations

→ Including baryons in simulations → Lead to cusp/core problem resolution

5.2. Baryons – "Missing Satellites" problem

Baryonic solutions to the "missing satellites" problem:

1. subhalo mass functions and survival

2. the mapping between the line-of-sight velocities of individual stars in galaxies and the maximum velocity of dark-matter halos

3. the probability that some subhalos have no visible baryons in them at all

→ Evidence that "Missing satellites" problem is solved in CDM context

Baryons can significantly reduce the abundance of dark matter halos at fixed maximum velocity in several ways

Baryonic outflows – Prevent halos to grow as fast

Halos fall into larger halos → Small halos easily destroyed in hydrodynamic simulations

5.3. Baryons – Too Big To Fail

Hydrodynamic CDM simulations → Baryons play an important role in shaping the central densties of MW satellites to solve TBTF

If baryons can push dark matter out of the cores of halos, then the central densities of halos can be low even if the total halo mass is high.

Low densities of some satellites remain difficult to reconcile with simulations of CDM + baryons

Baryons can address TBTF on halo mass scales $M_{\mathrm{halo}} \sim 10^{10}\, M_{\odot}$

5.4. Baryonic Tuller Fisher relation

Relationship between stellar and dark matter mass found in **hydrodynamic + CDM simulations** shows good agreement with extrapolations from empirical measurements for larger masses and inferences based on Local Group satellite populations.

The problem with Baryonic Tully-Fisher lies in the assignment of galaxies to halos based on rotation curves, both on the simulation and observational sides.

6. Overall
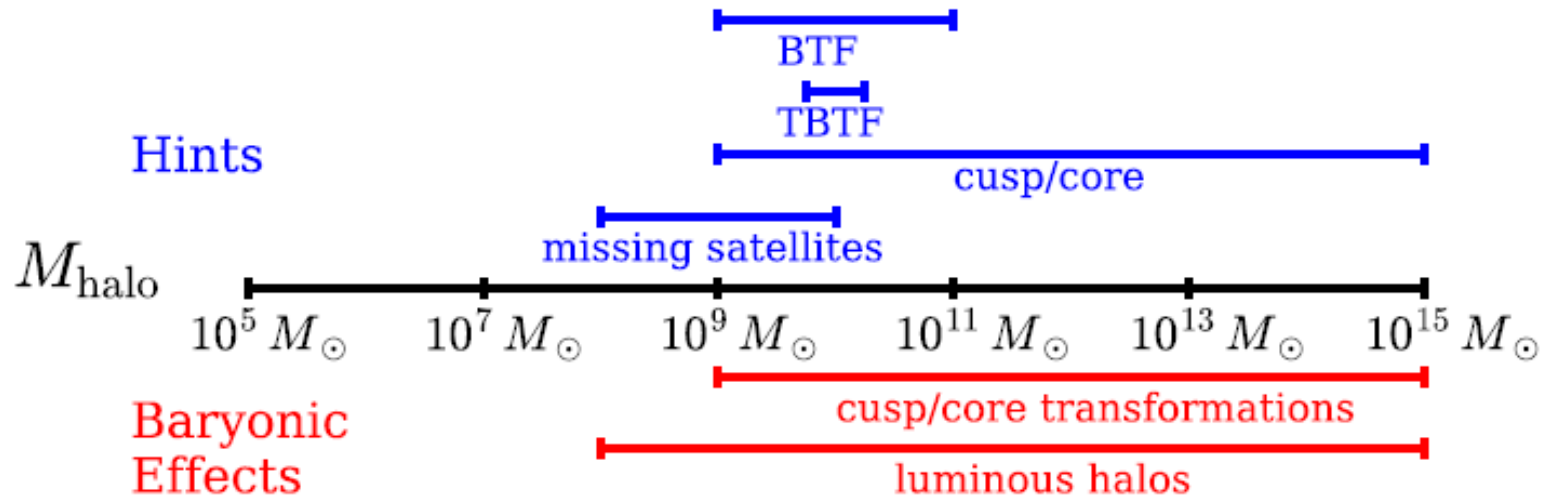
6. Conclusions

- We described 4 problems where we can see that CDM is an inadequate description of dark matter on scales from $10^9\,M_\odot$ to the $10^{15}\,M_\odot$.

- Baryons also affect halos on these scales. Baryons are important for $10^8\,M_\odot$ to the $10^{15}\,M_\odot$ and above. It is not clear if baryons can solve all small-scale problems with CDM, but the physics goes in a good direction.

- Regardless of what the true nature of dark matter is, its cosmic distribution is governed by the gravitational effects of baryons in addition to dark physics, and so the baryons must be well understood before non-gravitational interactions in the dark sector can be identified or ruled out with any confidence.

References

M. Buckley and A. Peter (2018) – Section 4:

https://arxiv.org/pdf/1712.06615.pdf

Outline

1. What is Line-Intensity Mapping?

2. Types of Line-Intensity Mapping

   - [CII] Fine Structure Line

   - Rotational CO Line

   - Lymann-α Line

   - 21-cm Line

3. Probing the Epoch of Reionization (EoR)

4. Conclusions

What is Line-Intensity Mapping?

~4 500 hours   ~1 500 hours

VLA   COMAP

0.5 Deg
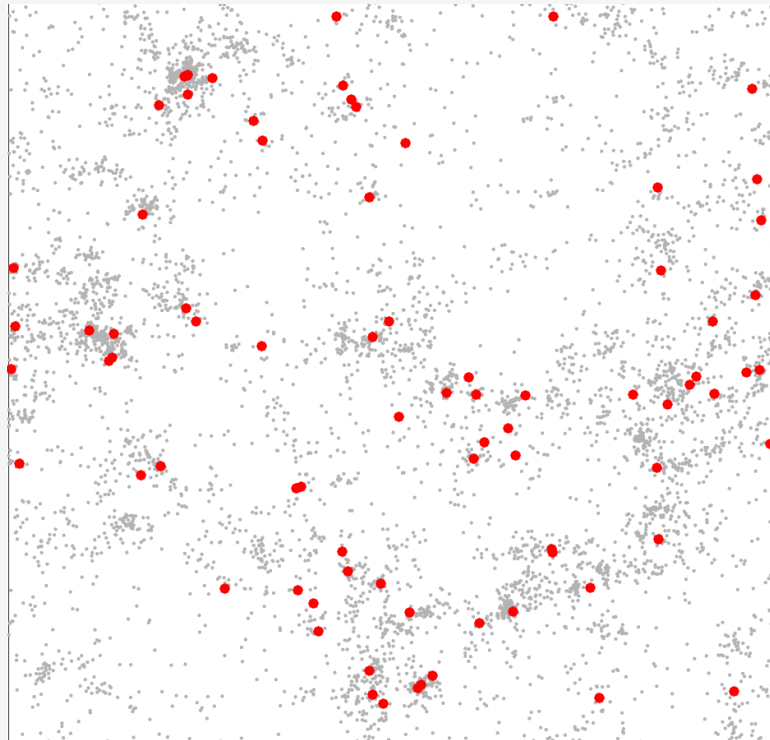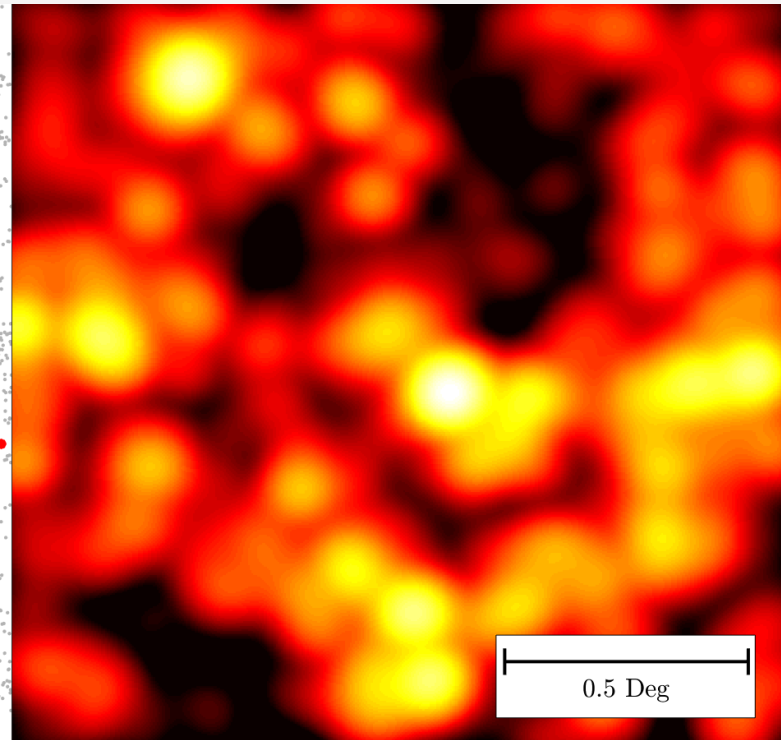
Credits: E. Kovetz et al (2017)

Galaxy Surveys	Intensity Mapping
Discrete objects whose emission lies above some flux limit	Sensitive to all sources of emission in the line
High angular resolution is required €€€€	High angular resolution not required €
Take a lot of time covering a specific area of the sky	Take less time covering a specific area of the sky

- Measures the spatial fluctuations in the spectral line emission in galaxies and/or the intergalactic medium (IGM).

- It does so in multiple redshift slices (different frequencies) resulting in a data cube.
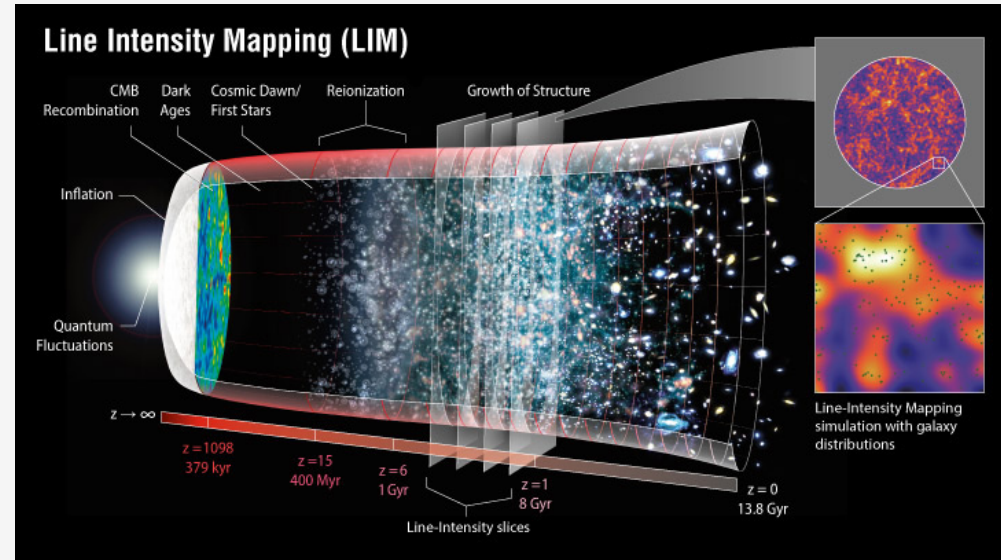
Credits: NASA / LAMBDA Archive Team
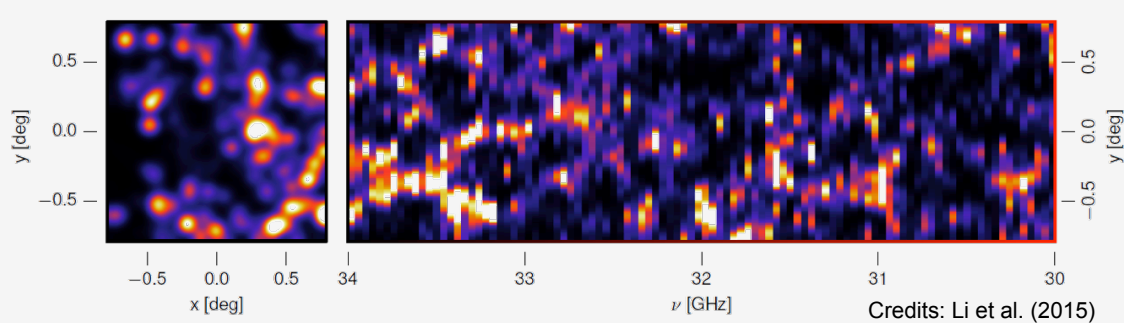
Credits: Li et al. (2015)

UNDERLYING POWER MATTER SPECTRUM

$$P_k(z) = \langle I(z) \rangle^2 b^2(z) P_m(k, z) + P_{\text{shot}}(z)$$

AVERAGE INTENSITY

REDSHIFT-DEPENDENT BIAS

SHOT NOISE POWER SPECTRUM

$$\langle I(z) \rangle \propto \int_0^\infty L \Phi(L, z) dL \qquad P_{\text{shot}}(z) \propto \int_0^\infty L^2 \Phi(L, z) dL$$

Types of Line-Intensity Mapping

- ## [CII] fine-structure line

  - λ = 157.7 µm (restframe)

  - Brightest among all metal lines emitted by the ISM of star formation galaxies

  - Traces gas in the Interstellar Medium (ISM), probes the Star Formation Rate (SFR)

- ## Rotational CO line

  - Rotational transitions, J $\rightarrow$ J-1

  - Ground-state CO(1-0) transition at 115.27GHz (λ = 2.6mm, restframe)

  - Traces H_2 gas (where stars form efficiently)

- ## Lymann-α line

  - ○ λ = 121.57 nm (restframe)

  - ○ Emitted when an electron jumps from n=2 to n=1

  - ○ Traces star formation

- ## 21-cm line [Chang et al. (2010)]

  - ○ Emitted when electron jumps between the 2 hyperfine levels of the hydrogen 1s ground state ("spin-flip")

  - ○ Traces HI in the IGM during reionization and in galaxies post-reionization
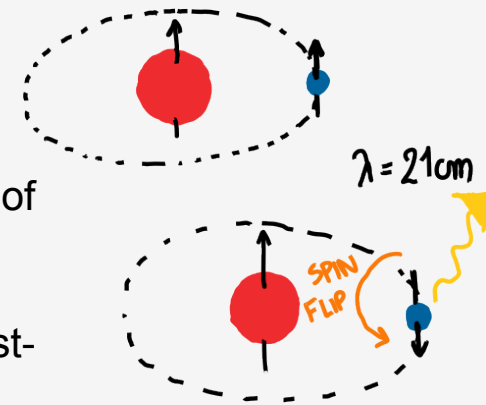
Types of Line-Intensity Mapping
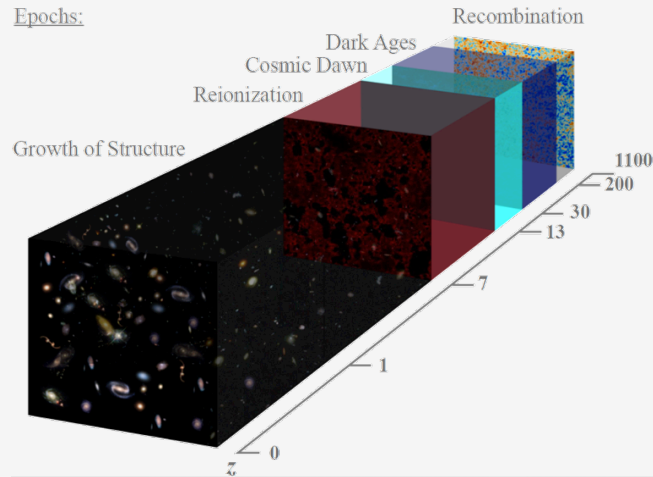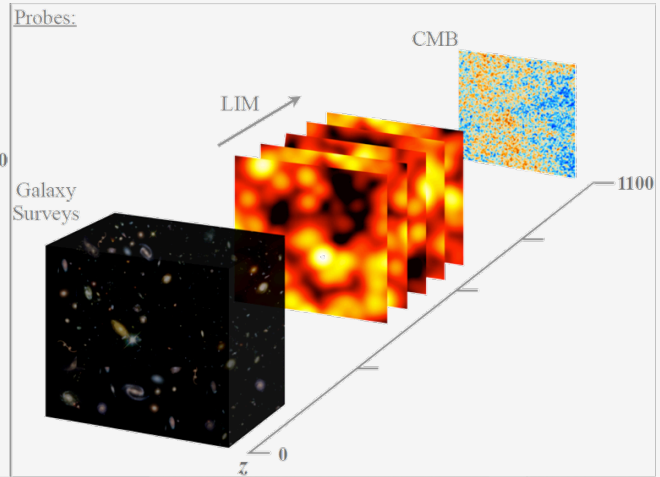
Credits: E. Kovetz et al (2019)
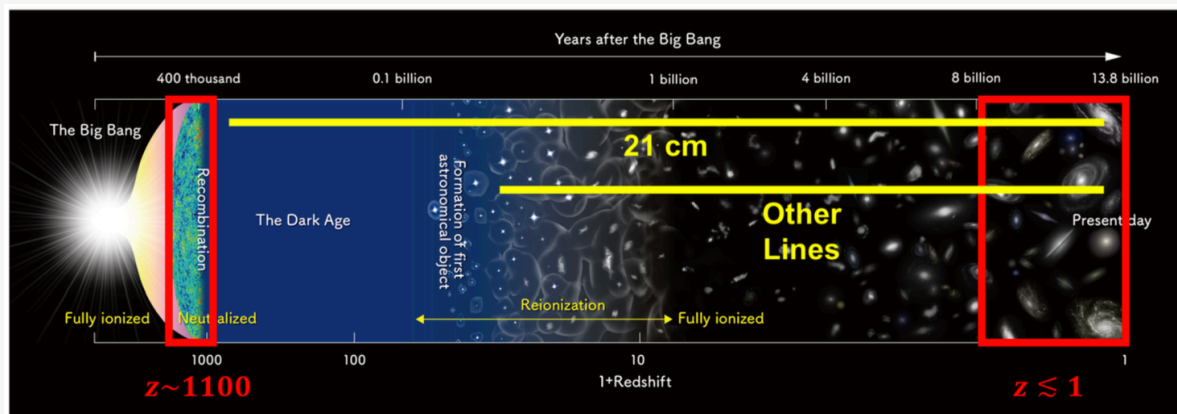
Credits: E. Kovetz et al (2017)

Probing the Epoch of Reionization (EoR)

What is the Epoch of Reionization?
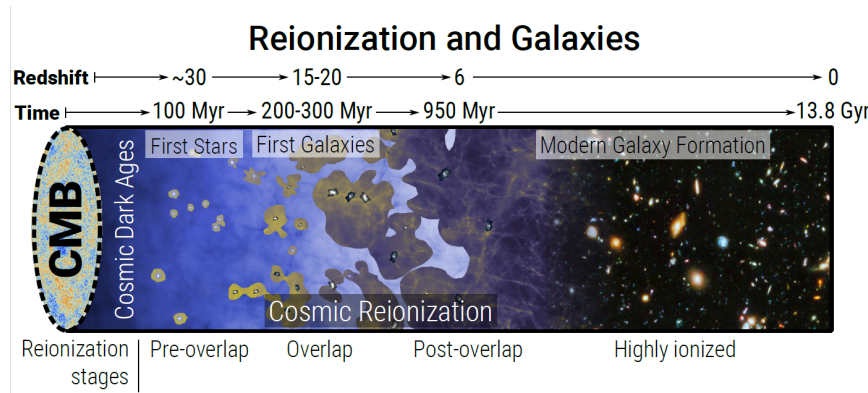
Credits: J. Wise et al (2019)
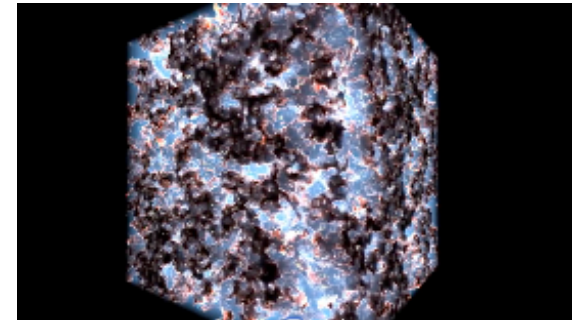
Credits: R. Kaehler, M. Alvarez & T. Abel

- Dark Ages: Universe consists mostly of HI formed after recombination

- Cosmic Dawn: First stars (population III) and galaxies form

- Epoch of Reionization: UV photons from stars reionize the intergalactic medium ("bubbles")

There are some questions…

- When does reionization begin and end?

    - Occurred between z = 6 – 15

- What sources were responsible for the reionization?

- How abundant are galaxies as a function of luminosity and redshift?

- How many ionizing photons escaped from these galaxies into the IGM?

INTENSITY MAPPING
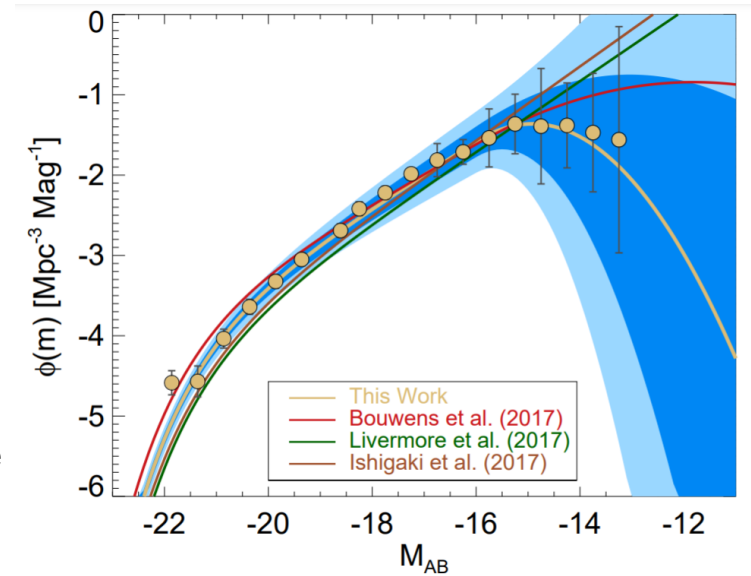
Credits: Atek et al. (2018)

- How do we know that an initial 21-cm detection is real and not residual foregrounds?

- Cross-correlation: Reionization involves the interplay between the ionizing sources and intergalactic hydrogen.
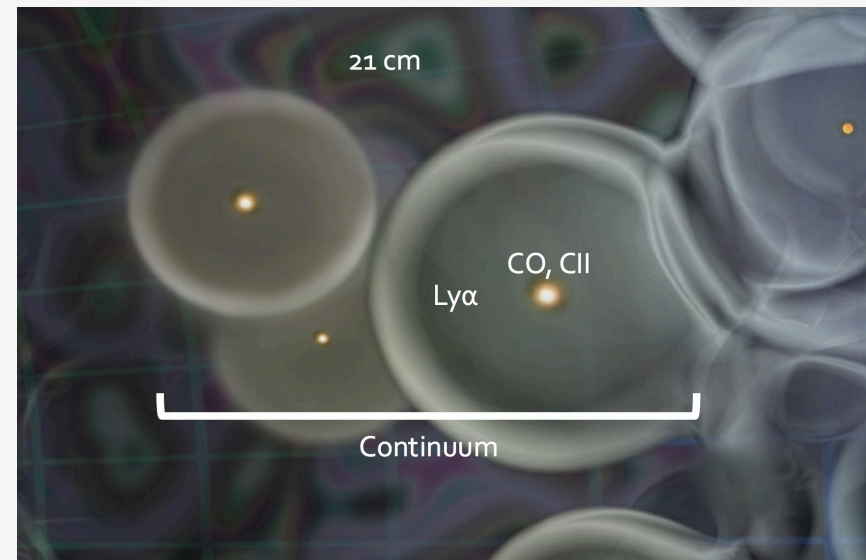
Credits: E. Kovetz et al (2017)
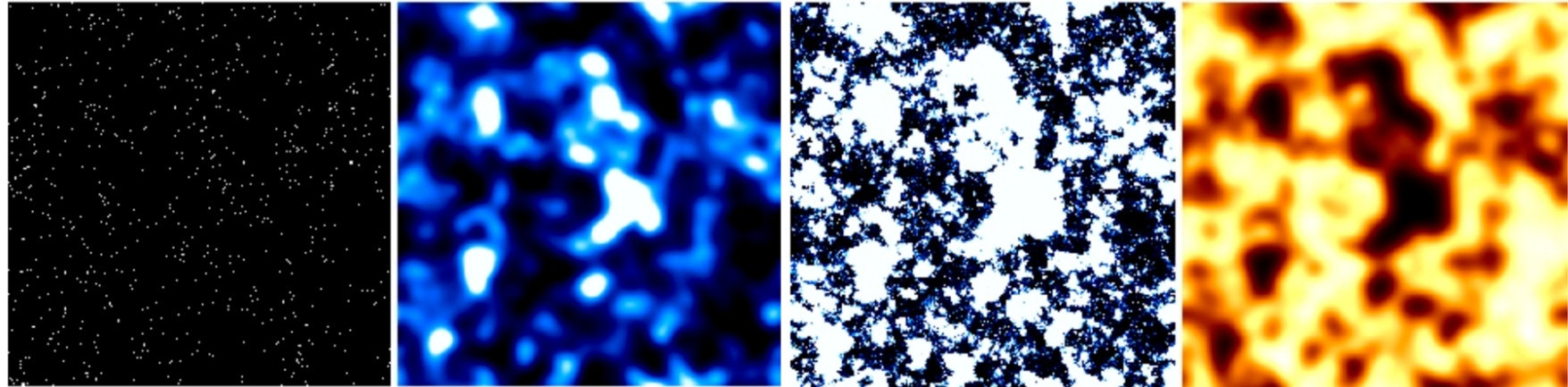
Credits: E. Kovetz et al (2017)

- <u>Solution:</u> Line-intensity mapping observations using various emission lines

- 21-cm and galaxy emission should be anti-correlated on large scales
- Cross-correlation sensitive to bubble sizes

Intensity Mapping Experiments
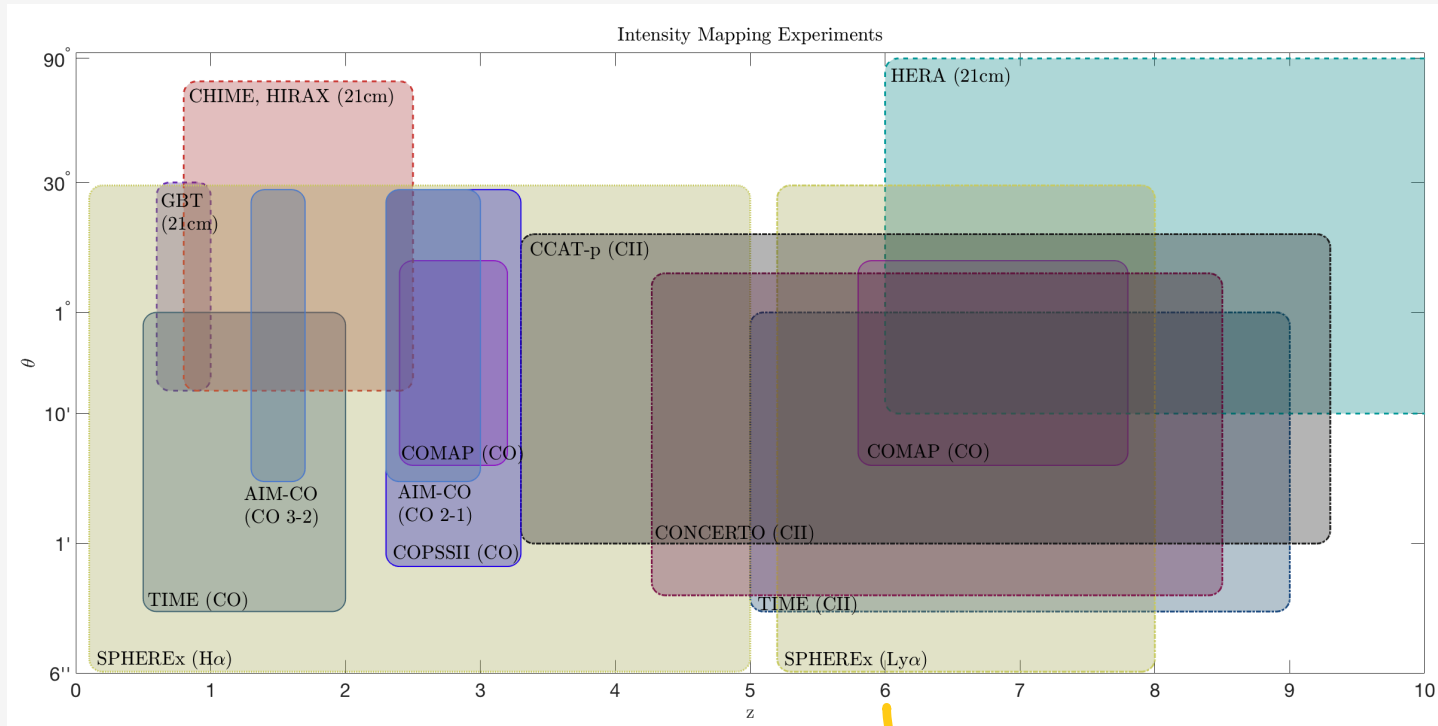
Credits: E. Kovetz et al (2017)

https://lambda.gsfc.nasa.gov/product/expt/lim_experiments.cfm

Conclusion

- Advantages over traditional galaxy surveys: can cover extremely large cosmological volumes in a relatively short time

- Astrophysical and Cosmological probe

  - Will provide a more detailed reconstruction of ionization history, star formation rates and growth of structure.

- Use of multiple line tracers enhances the picture of physical conditions and allows for consistency checks (21-cm, [CII], CO, Ly-α,…)

Thank you for your attention!

Intensity Mapping

Lara Piscarreta, nº 51121

Physical Cosmology

June 2021

References

- Kovetz, E., Breysse, P. C., Lidz, A., et al. 2019, BAAS, 51, 101. https://arxiv.org/abs/1903.04496

- Kovetz, E. D., Viero, M. P., Lidz, A., et al. 2017, arXiv e-prints, arXiv:1709.09066. https://arxiv.org/abs/1709.09066

- Wise J. H., 2019, arXiv e-prints, p. arXiv:1907.06653. https://arxiv.org/abs/1907.06653

III. Beyond ΛCDM
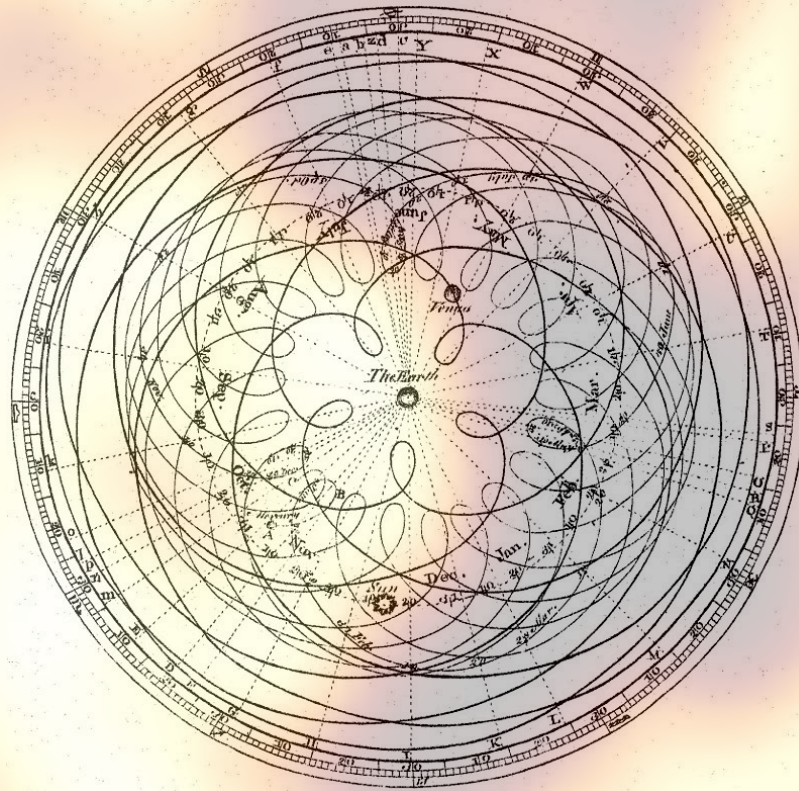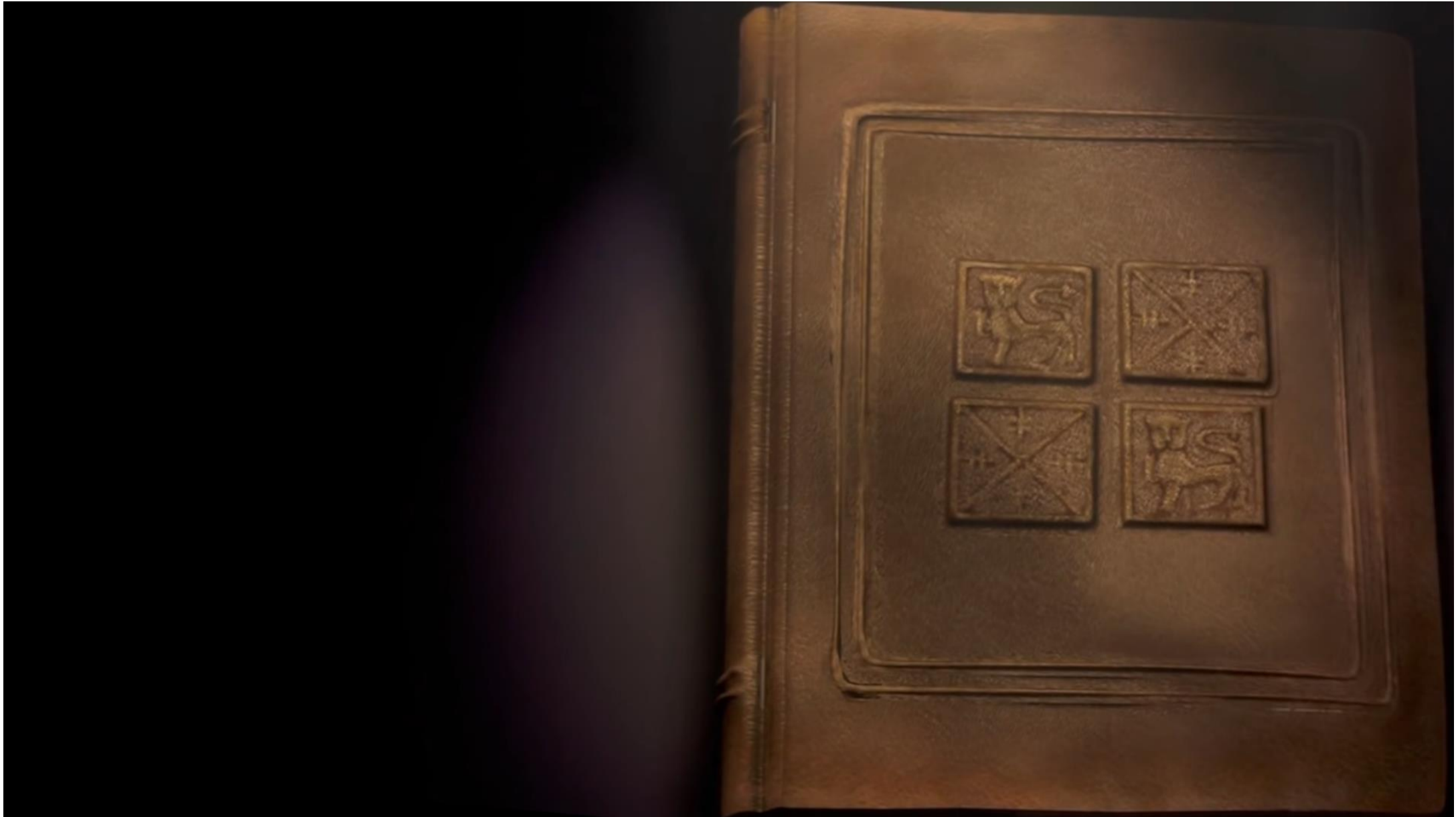
The Quintessence

By José Ferreira
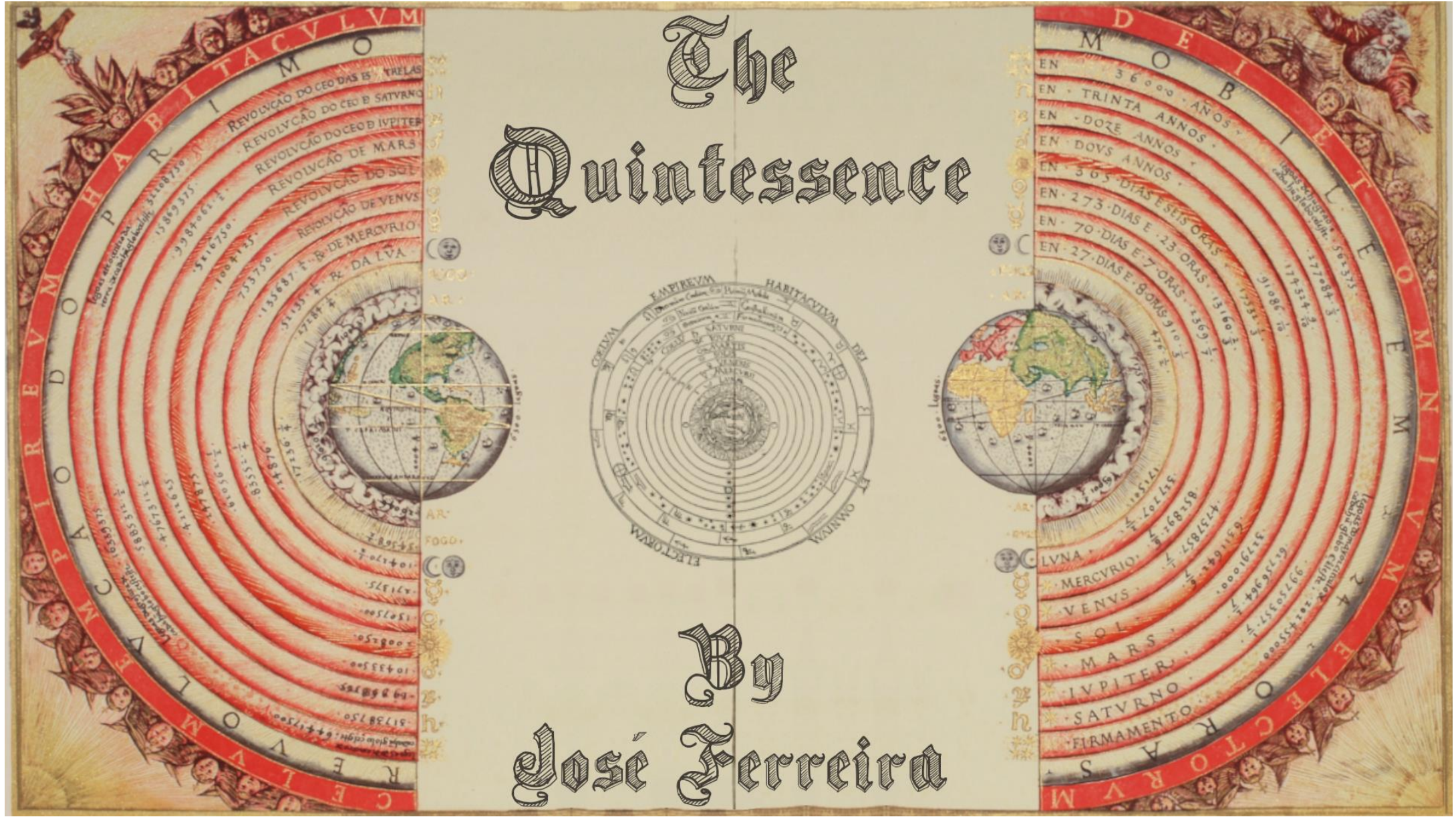
The Index

1. Historical Remarks

Le j. liure.
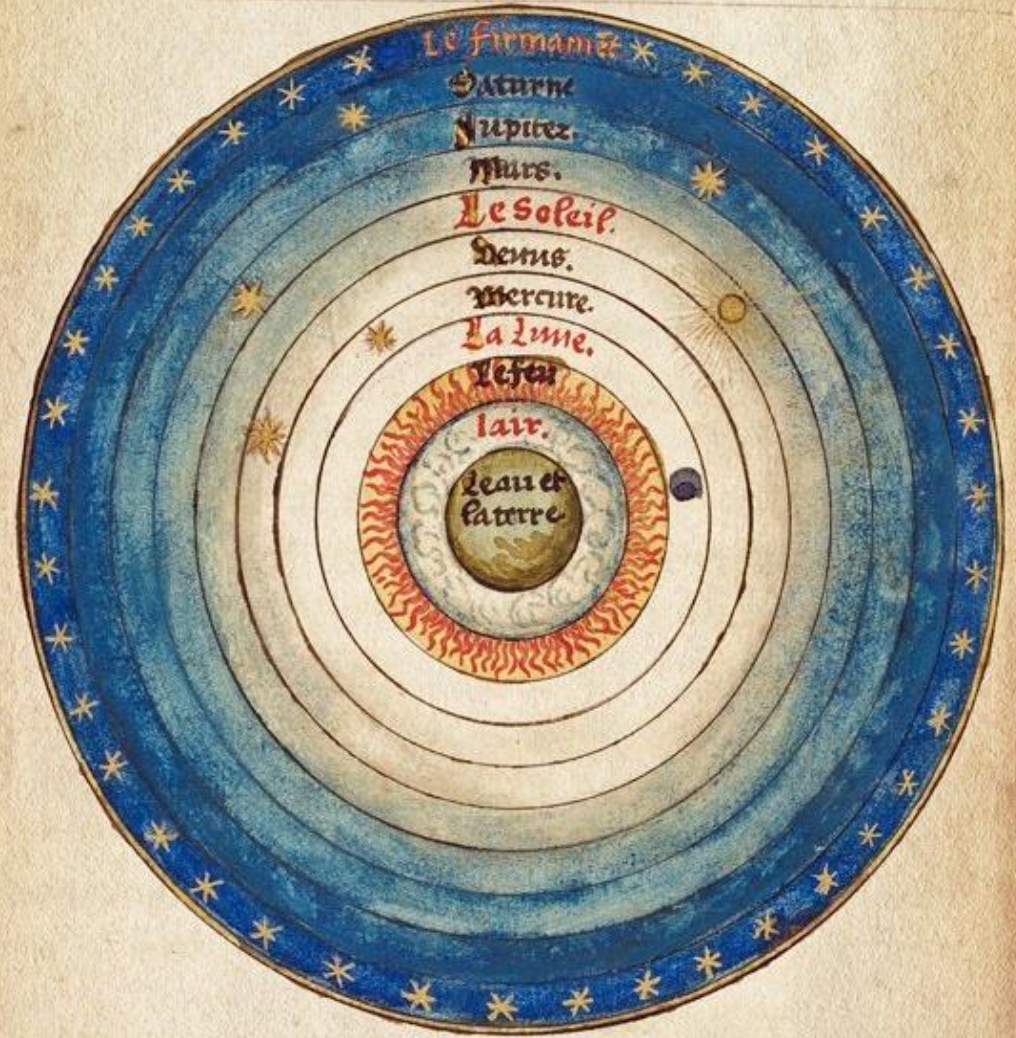
In the Begging there was…

△

Fire

▽

Water

A̶

Air

∀

Earth

5

And then it became…

6
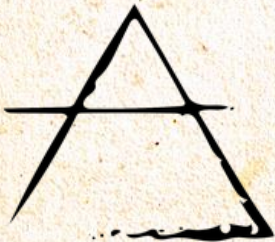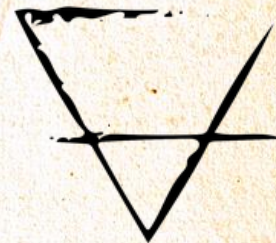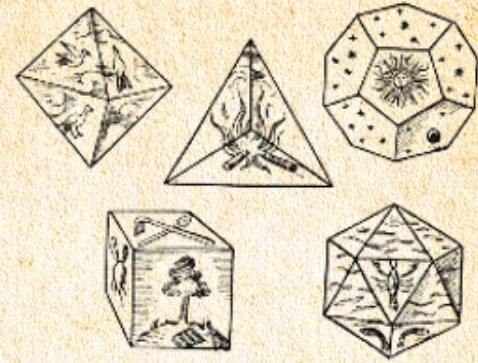
Introduction to Field Theory
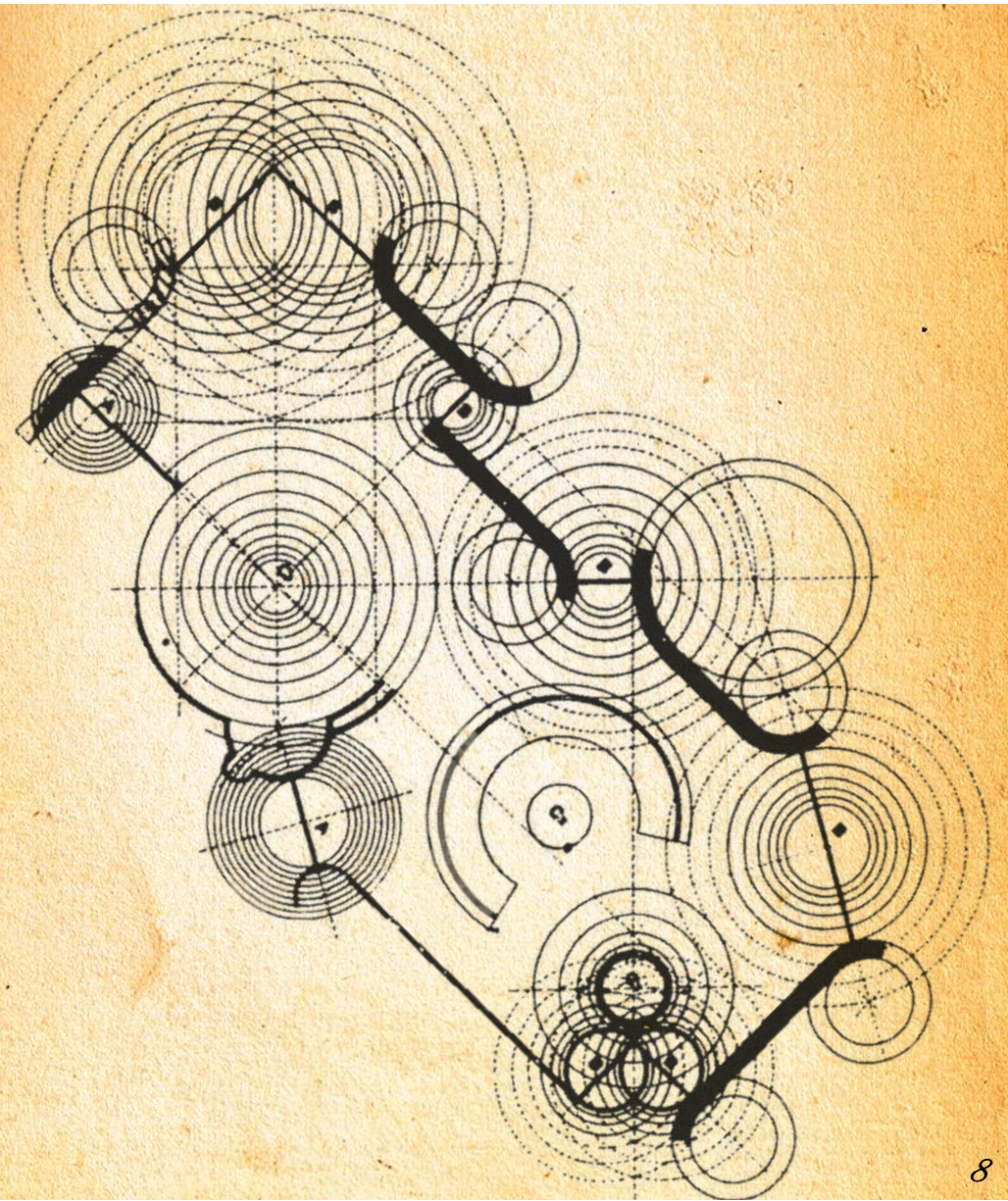
Classical Action

The action is defined as:

$$S = \int_{-\infty}^{\infty} L\,dt$$

A small change δ in S is:

$$\delta S = \int_{-\infty}^{\infty} \left(\frac{\partial L}{\partial q} \delta q + \frac{\partial L}{\partial \dot{q}} \delta \dot{q} \right) dt$$

The action principle states:

$$\delta S = 0$$

Using the action principle:

$$\frac{\partial L}{\partial q} - \frac{\partial}{\partial t} \left(\frac{\partial L}{\partial \dot{q}} \right) = 0$$

Field Theory Action

To respect the relativity principle:

$$L = \int \mathcal{L} \, d^3 x$$

Where $\mathcal{L}$ is the Lagrangian density.

The action then becomes:

$$S = \int \mathcal{L} \, d^4 x$$

A small change δ in S is:

$$\delta S = \int \left(\frac{\partial \mathcal{L}}{\partial q} \delta q + \frac{\partial \mathcal{L}}{\partial (\partial_\mu q)} \delta(\partial_\mu q) \right) d^4 x$$

Using the action principle:

$$\frac{\partial \mathcal{L}}{\partial q} - \frac{\partial}{\partial x^\mu} \left(\frac{\partial \mathcal{L}}{\partial (\partial_\mu q)} \right) = 0$$

Scalar Field

A generic scalar field ϕ Lagrangian is:

$$\mathcal{L}_\phi = -\frac{1}{2}\partial_\mu \phi \partial^\mu \phi - V(\phi)$$

Using the Euler-Lagrange equation:

$$\frac{\partial \mathcal{L}}{\partial \phi} - \frac{\partial}{\partial x^\mu}\left(\frac{\partial \mathcal{L}}{\partial(\partial_\mu \phi)}\right) = 0$$

We obtain the following:

$$-\Box \phi + V'(\phi) = 0$$

Where the d'Alembertian is given by:

$$\Box = \frac{\partial^2}{\partial t^2} - \nabla^2$$

For a homogeneous field:

$$\ddot{\phi} + V'(\phi) = 0$$

Action for G.R.

Considering the action:

$$S = \int \sqrt{-g} \left[\frac{1}{2k^2} R + \mathcal{L} \right] d^4 x$$

Geometry (LHS)

Energy (RHS)

Where: $k^2 = 8\pi G$

Applying the action principle:

$$R_{\mu\nu} - \frac{1}{2} g_{\mu\nu} R = k^2 T_{\mu\nu}$$

Where:

$$T_{\mu\nu} = -\frac{2}{\sqrt{-g}} \frac{\delta \sqrt{-g} \mathcal{L}}{\delta g^{\mu\nu}}$$

Scalar field in G.R.

Considering the action:

$$S = \int \sqrt{-g}\,\mathcal{L}_\phi$$

Where ϕ is again a scalar field and:

$$\mathcal{L}_\phi = -\frac{1}{2}\partial_\mu \phi \partial^\mu \phi + V(\phi)$$

$$k^2 = 8\pi G$$

Using FLRW and the E-L equation:

$$\ddot{\phi} - a^{-2}\nabla^2 \phi + 3H\dot{\phi} + V'(\phi) = 0$$

Assuming that ϕ is homogeneous:

$$\ddot{\phi} + 3H\dot{\phi} + V'(\phi) = 0$$

Using the expression for $T_{\mu\nu}$:

$$T_{\mu\nu} = \partial_\mu \partial_\nu \phi - g_{\mu\nu}\left[\frac{1}{2}g^{\alpha\beta}\partial_\alpha \phi \partial_\beta \phi + V(\phi)\right]$$

The Quintessence
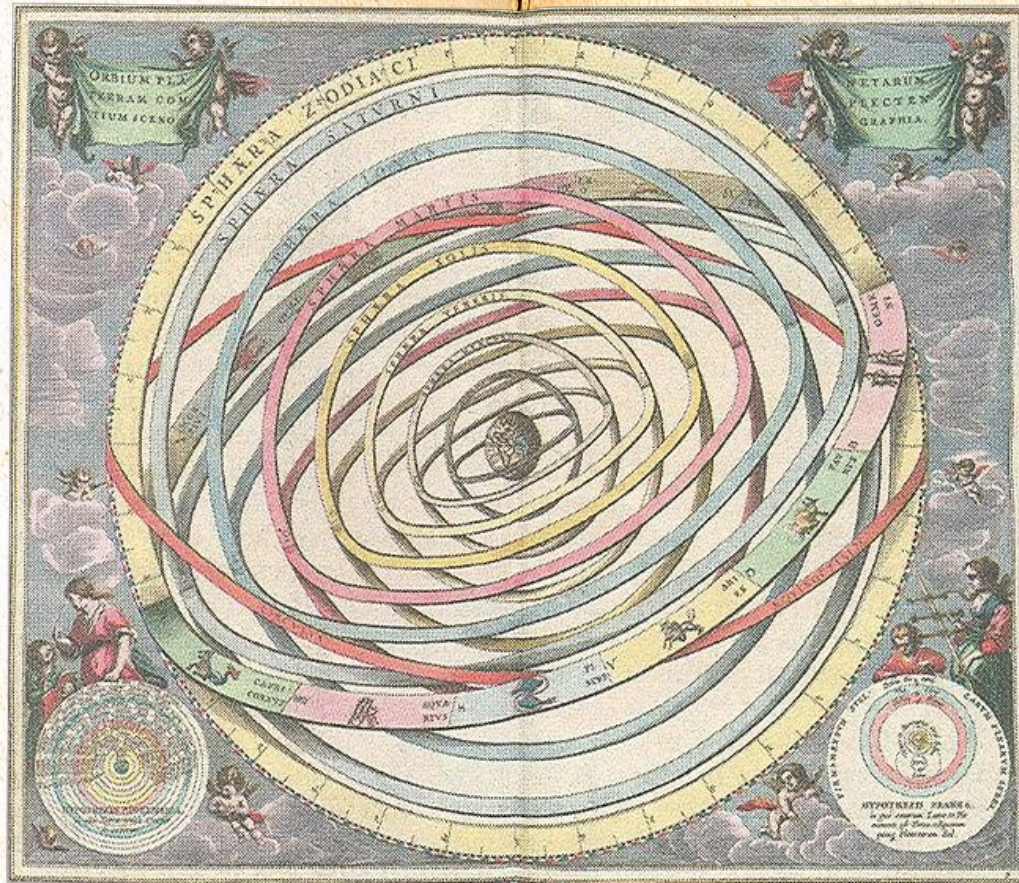
Equations of Motion

The Action is given by:

$$S = \int \sqrt{-g} \left[\frac{1}{2k^2} R + \mathcal{L}_\phi \right] d^4 x + S_m$$

Where:

$$\mathcal{L}_\phi = -\frac{1}{2} g^{\mu\nu} \partial_\mu \phi \partial_\nu \phi + V(\phi)$$

$$k^2 = 8\pi G$$

As we saw before, for the scalar field:

$$T_{\mu\nu}^{(\phi)} = \partial_\mu \partial_\nu \phi - g_{\mu\nu} \left[\frac{1}{2} g^{\alpha\beta} \partial_\alpha \phi \partial_\beta \phi + V(\phi) \right]$$

In a FLRW background:

$$P_\phi = \frac{1}{3} T_i^{i(\phi)} = \frac{1}{2} \dot{\phi}^2 - V(\phi)$$

$$\rho_\phi = -T_0^{0(\phi)} = \frac{1}{2} \dot{\phi}^2 + V(\phi)$$

The equation of state is:

$$\omega_\phi \equiv \frac{P_\phi}{\rho_\phi} = \frac{\dot{\phi}^2 - 2V(\phi)}{\dot{\phi}^2 + 2V(\phi)}$$

Assuming a flat universe:

$$H^2 = \frac{k^2}{3}\left[\frac{1}{2}\dot{\phi}^2 + V(\phi) + \rho_M\right]$$

$$\dot{H} = -\frac{k^2}{2}(\dot{\phi}^2 + \rho_M + P_M)$$

The equation of motion is:

$$\ddot{\phi} + 3H\dot{\phi} + V'(\phi) = 0$$

In radiation/matter dominated epochs:

$$\rho_M >> \rho_\phi \implies \frac{\dot{\phi}^2}{2} >> V(\phi)$$

In late time:

$$\omega_\phi < -\frac{1}{3} \implies \dot{\phi}^2 < V(\phi)$$

Analysis of motion

It is convenient to define:

$$x_1 \equiv \frac{k\dot{\phi}}{\sqrt{6}H}$$

$$x_2 \equiv \frac{k\sqrt{V}}{\sqrt{3}H}$$

The densities can be written as:

$$\Omega_M \equiv \frac{k^2 \rho_M}{3H^2} = 1 - x_1^2 - x_2^2$$

$$\Omega_\phi \equiv \frac{k^2 \rho_\phi}{3H^2} = x_1^2 + x_2^2$$

We can also rewrite the EoS:

$$\omega_\phi = \frac{x_1^2 - x_2^2}{x_1^2 + x_2^2}$$

The number of e-foldings is:

$$N = \ln a$$

$$\frac{dx_1}{dN} = -3x_1 + \frac{\sqrt{6}}{2}\lambda x_2^2 + \frac{3}{2}x_1[(1 - \omega_M)x_1^2 + (1 + \omega_M)(1 - x_2^2)]$$

$$\frac{dx_2}{dN} = -\frac{\sqrt{6}}{2}\lambda x_1 x_2 + \frac{3}{2}x_2[(1 - \omega_M)x_1^2 + (1 + \omega_M)(1 - x_2^2)]$$

Where:

$$\lambda \equiv -\frac{V_{,\phi}}{kV}$$

$$\omega_M = \frac{P_M}{\rho_M}$$

x_1	x_2	Ω_ϕ	ω_ϕ	Stability
0	0	0	undefined	Saddle
1	0	1	1	Unstable ($\lambda < \sqrt{6}$) or Saddle
-1	0	1	1	Unstable ($\lambda > -\sqrt{6}$) or Saddle
$\frac{\lambda}{\sqrt{6}}$	$\sqrt{1 - \frac{\lambda^2}{6}}$	1	$-1 + \frac{\lambda^2}{3}$	Stable ($\lambda^2 < 3(1 + \omega_M)$) or Saddle
$\sqrt{\frac{3}{2}}\frac{1+\omega_M}{\lambda}$	$\sqrt{\frac{3(1-\omega_M^2)}{2\lambda^2}}$	$\frac{3(1+\omega_M)}{\lambda^2}$	ω_M	Saddle, Stable or Stable spiral

Matter dominated
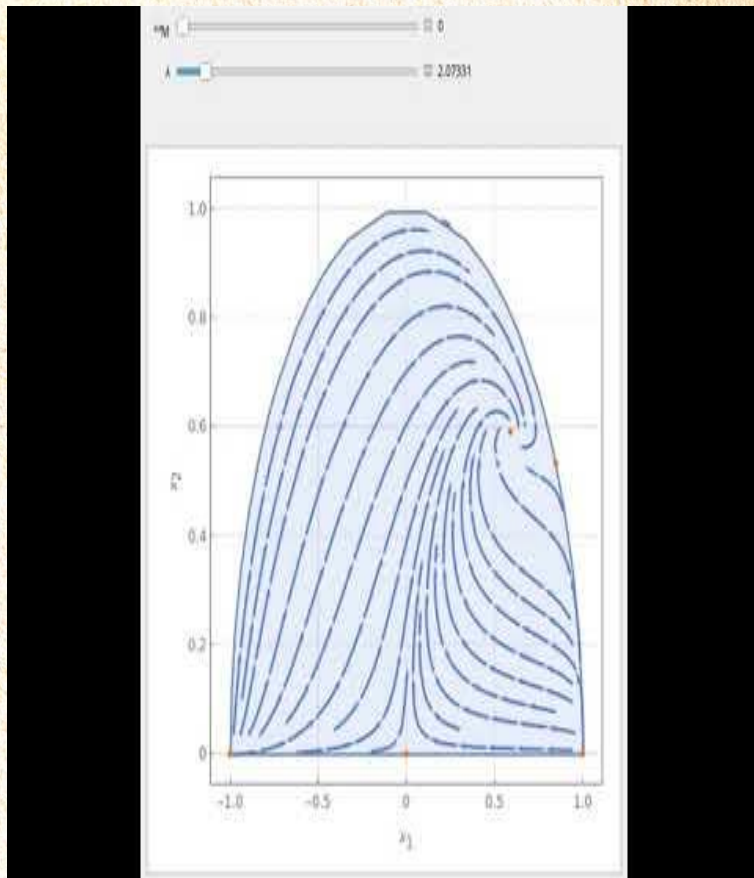
Radiation dominated
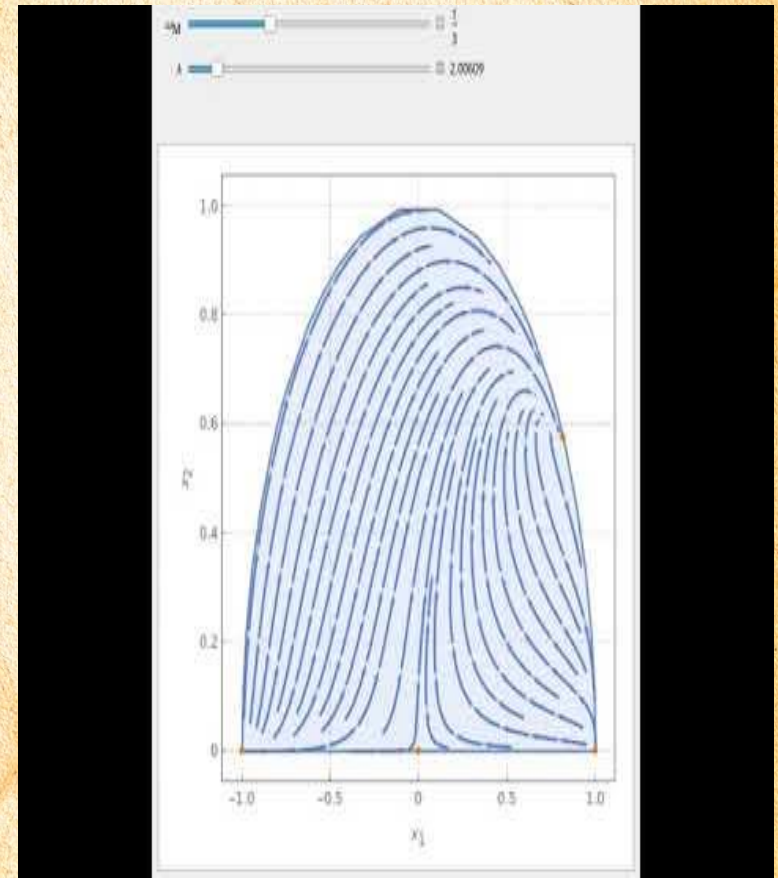
The End?
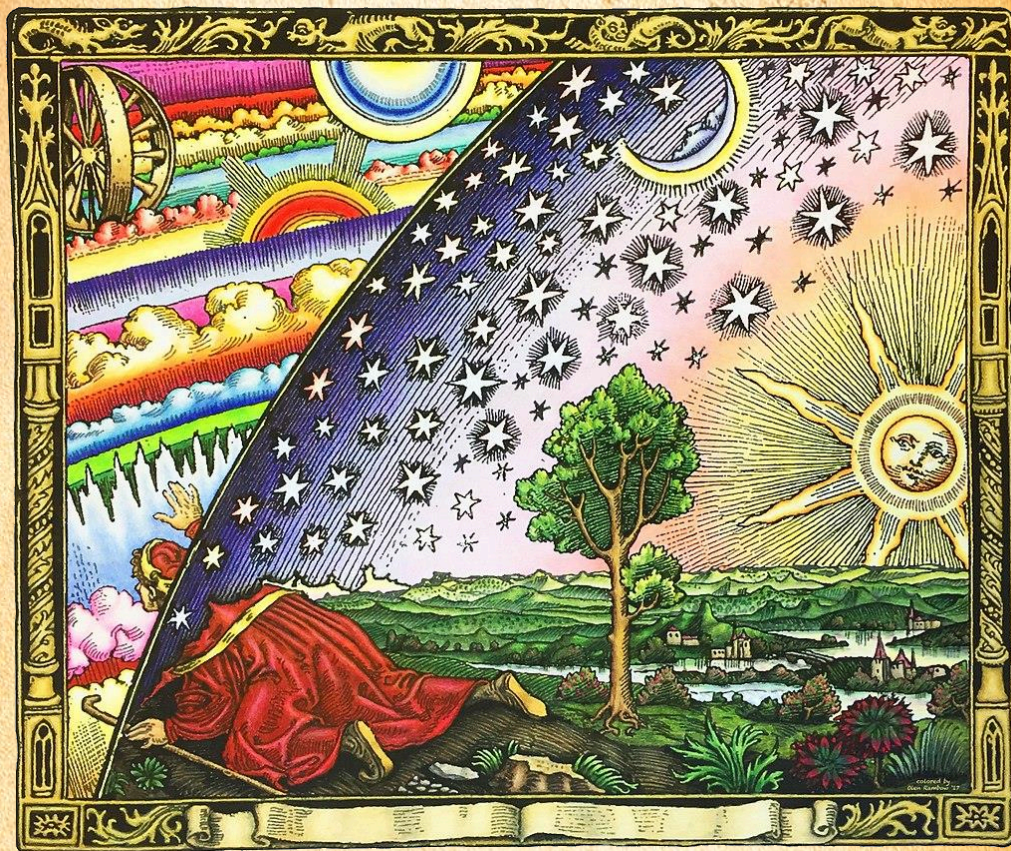
Modifications to General Relativity

A Phenomenological Approach

Maria Gonçalves

Faculdade de Ciências da Universidade de Lisboa

Table of contents

1

INTRODUCTION

How can we modify GR?

- At the level of the action and its Lagrangian;
- At the level of the perturbed Einstein's equations.

Observational Constraints

Methods
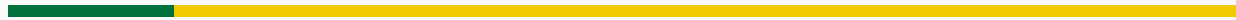
EFT APPROACH TO DARK ENERGY AND MODIFIED GRAVITY

EFT approach

- Lagrangian with scalar terms for a perturbed FLRW metric
- Action in terms of the metric and its derivatives with no scalar field perturbations

EFT covers the background evolution and the linear perturbations of the metric

Provides equations and parameterization

Compare with observations
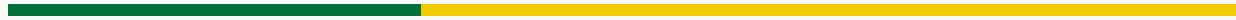
OBSERVATIONAL CONSTRAINTS

Modified Equations

$$k^2 \Psi = -4\pi G a^2 \sum_i \bar{\rho}_i \delta_i \mu(k, a)$$

$$\frac{\Phi}{\Psi} = \eta(k, a)$$

$$\Sigma(k, a) \equiv \frac{\mu(k, a)[1 + \eta(k, a)]}{2}$$

Dependencies

- Scale dependencies;
- Time dependencies:
  - effective dark energy density, $\Omega_{DE}(a)$;
  - scale factor, a.

Credits: [1]
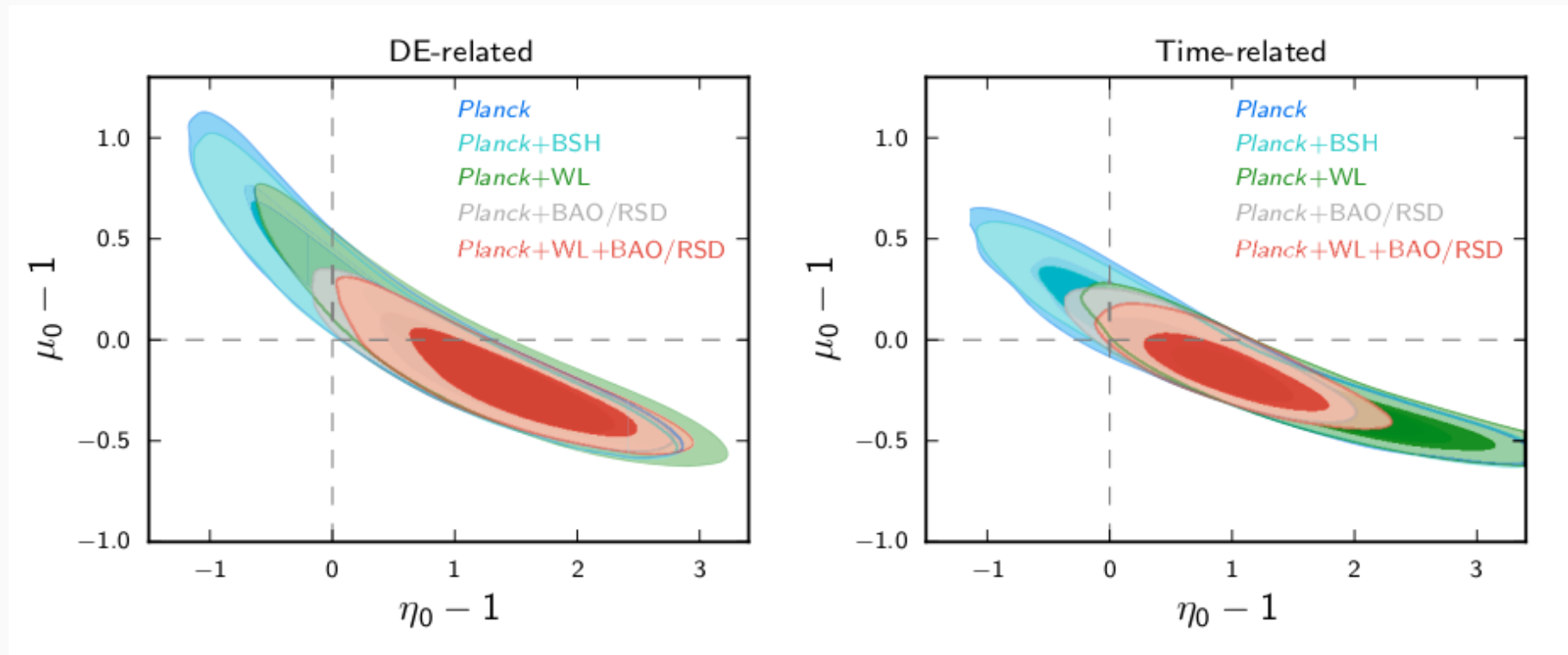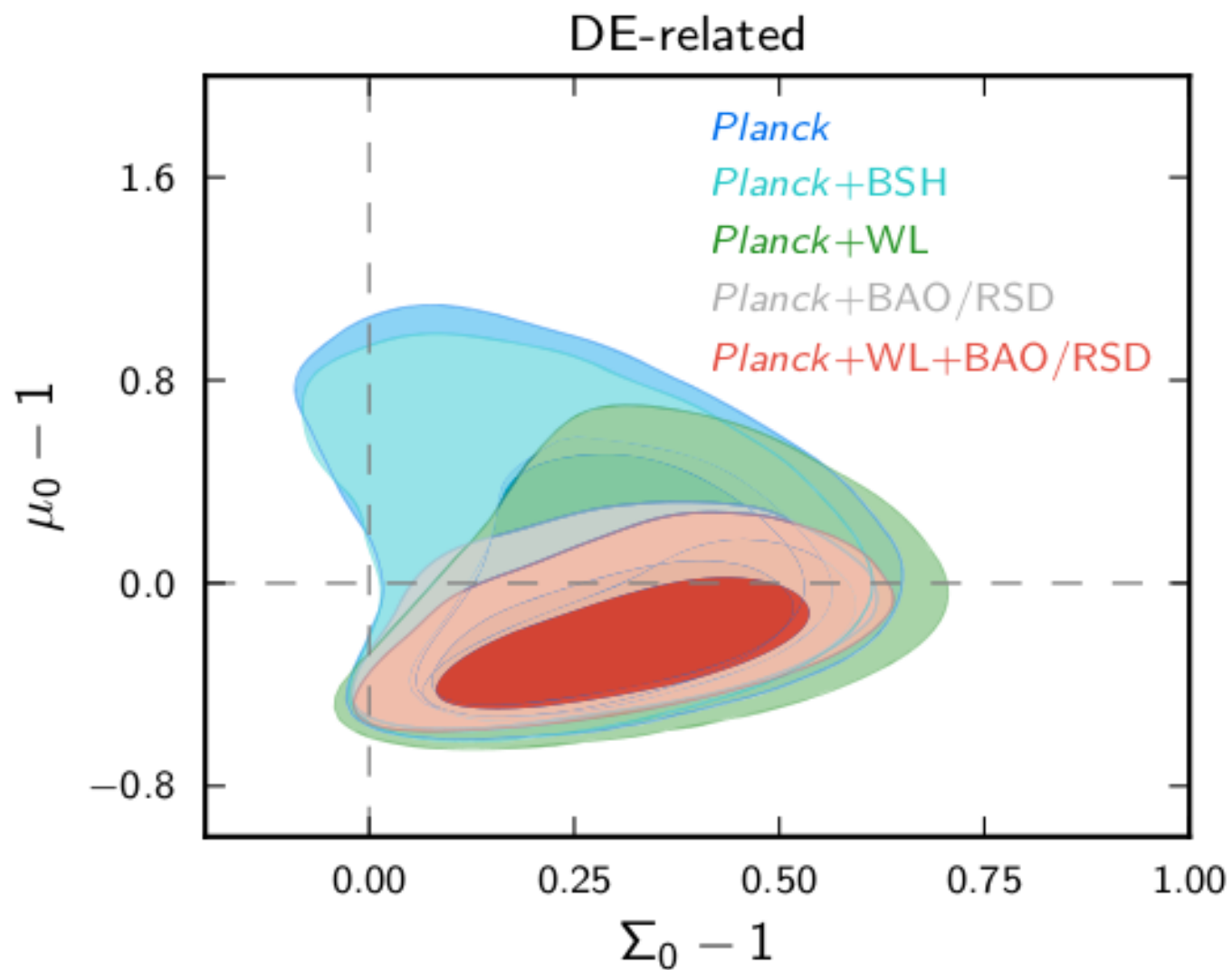
Credits: [1]

Modified Equations

$$k^2\Phi = -4\pi G a^2 \sum_i \bar{\rho}_i \delta_i Q(k, a)$$

$$k^2(\Psi - R(k, a)\Phi) = -12\pi G a^2 \sum_i \bar{\rho}_i (1 + w_i)\sigma_i Q(k, a)$$

Credits: [1]
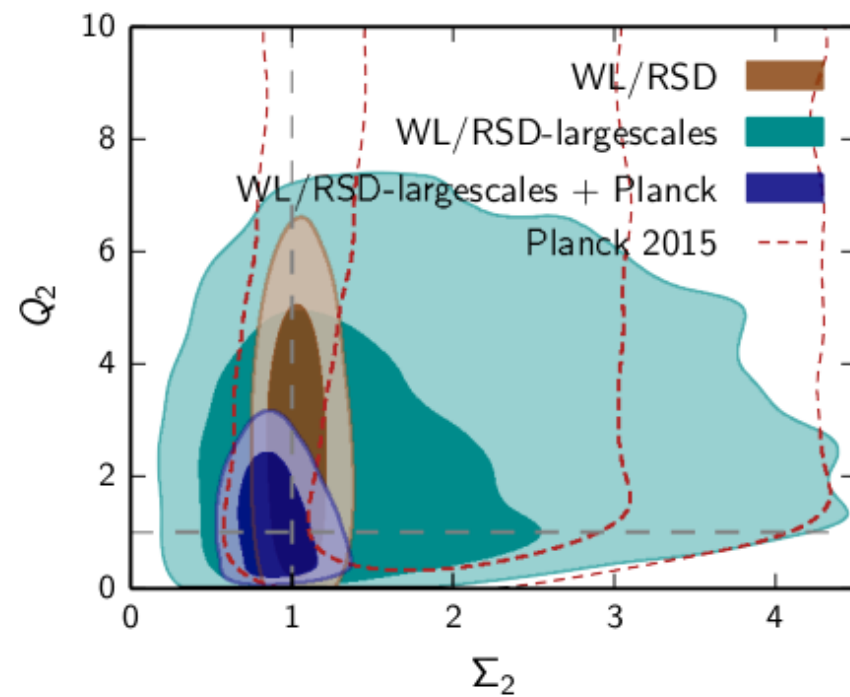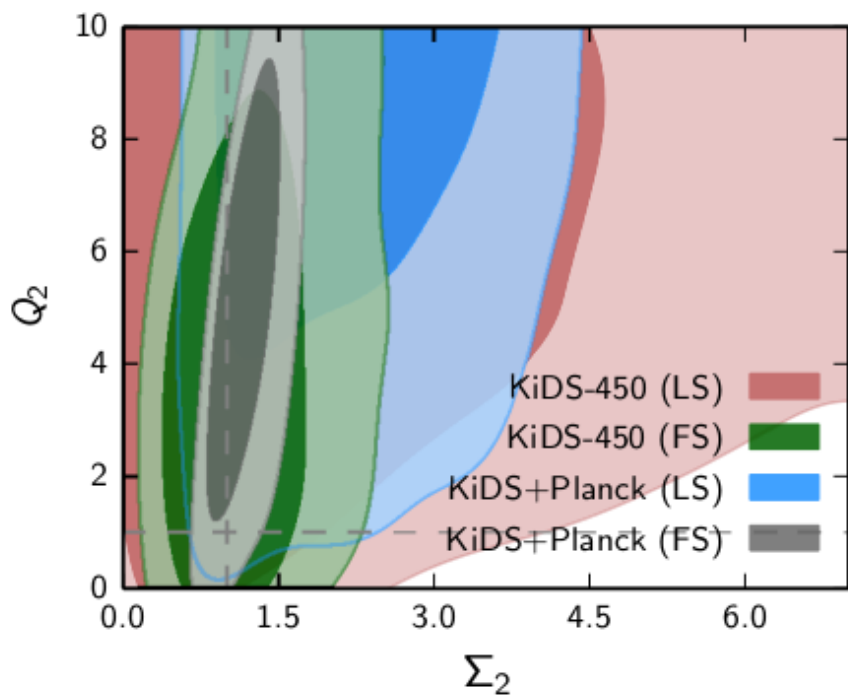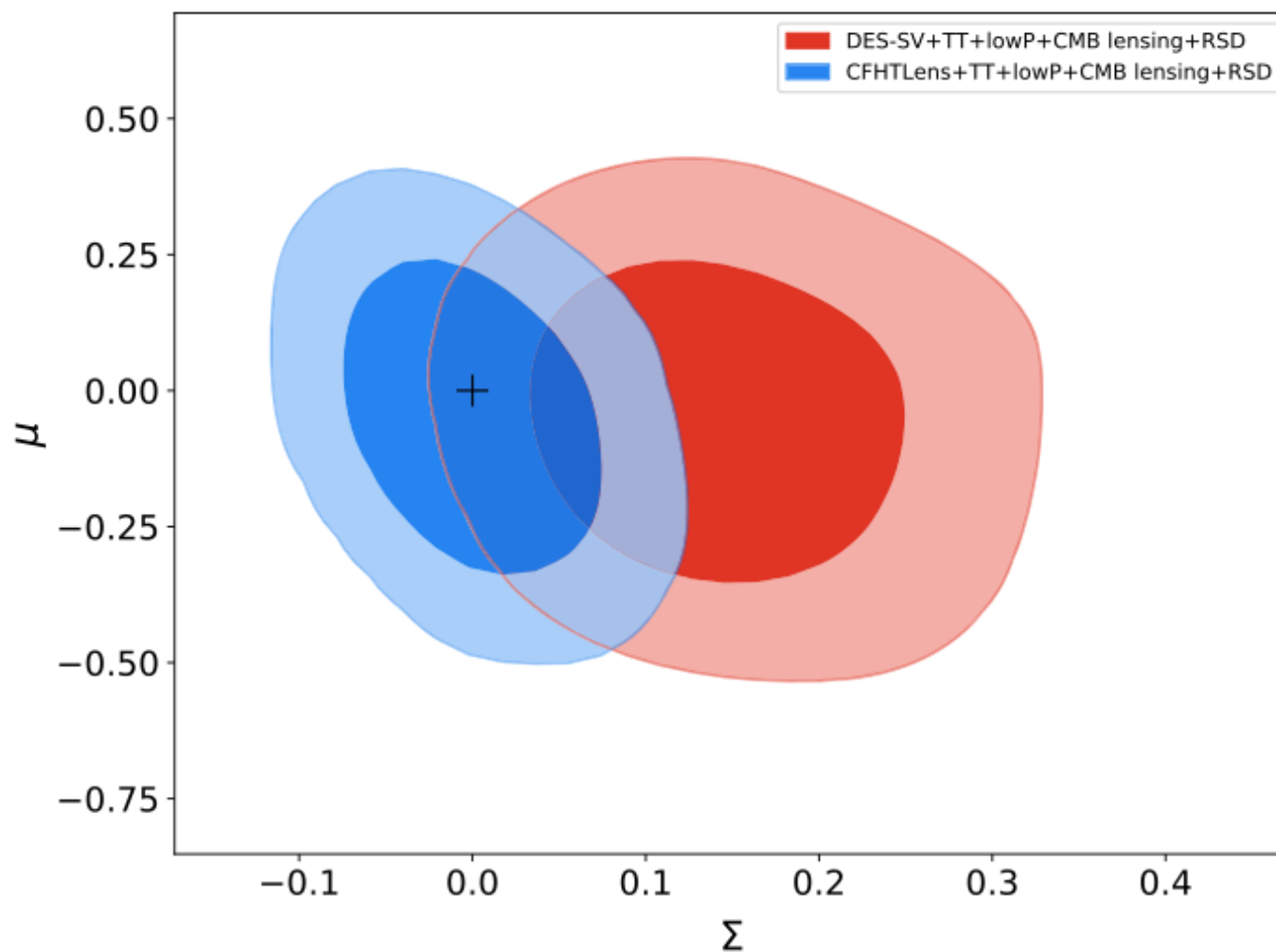
Credits: [1]

fσ_8

- $f = \Omega_m^{\gamma}$

- $\sigma_8 \to$ rms of matter fluctuations at $8h^{-1}Mpc$

Definition

$$f\sigma_8 \to f\sigma_8[A_{f\sigma_8} + B_{f\sigma_8}(z - z_p)]$$

where $z_p = 0.51$ and in GR $A_{f\sigma_8} = 1$ and $B_{f\sigma_8} = 0$.
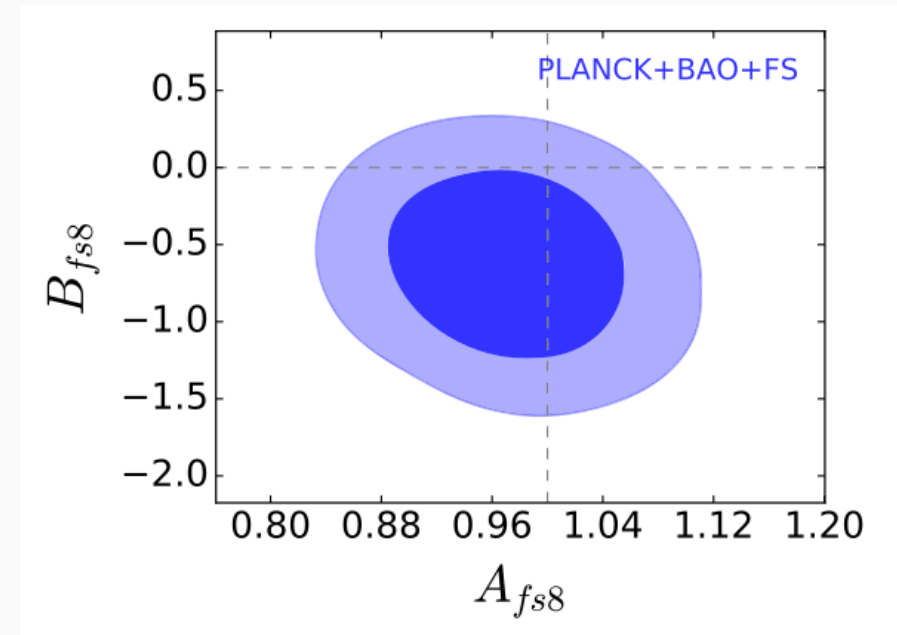
Credits: [1]

Sensitive to

- growth of structure
- mean matter density in the Universe

Results

- $E_G(z = 0.6) = 0.16 \pm 0.09$
- $E_G(z = 0.86) = 0.09 \pm 0.07$
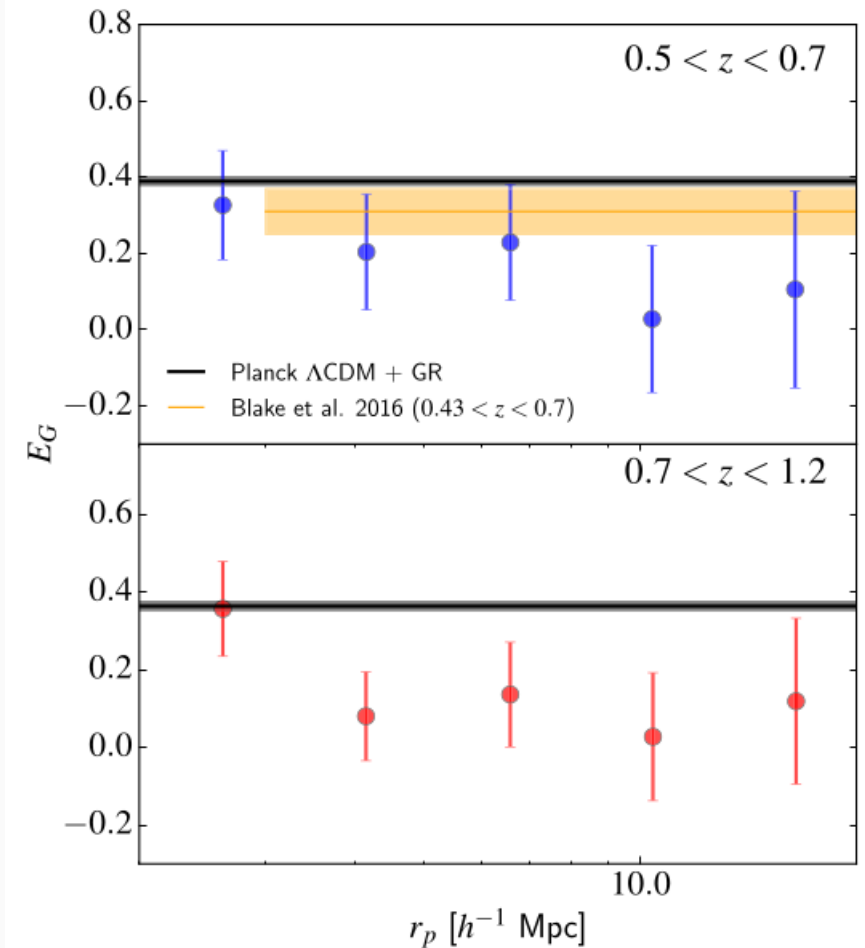
Credits: [1]

DE and MG models

Standard dark energy models

- DE has no clustering on sub-horizon scales;
- Example: Quintessence.

Clustering dark energy

- DE has fluctuations and can cluster on sub-horizon scales;
- Example: k-essence.

Modified gravity models

- Characterized by the presence of fifth force and violate the SEP;
- Example: f(R).

Conclusion

Summary

- Modify GR using different methods
- Get new parameters
- Observational constraints

Better Theory

Questions?

M. Ishak.
Testing general relativity in cosmology.
Living Reviews in Relativity, 22(1):1, Dec. 2019.

IV. Structure formation
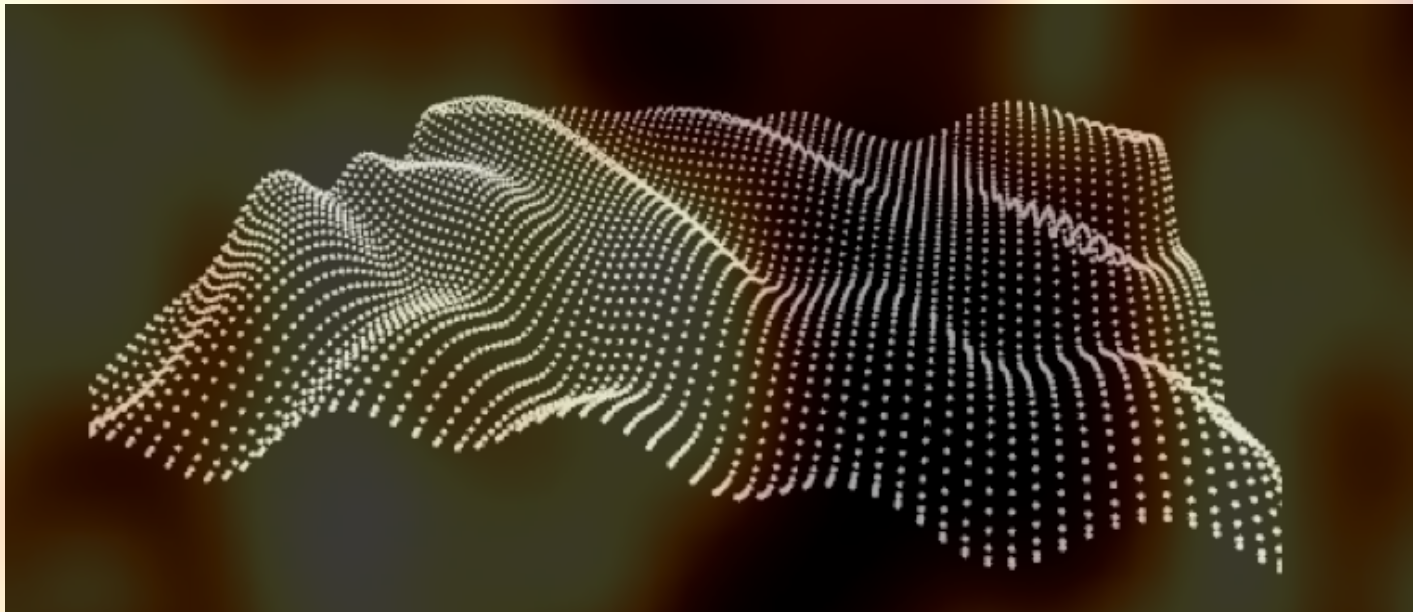
Boltzmann Equation

The Cold Dark Matter Case
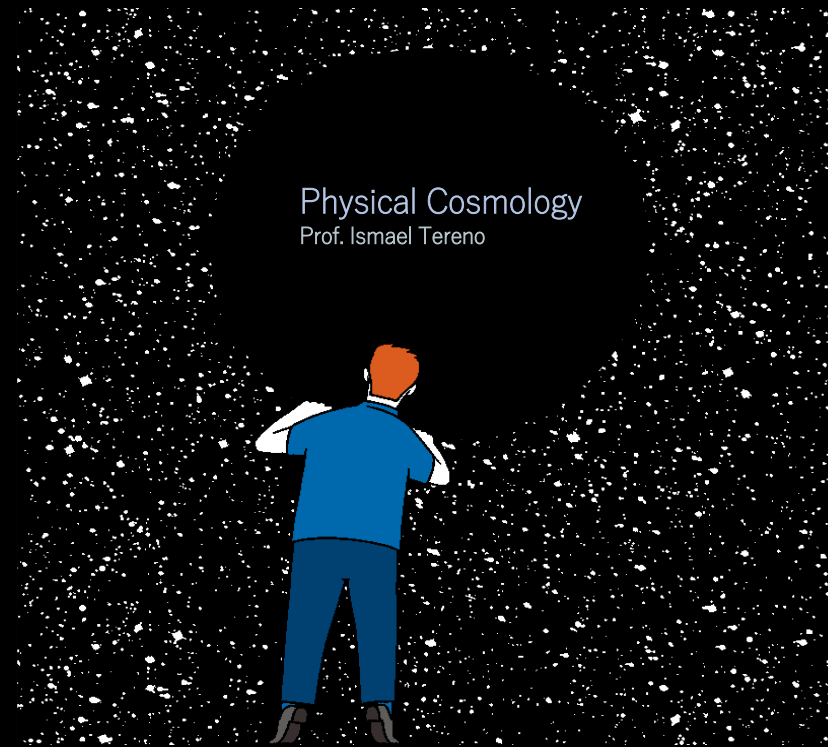
Physical Cosmology
Prof. Ismael Tereno

Miguel Pinto Nº 51135

Ciências
ULisboa
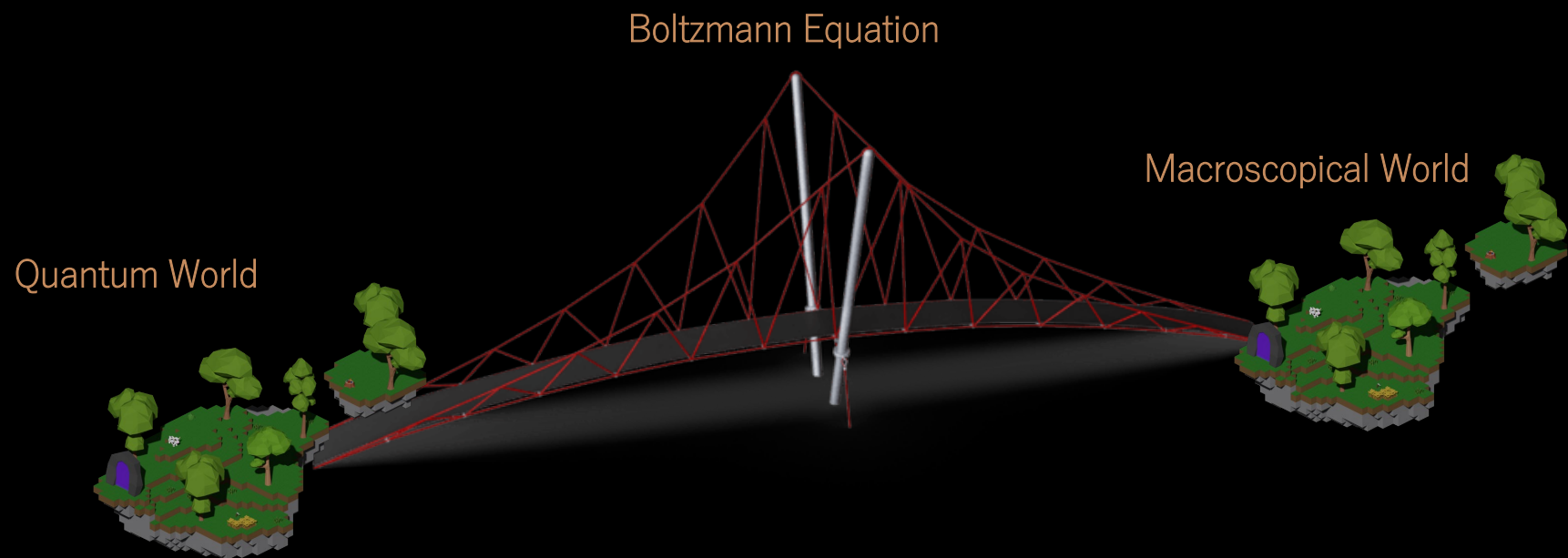
Introduction

Introduction

Distribution Function $\quad f = f(\vec{x}, \vec{p}, t)$

Number of particles $\quad N(\vec{x}, \vec{p}, t) = f(\vec{x}, \vec{p}, t)(\Delta x)^3 \dfrac{(\Delta p)^3}{(2\pi)^3}$

$$\frac{dN}{dt} = 0 \implies \frac{df}{dt} = 0$$

Particle conservation implies conservation of the distribution function

Taking the total time derivative of f we get:

$$\frac{df}{dt} = \frac{\partial f}{\partial t} + \frac{\partial f}{\partial x^i} \cdot \frac{dx^i}{dt} + \frac{\partial f}{\partial p}\frac{dp}{dt} + \frac{\partial f}{\partial \hat{p}^i} \cdot \frac{d\hat{p}^i}{dt} \qquad \frac{df}{dt} = C[f]$$

$$\underbrace{\frac{\partial f}{\partial t} + \frac{\partial f}{\partial x^i} \cdot \frac{dx^i}{dt} + \frac{\partial f}{\partial p}\frac{dp}{dt} + \frac{\partial f}{\partial \hat{p}^i} \cdot \frac{d\hat{p}^i}{dt}}_{\text{Gravity Effects}} = \underbrace{C[f]}_{\substack{\text{Fundamental} \\ \text{Interactions}}}$$

Inhomogeneous Universe

Metric

Metric Elements
$$g_{00}(\vec{x}, t) = -1 - 2\Psi(\vec{x}, t)$$

$$g_{0i}(\vec{x}, t) = 0 \qquad \qquad \text{Conformal Newtonian Gauge}$$

$$g_{ij}(\vec{x}, t) = a^2(t)\, \delta_{ij}\, [1 + 2\Phi(\vec{x}, t)]$$

- Ψ corresponds to the Newtonian gravitational potential, which governs the dynamics of the nonrelativistic regime.

- Φ is a perturbation to the spacial curvature, but it also can be seen as a local perturbation to the scale factor:

$$a(t) \rightarrow a(\vec{x}, t) = a(t)\sqrt{1 + 2\Phi(\vec{x}, t)}$$

3

Boltzmann Equation

In an Inhomogeneous Universe

Its 0-th order does not depend on position and momentum vector – We assume that the equilibrium distribution is isotropic: $\frac{\partial f}{\partial \hat{p}^i}$ and $\frac{\partial f}{\partial x^i}$ are first order perturbative terms.

These terms are of the same order of the Bardeen fields Ψ and Φ

After many tedious steps one can get the

(Perturbed Linearized) Boltzmann Equation

in an Inhomogeneous Universe

$$\frac{\partial f}{\partial t} + \frac{p}{E}\frac{\hat{p}^i}{a}\frac{\partial f}{\partial x^i} - \left[H + \dot{\Phi} + \frac{E}{ap}\hat{p}^i\Psi_{,i}\right]p\frac{\partial f}{\partial p} = C[f]$$

Boltzmann Equation

For Cold Dark Matter

$\frac{\partial f}{\partial \hat{p}^i}$ and $\frac{\partial f}{\partial x^i}$ are of the same order as the Bardeen fields

- Distribution Function $\quad f \longrightarrow f_c \quad \Longrightarrow \quad$ Its 0-th order does not depend on position and momentum vector

Vanishes at $p = 0$ and $p \to +\infty$

- Cold Dark Matter does not have interactions $\quad \Longrightarrow \quad \dfrac{df_c}{dt} = C[f_c] = 0 \quad$ The collision term is gone!

- Cold Dark Matter is very nonrelativistic $\quad \Longrightarrow \quad E(p) \approx m \Longrightarrow \left(\dfrac{p}{m}\right)^2 \sim 0 \quad$ Higher-order powers of p are negligible!

Collisionless Boltzmann Equation for Cold Dark Matter

$$\frac{\partial f_c}{\partial t} + \frac{p}{E}\frac{\hat{p}^i}{a}\frac{\partial f_c}{\partial x^i} - \left[H + \dot{\Phi} + \frac{E}{ap}\hat{p}^i \Psi_{,i}\right] p \frac{\partial f_c}{\partial p} = 0$$

5

Boltzmann Equation
Taking Its 0-th Moment

Multiplying the Boltzmann Equation by the phase space volume $d^3p/(2\pi)^3$ and integrate we get:

$$\int \left\{ \frac{\partial f_c}{\partial t} + \frac{p}{E} \frac{\hat{p}^i}{a} \frac{\partial f_c}{\partial x^i} - \left[H + \dot{\Phi} + \frac{E}{ap} \hat{p}^i \Psi_{,i} \right] p \frac{\partial f_c}{\partial p} \right\} \frac{d^3p}{(2\pi)^3} = \int 0 \times \frac{d^3p}{(2\pi)^3}$$

$$\Leftrightarrow \underbrace{\frac{\partial}{\partial t} \int f_c \frac{d^3p}{(2\pi)^3}}_{(1)} + \underbrace{\frac{1}{a} \frac{\partial}{\partial x^i} \int f_c \frac{p}{E(p)} \hat{p}^i \frac{d^3p}{(2\pi)^3}}_{(2)} - \underbrace{(H + \dot{\Phi}) \int p \frac{\partial f_c}{\partial p} \frac{d^3p}{(2\pi)^3}}_{(3)} - \underbrace{\frac{1}{a} \frac{\partial \Psi}{\partial x^i} \int E(p) \hat{p}^i p \frac{\partial f_c}{\partial p}}_{(4)} = 0$$

6

Boltzmann Equation

Taking Its 0-th Moment

CDM Density Number $\quad n_c \equiv \int f_c \dfrac{d^3p}{(2\pi)^3}$

CDM Fluid Velocity $\quad u_c^i \equiv \dfrac{1}{n_c} \int f_c \dfrac{p}{E(p)} \hat{p}^i \dfrac{d^3p}{(2\pi)^3}$

Expressing (1), (2) and (3) in terms of n_c and u_c^i we get:

(1) - $\dfrac{\partial}{\partial t} \underbrace{\int f_c \dfrac{d^3p}{(2\pi)^3}}_{n_c} = \dfrac{\partial n_c}{\partial t}$

(3) - $(H + \dot{\Phi}) \int p \dfrac{\partial f_c}{\partial p} \dfrac{d^3p}{(2\pi)^3} = (H + \dot{\Phi}) \int_0^{+\infty} p^3 \dfrac{\partial f_c}{\partial p} \dfrac{dp}{(2\pi)^3} \int d\Omega$

$= (H + \dot{\Phi}) \left\{ \left[\dfrac{p^3 f_c(p)}{(2\pi)^3} \right]_0^{+\infty} \int d\Omega - \int_0^{+\infty} 3p^2 f_c \dfrac{dp}{(2\pi)^3} \int d\Omega \right\}$

(2) - $\dfrac{1}{a} \dfrac{\partial}{\partial x^i} \underbrace{\int \dfrac{p}{E(p)} \hat{p}^i \dfrac{d^3p}{(2\pi)^3}}_{u_c^i \, n_c} = \dfrac{1}{a} \dfrac{\partial (u_c^i \, n_c)}{\partial x^i}$

$= -3(H + \dot{\Phi}) \underbrace{\int f_c \dfrac{d^3p}{(2\pi)^3}}_{n_c} = 3(H + \dot{\Phi}) n_c$

7

Boltzmann Equation

Taking Its 0-th Moment

Thus we obtain
$$\frac{\partial n_c}{\partial t} + \frac{1}{a}\frac{\partial(u_c^i\, n_c)}{\partial x^i} + 3(H + \dot{\Phi})n_c = 0$$

Expanding the number density $n_c(\vec{x}, t) = \bar{n}_c(t) + \bar{n}_c(t)\delta_c(\vec{x}, t)$ and plugging in the eq. above we get

$$\frac{\partial(\bar{n}_c(1 + \delta_c))}{\partial t} + \frac{1}{a}\frac{\partial\left(u_c^i\bar{n}_c(1 + \delta_c)\right)}{\partial x^i} + 3(H + \dot{\Phi})\,\bar{n}_c(1 + \delta_c) = 0$$

$$\Leftrightarrow \frac{\partial\bar{n}_c}{\partial t} + 3H\bar{n}_c + \frac{\partial\bar{n}_c}{\partial t}\delta_c + \frac{\partial\delta_c}{\partial t}\bar{n}_c + 3H\bar{n}_c\delta_c + 3\dot{\Phi}\bar{n}_c + \frac{\bar{n}_c}{a}\frac{\partial u_c^i}{\partial x^i} + \frac{\bar{n}_c}{a}u_c^i\frac{\partial\delta_c}{\partial x^i} + \frac{\bar{n}_c}{a}\frac{\partial u_c^i}{\partial x^i}\delta_c + 3\dot{\Phi}\bar{n}_c\delta_c = 0$$

Zeroth-order   First-order   Second-order

8

Boltzmann Equation

Collecting the zeroth-order terms we get:

$$\frac{\partial \bar{n}_c}{\partial t} + 3H\bar{n}_c = 0 \Longleftrightarrow \frac{\partial \bar{n}_c}{\partial t} = -3H\bar{n}_c \Longleftrightarrow \frac{1}{\bar{n}_c}\frac{\partial \bar{n}_c}{\partial t} = -3\frac{1}{a}\frac{\partial a}{\partial t} \Longrightarrow \bar{n}_c \propto a^{-3}$$

Continuity equation for the Cold Dark Matter in the homogeneous universe!

Doing the same with the first-order terms we obtain:

$$\frac{\partial \bar{n}_c}{\partial t}\delta_c + \frac{\partial \delta_c}{\partial t}\bar{n}_c + 3H\bar{n}_c\delta_c + 3\dot{\Phi}\bar{n}_c + \frac{\bar{n}_c}{a}\frac{\partial u_c^i}{\partial x^i} = 0 \Longleftrightarrow \boxed{\frac{\partial \delta_c}{\partial t} + \frac{1}{a}\frac{\partial u_c^i}{\partial x^i} + 3\dot{\Phi} = 0}$$

$$\underbrace{\phantom{\frac{\partial \bar{n}_c}{\partial t}}}_{-3H\bar{n}_c}$$

Perturbed linearized Continuity Equation for the Cold Dark Matter!

9

Boltzmann Equation
Taking Its 1-st Moment

$$\frac{\partial f_c}{\partial t} + \frac{p}{E} + \frac{\hat{p}^i}{a}\frac{\partial f_c}{\partial x^i} - \left[H + \dot{\Phi} + \frac{E}{ap}\hat{p}^i\Psi_{,i}\right]p\frac{\partial f_c}{\partial p} = 0$$

One equation for two perturbation variables... We need to find another!

Multiplying the Boltzmann Equation by $(p\hat{p}^j/E)d^3p/(2\pi)^3$ and integrate we get:

$$\int \left\{ \frac{\partial f_c}{\partial t} + \frac{p}{E}\frac{\hat{p}^i}{a}\frac{\partial f_c}{\partial x^i} - \left[H + \dot{\Phi} + \frac{E}{ap}\hat{p}^i\Psi_{,i}\right]p\frac{\partial f_c}{\partial p}\right\} \frac{p}{E(p)}\hat{p}^j\frac{d^3p}{(2\pi)^3} = \int 0 \times \frac{p}{E(p)}\hat{p}^j\frac{d^3p}{(2\pi)^3}$$

$$\Leftrightarrow \underbrace{\frac{\partial}{\partial t}\int f_c\frac{p}{E(p)}\hat{p}^j\frac{d^3p}{(2\pi)^3}}_{(1)} + \frac{1}{a}\frac{\partial}{\partial x^i}\int \underbrace{\frac{p^2}{E^2(p)}}_{\approx\left(\frac{p}{m}\right)^2\sim 0}f_c\hat{p}^i\hat{p}^j\frac{d^3p}{(2\pi)^3} - \underbrace{(H+\dot{\Phi})\int\frac{p^2}{E(p)}\hat{p}^j\frac{\partial f_c}{\partial p}\frac{d^3p}{(2\pi)^3}}_{(3)}$$

with (1), (2), (3) labels over the three terms.

$$\underbrace{-\frac{1}{a}\frac{\partial\Psi}{\partial x^i}\int p\frac{\partial f_c}{\partial p}\hat{p}^i\hat{p}^j\frac{d^3p}{(2\pi)^3}}_{(4)} = 0$$

10

Boltzmann Equation

Taking Its 1-st Moment

$$n_c \equiv \int f_c \frac{d^3p}{(2\pi)^3} \qquad u_c^i \equiv \frac{1}{n_c} \int f_c \frac{p}{E(p)} \hat{p}^i \frac{d^3p}{(2\pi)^3}$$

Expressing (1) and (3) in terms of n_c and u_c^i we get:

(1) - $\displaystyle \frac{\partial}{\partial t} \underbrace{\int f_c \frac{p}{E(p)} \hat{p}^j \frac{d^3p}{(2\pi)^3}}_{u_c^j\, n_c} = \frac{\partial (u_c^j\, n_c)}{\partial t}$

$$E(p) = \sqrt{p^2 + m^2} \approx m$$

(3) - $\displaystyle (H + \dot{\Phi}) \int \frac{p^2}{E(p)} \hat{p}^j \frac{\partial f_c}{\partial p} \frac{d^3p}{(2\pi)^3} = (H + \dot{\Phi}) \int \frac{\hat{p}^j}{(2\pi)^3} d\Omega \int_0^{+\infty} \frac{p^4}{E(p)} \frac{\partial f_c}{\partial p} dp$

$$= (H + \dot{\Phi}) \int \frac{\hat{p}^j}{(2\pi)^3} d\Omega \left\{ \left[\frac{p^4}{E(p)} f_c \right]_0^{+\infty} - \int_0^{+\infty} \frac{\partial}{\partial p} \left(\frac{p^4}{E(p)} \right) f_c\, dp \right\}$$

$$= -(H + \dot{\Phi}) \int \frac{\hat{p}^j}{(2\pi)^3} d\Omega \int_0^{+\infty} \left(4 \frac{p^3}{E(p)} - \underbrace{\frac{p^5}{E^3(p)}}_{\approx \left(\frac{p}{m} \right)^2 \frac{p^3}{m} \sim 0} \right) f_c\, dp = -4(H + \dot{\Phi}) \underbrace{\int f_c \frac{p}{E(p)} \hat{p}^j \frac{d^3p}{(2\pi)^3}}_{u_c^j\, n_c}$$

$$= -4(H + \dot{\Phi}) u_c^j\, n_c$$

11

Boltzmann Equation

Taking Its 1-st Moment

Expressing (4) in terms of n_c and u_c^i we get:

(4) - $\dfrac{1}{a}\dfrac{\partial \Psi}{\partial x^i}\displaystyle\int p\,\dfrac{\partial f_c}{\partial p}\,\hat{p}^i\hat{p}^j\,\dfrac{d^3 p}{(2\pi)^3}$

$$= \dfrac{1}{a}\dfrac{\partial \Psi}{\partial x^i}\int \dfrac{\hat{p}^i\hat{p}^j}{(2\pi)^3}\,d\Omega \int_0^{+\infty} p^3\,\dfrac{\partial f_c}{\partial p}\,dp$$

$$= \dfrac{1}{a}\dfrac{\partial \Psi}{\partial x^i}\int \dfrac{\hat{p}^i\hat{p}^j}{(2\pi)^3}\,d\Omega \left\{ [p^3 f_c]_0^{+\infty} - \int_0^{+\infty} 3p^2 f_c\,dp \right\}$$

$$= -\dfrac{1}{a}\dfrac{\partial \Psi}{\partial x^i}\,\delta^{ij}\underbrace{\int f_c\,\dfrac{d^3 p}{(2\pi)^3}}_{n_c} = -\dfrac{1}{a}\dfrac{\partial \Psi}{\partial x^j}\,n_c$$

$$n_c \equiv \int f_c\,\dfrac{d^3 p}{(2\pi)^3}$$

$$u_c^i \equiv \dfrac{1}{n_c}\int f_c\,\dfrac{p}{E(p)}\,\hat{p}^i\,\dfrac{d^3 p}{(2\pi)^3}$$

$$\int \dfrac{\hat{p}^i\hat{p}^j}{(2\pi)^3}\,d\Omega = \delta^{ij}\,\dfrac{4\pi}{3}$$

Boltzmann Equation

We can set everywhere

$$n_c \longrightarrow \bar{n}_c$$

So we get

$$\frac{\partial(u_c^j \, n_c)}{\partial t} + 4(H + \dot{\Phi})u_c^j \, n_c + \frac{1}{a}\frac{\partial \Psi}{\partial x^j} n_c = 0$$

because this eq. does not have 0th-terms

Hence

$$\frac{\partial(u_c^j \bar{n}_c)}{\partial t} + 4Hu_c^j \bar{n}_c + \frac{1}{a}\frac{\partial \Psi}{\partial x^j} \bar{n}_c = 0$$

$$\Leftrightarrow \bar{n}_c \frac{\partial u_c^j}{\partial t} + u_c^j \overbrace{\frac{\partial n_c}{\partial t}}^{-3H\bar{n}_c} + 4Hu_c^j \bar{n}_c + \frac{1}{a}\frac{\partial \Psi}{\partial x^j} \bar{n}_c = 0$$

$$\boxed{\frac{\partial u_c^j}{\partial t} + Hu_c^j + \frac{1}{a}\frac{\partial \Psi}{\partial x^j} = 0}$$

Perturbed linearized Euler Equation
for the Cold Dark Matter!

13

Boltzmann Equation

Continuity and Euler Equations

$$\left[\begin{array}{l} \dfrac{\partial \delta_c}{\partial t} + \dfrac{1}{a}\dfrac{\partial u_c^i}{\partial x^i} + 3\dot{\Phi} = 0 \qquad \text{Continuity Equation} \\[3em] \dfrac{\partial u_c^j}{\partial t} + H u_c^j + \dfrac{1}{a}\dfrac{\partial \Psi}{\partial x^j} = 0 \qquad \text{Euler Equation} \end{array}\right.$$

	Probability Density Funtion	Distribution Function	Boltzmann Equation
0-th Moment	1	n_c	Generalization of the Continuity Equation
1-st Moment	Mean Value	u_c^i	Generalization of the Euler Equation
2-nd Moment	Variance	Velocity Dispersion	

14

Boltzmann Equation

Continuity Equation in a conformal way in Fourier Space

Continuity Equation $\quad \dfrac{\partial \delta_c}{\partial t} + \dfrac{1}{a}\dfrac{\partial u_c^i}{\partial x^i} + 3\dot{\Phi} = 0 \qquad\qquad$ Physical Time $\quad dt = a\,d\tau$

Velocity Component $\quad u_c^i = \dfrac{k^i}{k} u_c \qquad \dfrac{\partial u_c^i}{\partial x^i} = \dfrac{\partial}{\partial x^i}\left(\dfrac{k^i}{k} u_c\right) = \dfrac{k^i}{k}\dfrac{\partial u_c}{\partial x^i} = i\dfrac{k^i}{k} k_i u_c = i\dfrac{k^2}{k} u_c = iku_c$

The Continuity Equation becomes $\qquad \dfrac{1}{a}\dfrac{\partial \delta_c}{\partial \tau} + \dfrac{1}{a} iku_c + 3\dfrac{1}{a}\dfrac{\partial \Phi}{\partial \tau} = 0$

$$\Downarrow \quad \dfrac{\partial}{\partial \tau} \equiv {}'$$

$$\boxed{\delta_c' + iku_c + 3\Phi' = 0}$$

15

Boltzmann Equation

Euler Equation in a conformal way in Fourier Space

Euler Equation $\quad \dfrac{\partial u_c^j}{\partial t} + H u_c^j + \dfrac{1}{a}\dfrac{\partial \Psi}{\partial x^j} = 0$

Potential $\quad \dfrac{\partial \Psi}{\partial x^j} = i k_j \Psi$

Velocity Component $\quad u_c^j = \dfrac{k^j}{k} u_c \qquad \dfrac{\partial u_c^j}{\partial t} = \dfrac{\partial}{\partial t}\left(\dfrac{k^j}{k} u_c\right) = \dfrac{k^j}{k}\dfrac{\partial u_c}{\partial t}$

Physical Time $\quad dt = a\, d\tau$

The Euler Equation becomes $\quad \dfrac{k^j}{k}\dfrac{1}{a}\dfrac{\partial u_c}{\partial \tau} + \dfrac{1}{a^2}\dfrac{\partial a}{\partial \tau}\dfrac{k^j}{k} u_c + \dfrac{1}{a} i k_j \Psi = 0$

$$\dfrac{a'}{a} \equiv \mathcal{H} \qquad \Downarrow \qquad \dfrac{\partial}{\partial \tau} = {}'$$

$$\boxed{u_c' + \mathcal{H} u_c + i k \Psi = 0}$$

16

Summary

➤ The Boltzmann Equation makes the bridge between fundamental interactions and the effects of gravity and the distribution function evolution;

➤ The equations which arise from its moments describe the evolution of a certain species;

➤ The integrated Boltzmann Equation for the n-th moment depends on the moment of order n+1.

➤ For Cold Dark Matter we deduce a close set of two equations

Bibliography

➤ S. Dodelson and F. Schmidt (2021) "Modern Cosmology, 2nd edition"
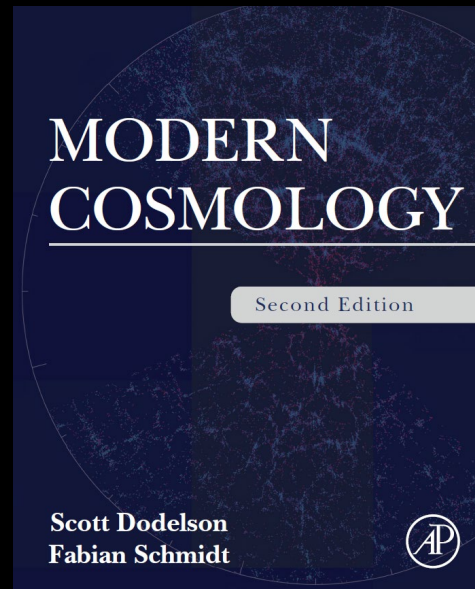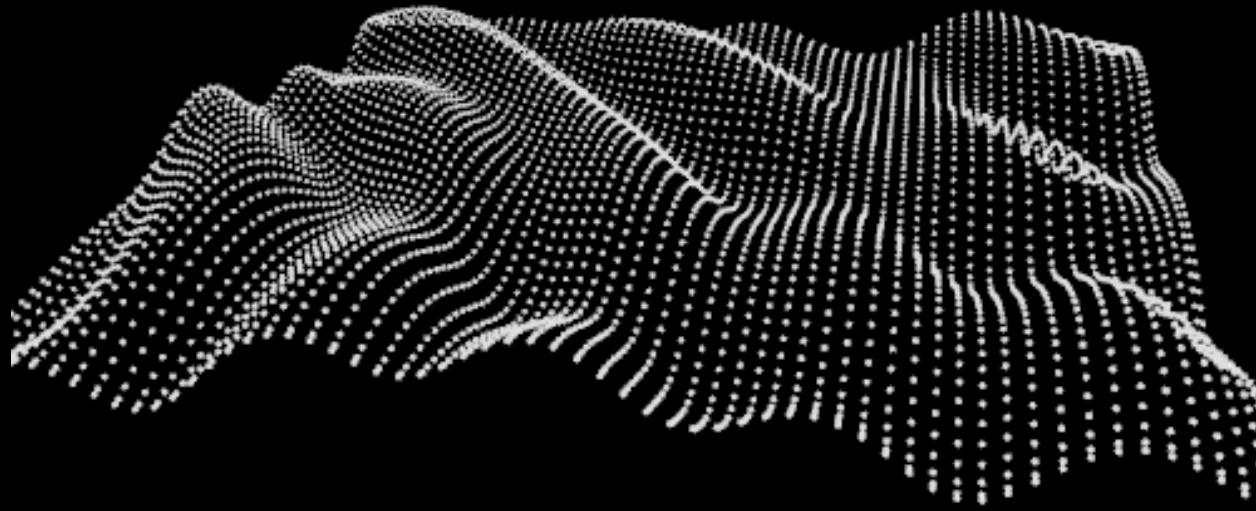
Structure formation
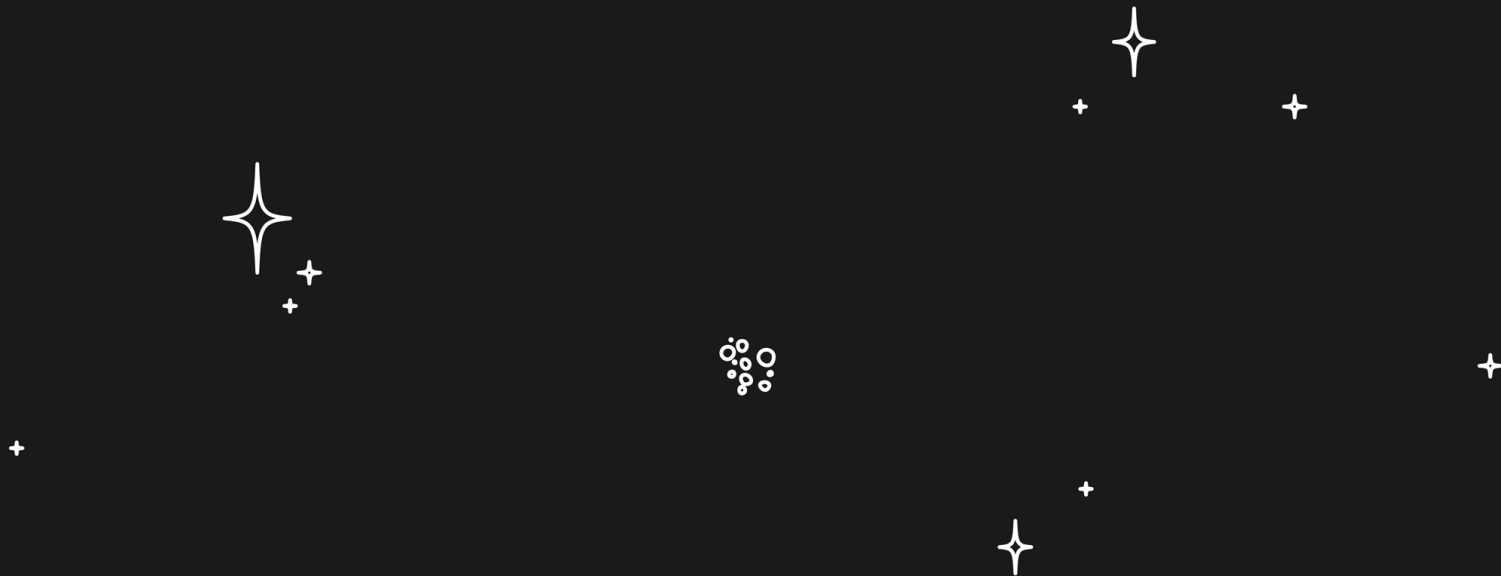
$$R_{\mu\nu} - \frac{1}{2}g_{\mu\nu}R + \Lambda g_{\mu\nu} = 8\pi G T_{\mu\nu}$$

Key Concepts – Structure Formation

For realistic models of structure formation, the initial spectrum of perturbations is such that at large scales, fluctuations are small and reflect the primordial spectrum

The angular power spectrum characterizes the size of the fluctuations as a function of angular scale

The angular power spectrum from CMB temperature fluctuations contains a convolved signal of the shape of initial fluctuation, i.e. the primordial power spectrum

rimordial spectrum**
formation**, the initial spectrum of perturbations is
such that at large scales, **fluctuations are small** and reflect the **per****, the growth of density perturbations can be
described by **linear perturbation theory**

The **variance of density fluctuations** is a
decreasing function of scale *R* $\longrightarrow$ $\sigma^2(R)$

Linear regime
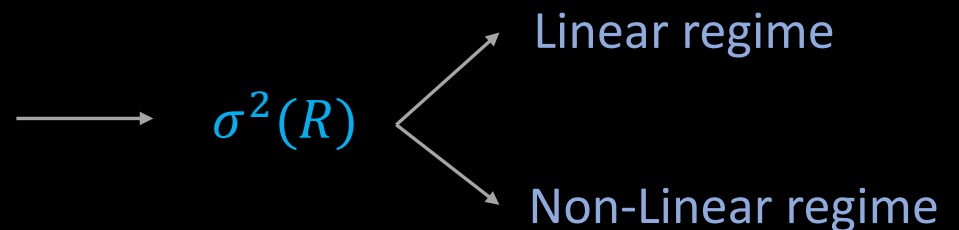
Non-Linear regime

Key Concepts – Linear Regime

Since $\sigma^2(R)$ decreases with R then the Linear regime at large scales is characterized by
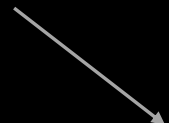
$$\sigma^2(R) \ll 1$$

In the linear regime, perturbation Fourier modes evolve independently of one another.

1. Conserves the statistical properties of the primordial fluctuations
2. Density and velocity fields are completely determined by the two-point correlation function or the power spectrum

Key Concepts – Non-Linear Regime

The Non-Linear regime at small scales is characterized by

$$\sigma^2(R) \gg 1$$

When the fluctuations become non-linear, coupling between different Fourier modes becomes important

The correlation length R_0 is defined where $\sigma^2(R_0) = 1$.
Because of gravitational instability, R_0 grows with time and therefore a given scale eventually becomes non-linear under time evolution

Non-linear Cosmological Perturbation Theory

Is a theoretical framework for the calculation of the induced higher-order correlation functions in the weakly non-linear regime, defined by scales R such that $\sigma(R) \lesssim 1$

And tree-level (leading order) perturbation theory quantities at the largest scales

Contains no closed loops $\sigma^2(R) \ll 1$

Next to leading order (loop) are corrections to the tree-level results which are expected to become important in the non-linear regime

$\sigma^2(R) \gg 1$

Non-linear Cosmological Perturbation Theory

Our understanding of non-linear clustering can be extended from the largest scales into the transition region to the non-linear regime?

Extend the leading order calculations to one-loop, in order to understand better the limitations of the tree-level results and see the extent to which one can improve the agreement of perturbation theory with fully non-linear numerical simulations.

Non-linear Cosmological Perturbation Theory

We concentrate on one-loop corrections to the three-point function of density perturbations in Fourier space, also known as the bispectrum, and its one-point counterpart, the skewness

The bispectrum is the lowest order correlation function which, for Gaussian initial conditions, vanishes in the linear regime and its structure therefore reflects truly non-linear properties of the matter distribution giving direct physical information on the anisotropic structures and flows generated by gravitational instability.

Dynamics and Perturbation Theory

Equations of motion relevant to gravitational instability referred as "exact dynamics" (ED)

$$\frac{\partial \delta(\mathbf{x}, \tau)}{\partial \tau} + \nabla \cdot \{[1 + \delta(\mathbf{x}, \tau)]\mathbf{v}(\mathbf{x}, \tau)\} = 0,$$ — Continuity Equation

$$\frac{\partial \mathbf{v}(\mathbf{x}, \tau)}{\partial \tau} + \mathcal{H}(\tau)\,\mathbf{v}(\mathbf{x}, \tau) + [\mathbf{v}(\mathbf{x}, \tau) \cdot \nabla]\mathbf{v}(\mathbf{x}, \tau) = -\nabla\Phi(\mathbf{x}, \tau),$$ — Euler Equation

$$\nabla^2\Phi(\mathbf{x}, \tau) = \frac{3}{2}\Omega\mathcal{H}^2(\tau)\delta(\mathbf{x}, \tau)$$ — Poisson Equation

Further notes on this derivation can be seen in Peebles, P. J. E. 1980, The Large-Scale Structure of the Universe

Dynamics and Perturbation Theory

Equations of motion relevant to gravitational instability (ED)

$$\frac{\partial \delta(\mathbf{x}, \tau)}{\partial \tau} + \nabla \cdot \{[1 + \delta(\mathbf{x}, \tau)]\mathbf{v}(\mathbf{x}, \tau)\} = 0,$$

$$\frac{\partial \mathbf{v}(\mathbf{x}, \tau)}{\partial \tau} + \mathcal{H}(\tau)\,\mathbf{v}(\mathbf{x}, \tau) + [\mathbf{v}(\mathbf{x}, \tau) \cdot \nabla]\mathbf{v}(\mathbf{x}, \tau) = -\nabla\Phi(\mathbf{x}, \tau),$$

$$\nabla^2\Phi(\mathbf{x}, \tau) = \frac{3}{2}\Omega\mathcal{H}^2(\tau)\delta(\mathbf{x}, \tau)$$

$\mathbf{x} \equiv$ Comoving spatial coordinates

$\tau \equiv$ Conformal time

$a(\tau) \equiv$ Cosmic scale factor

$\delta(\mathbf{x}, \tau) \equiv$ Density contrast

$\mathcal{H} \equiv$ Conformal expansion rate

$$\delta(\mathbf{x}, \tau) \equiv \rho(\mathbf{x}, \tau)/\bar{\rho} - 1$$

Further notes on this derivation can be seen in Peebles, P. J. E. 1980, The Large-Scale Structure of the Universe

Dynamics and Perturbation Theory

Taking the divergence of Euler equation and Fourier transforming the result equations we get

$$\frac{\partial \tilde{\delta}(\mathbf{k}, \tau)}{\partial \tau} + \tilde{\theta}(\mathbf{k}, \tau) = -\int d^3 k_1 \int d^3 k_2 \delta_D(\mathbf{k} - \mathbf{k}_1 - \mathbf{k}_2) \alpha(\mathbf{k}, \mathbf{k}_1) \tilde{\theta}(\mathbf{k}_1, \tau) \tilde{\delta}(\mathbf{k}_2, \tau),$$

$$\frac{\partial \tilde{\theta}(\mathbf{k}, \tau)}{\partial \tau} + \mathcal{H}(\tau) \, \tilde{\theta}(\mathbf{k}, \tau) + \frac{3}{2} \mathcal{H}^2(\tau) \tilde{\delta}(\mathbf{k}, \tau) = -\int d^3 k_1 \int d^3 k_2 \delta_D(\mathbf{k} - \mathbf{k}_1 - \mathbf{k}_2) \beta(\mathbf{k}, \mathbf{k}_1, \mathbf{k}_2) \tilde{\theta}(\mathbf{k}_1, \tau) \tilde{\theta}(\mathbf{k}_2, \tau),$$

Where was defined:

$$\alpha(\mathbf{k}, \mathbf{k}_1) \equiv \frac{\mathbf{k} \cdot \mathbf{k}_1}{k_1^2}$$

$$\beta(\mathbf{k}, \mathbf{k}_1, \mathbf{k}_2) \equiv \frac{k^2(\mathbf{k}_1 \cdot \mathbf{k}_2)}{2 k_1^2 k_2^2}$$

Dynamics and Perturbation Theory

The matrix γ constituting the mode coupling can be written in symmetric form with the elements

$$\gamma_{121} = \alpha(k_1, k_2)/2, \quad \gamma_{112} = \alpha(k_2, k_1)/2, \quad \gamma_{222} = \beta(k_1, k_2),$$

$$\alpha(\mathbf{k}, \mathbf{k}_1) \equiv \frac{\mathbf{k} \cdot \mathbf{k}_1}{k_1^2}$$

$$\beta(\mathbf{k}, \mathbf{k}_1, \mathbf{k}_2) \equiv \frac{k^2(\mathbf{k}_1 \cdot \mathbf{k}_2)}{2k_1^2 k_2^2}$$

Perturbation Theory Solutions

We want a statistical description of cosmological perturbations.
So as a general solution for the ED's:

$$\tilde{\delta}(\mathbf{k}, \tau) = \sum_{n=1}^{\infty} a^n(\tau)\delta_n(\mathbf{k}),$$

$$\tilde{\theta}(\mathbf{k}, \tau) = \mathcal{H}(\tau) \sum_{n=1}^{\infty} a^n(\tau)\theta_n(\mathbf{k})$$

The density contrast δ(x) is usually written in terms of its Fourier components

And where we define

$$\delta_n(\mathbf{k}) = \int d^3q_1 \ldots \int d^3q_n \delta_D(\mathbf{k} - \mathbf{q}_1 - \ldots - \mathbf{q}_n) F_n^{(s)}(\mathbf{q}_1, \ldots, \mathbf{q}_n)\delta_1(\mathbf{q}_1) \ldots \delta_1(\mathbf{q}_n),$$

$$\theta_n(\mathbf{k}) = -\int d^3q_1 \ldots \int d^3q_n \delta_D(\mathbf{k} - \mathbf{q}_1 - \ldots - \mathbf{q}_n) G_n^{(s)}(\mathbf{q}_1, \ldots, \mathbf{q}_n)\delta_1(\mathbf{q}_1) \ldots \delta_1(\mathbf{q}_n),$$

Perturbation Theory Solutions

$$\delta_n(\mathbf{k}) = \int d^3 q_1 \ldots \int d^3 q_n \delta_D(\mathbf{k} - \mathbf{q}_1 - \ldots - \mathbf{q}_n) F_n^{(s)}(\mathbf{q}_1, \ldots, \mathbf{q}_n) \delta_1(\mathbf{q}_1) \ldots \delta_1(\mathbf{q}_n),$$

$$\theta_n(\mathbf{k}) = -\int d^3 q_1 \ldots \int d^3 q_n \delta_D(\mathbf{k} - \mathbf{q}_1 - \ldots - \mathbf{q}_n) G_n^{(s)}(\mathbf{q}_1, \ldots, \mathbf{q}_n) \delta_1(\mathbf{q}_1) \ldots \delta_1(\mathbf{q}_n),$$

$$
\begin{aligned}
F_n(\mathbf{q}_1, \ldots, \mathbf{q}_n) = \; & \sum_{m=1}^{n-1} \frac{G_m(\mathbf{q}_1, \ldots, \mathbf{q}_m)}{(2n+3)(n-1)} \Big[(2n+1)\alpha(\mathbf{k}, \mathbf{k}_1) F_{n-m}(\mathbf{q}_{m+1}, \ldots, \mathbf{q}_n) \\
& + \; 2\beta(\mathbf{k}, \mathbf{k}_1, \mathbf{k}_2) G_{n-m}(\mathbf{q}_{m+1}, \ldots, \mathbf{q}_n) \Big],
\end{aligned}
$$

$$
\begin{aligned}
G_n(\mathbf{q}_1, \ldots, \mathbf{q}_n) = \; & \sum_{m=1}^{n-1} \frac{G_m(\mathbf{q}_1, \ldots, \mathbf{q}_m)}{(2n+3)(n-1)} \Big[3\alpha(\mathbf{k}, \mathbf{k}_1) F_{n-m}(\mathbf{q}_{m+1}, \ldots, \mathbf{q}_n) \\
& + \; 2n\beta(\mathbf{k}, \mathbf{k}_1, \mathbf{k}_2) G_{n-m}(\mathbf{q}_{m+1}, \ldots, \mathbf{q}_n) \Big],
\end{aligned}
$$

Statistics and Diagrammatics

Fluctuations can be described by statistically homogeneous and isotropic random fields

Ergodicity - approximate a statistical ensemble, so that
spatial averages are equivalent to ensemble averages

The non-linear evolution of the three-point cumulant of the density field, the bispectrum $B(k_1, K_2, \tau)$, and its 1-point counterpart, the skewness factor $S_3(R, \tau)$.

$$\left\langle \tilde{\delta}(\mathbf{k}_1, \tau) \tilde{\delta}(\mathbf{k}_2, \tau) \tilde{\delta}(\mathbf{k}_3, \tau) \right\rangle_c = \delta_D(\mathbf{k}_1 + \mathbf{k}_2 + \mathbf{k}_3) \ B(\mathbf{k}_1, \mathbf{k}_2, \tau)$$

The subscript "c" stands for the connected contribution

$$S_3(R, \tau) = \frac{1}{\sigma^4(R, \tau)} \int B(\mathbf{k}_1, \mathbf{k}_2, \tau) \ W(k_1 R) W(k_2 R) W(|\mathbf{k}_1 + \mathbf{k}_2| R) \ d^3 k_1 d^3 k_2,$$

$$W_{\mathrm{TH}}(u) = \frac{3}{u^3} \left[\sin(u) - u \cos(u) \right] \qquad W_{\mathrm{G}}(u) = \exp(-u^2/2).$$

Statistics and Diagrammatics

Where we defined variance of density fluctuations

$$\sigma^2(R, \tau) = \int P(k, \tau)\, W^2(kR)\, d^3k = \left\langle \delta^2(R, \tau) \right\rangle$$

Giving us the new power-spectrum

$$\left\langle \tilde{\delta}(\mathbf{k}, \tau)\tilde{\delta}(\mathbf{k}', \tau) \right\rangle_c = \delta_D(\mathbf{k} + \mathbf{k}')P(k, \tau)$$

$$P(k, \tau) = P^{(0)}(k, \tau) + P^{(1)}(k, \tau) + \ldots$$

(n) denotes an n-loop contribution

Statistics and Diagrammatics

$$P(k, \tau) = P^{(0)}(k, \tau) + P^{(1)}(k, \tau) + \dots$$

(n) denotes an n-loop contribution

$$P^{(0)}(k, \tau) = P_{11}(k, \tau)$$

$$P^{(1)}(k, \tau) = \boxed{P_{22}(k, \tau)} + \boxed{P_{13}(k, \tau)}.$$

$$P_{22}(k, \tau) \equiv 2 \int [F_2^{(s)}(\mathbf{k} - \mathbf{q}, \mathbf{q})]^2 P_{11}(|\mathbf{k} - \mathbf{q}|, \tau) P_{11}(q, \tau) d^3 q$$

$$P_{13}(k, \tau) \equiv 6 \int F_3^{(s)}(\mathbf{k}, \mathbf{q}, -\mathbf{q}) P_{11}(k, \tau) P_{11}(q, \tau) d^3 q.$$

P_{ij} denotes the amplitude given by the above rules for a connected diagram representing the contribution from $\langle \delta_i \delta_j \rangle_c$ to the power spectrum

Feynman rules of standard perturbation theory

$$P(k, \tau) = P^{(0)}(k, \tau) + P^{(1)}(k, \tau) + \ldots$$

$$P^{(0)}(k, \tau) = P_{11}(k, \tau)$$

$$P^{(1)}(k, \tau) = P_{22}(k, \tau) + P_{13}(k, \tau)$$

Diagrams for the power spectrum up to one-loop

(P_{11}) (P_{22}) (P_{13})
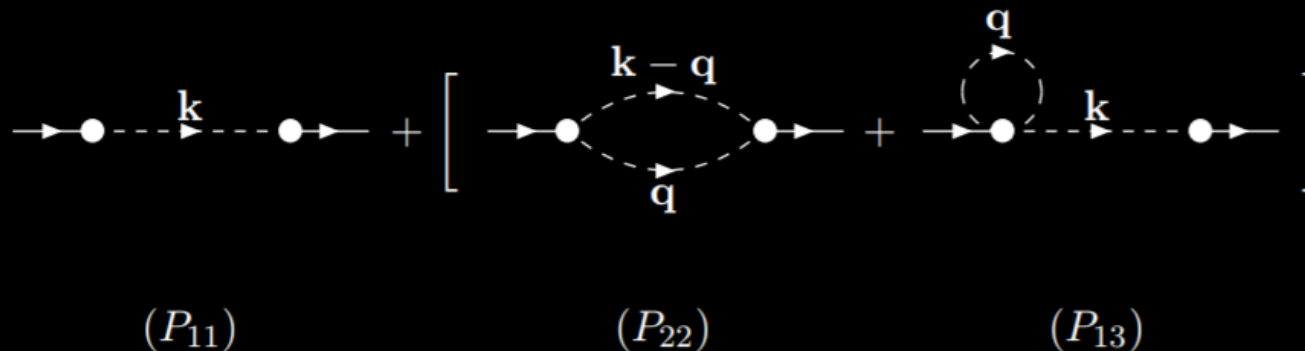
p-point cumulants of the density field come from connected diagrams with p external (solid) lines and r = p −1, p, . . . internal (dashed) lines

Bispectrum
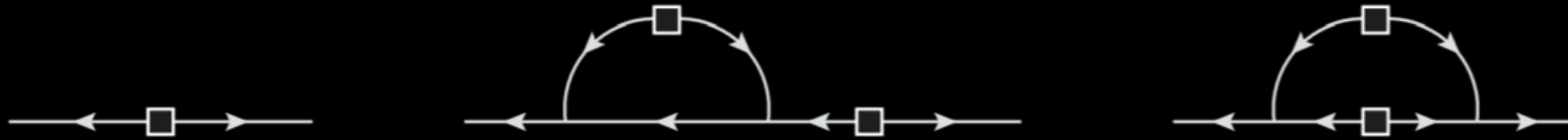
All tree level and one-loop contributions to the power spectrum.

The loop expansion for the bispectrum reads

$$B(\mathbf{k}_1, \mathbf{k}_2, \tau) = B^{(0)}(\mathbf{k}_1, \mathbf{k}_2, \tau) + B^{(1)}(\mathbf{k}_1, \mathbf{k}_2, \tau) + \ldots,$$

$$B^{(1)}(\mathbf{k}_1, \mathbf{k}_2, \tau) \equiv B_{222}(\mathbf{k}_1, \mathbf{k}_2, \tau) + B_{321}^{I}(\mathbf{k}_1, \mathbf{k}_2, \tau) + B_{321}^{II}(\mathbf{k}_1, \mathbf{k}_2, \tau) + B_{411}(\mathbf{k}_1, \mathbf{k}_2, \tau)$$

Bispectrum

We have Tree-level part is given

$$
\begin{aligned}
B^{(0)}(\mathbf{k}_1, \mathbf{k}_2, \tau) &\equiv 2P_{11}(k_1, \tau)P_{11}(k_2, \tau)F_2^{(s)}(\mathbf{k}_1, \mathbf{k}_2) + 2P_{11}(k_2, \tau)P_{11}(k_3, \tau) \\
&\quad \times F_2^{(s)}(\mathbf{k}_2, \mathbf{k}_3) + 2P_{11}(k_3, \tau)P_{11}(k_1, \tau)F_2^{(s)}(\mathbf{k}_3, \mathbf{k}_1).
\end{aligned}
$$
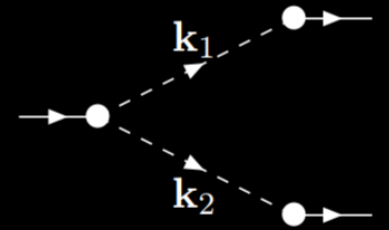
(B_{211})

The one-loop contribution consists of four distinct diagrams

$$
\begin{aligned}
B_{222} &\equiv 8\int d^3q\, P_{11}(q, \tau)F_2^{(s)}(-\mathbf{q}, \mathbf{q}+\mathbf{k}_1)P_{11}(|\mathbf{q}+\mathbf{k}_1|, \tau)F_2^{(s)}(-\mathbf{q}-\mathbf{k}_1, \mathbf{q}-\mathbf{k}_2) \\
&\quad \times P_{11}(|\mathbf{q}-\mathbf{k}_2|, \tau)F_2^{(s)}(\mathbf{k}_2-\mathbf{q}, \mathbf{q}), \\
B_{321}^{I} &\equiv 6P_{11}(k_3, \tau)\int d^3q\, P_{11}(q, \tau)F_3^{(s)}(-\mathbf{q}, \mathbf{q}-\mathbf{k}_2, -\mathbf{k}_3)P_{11}(|\mathbf{q}-\mathbf{k}_2|, \tau) \\
B_{321}^{II} &\equiv 6P_{11}(k_2, \tau)P_{11}(k_3, \tau)F_2^{(s)}(\mathbf{k}_2, \mathbf{k}_3)\int d^3q\, P_{11}(q, \tau)F_3^{(s)}(\mathbf{k}_3, \mathbf{q}, -\mathbf{q}) \\
&\quad +\text{permutations}, \\
B_{411} &\equiv 12P_{11}(k_2, \tau)P_{11}(k_3, \tau)\int d^3q\, P_{11}(q, \tau)F_4^{(s)}(\mathbf{q}, -\mathbf{q}, -\mathbf{k}_2, -\mathbf{k}_3) \\
&\quad +\text{permutations}.
\end{aligned}
$$

Bispectrum

The one-loop contribution consists of four distinct diagrams
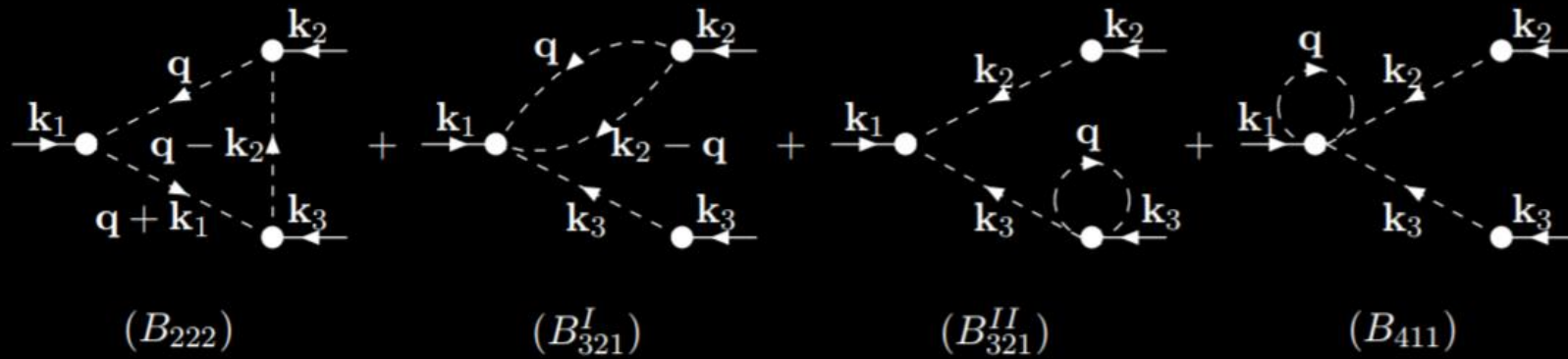
Thanks!

Any questions?
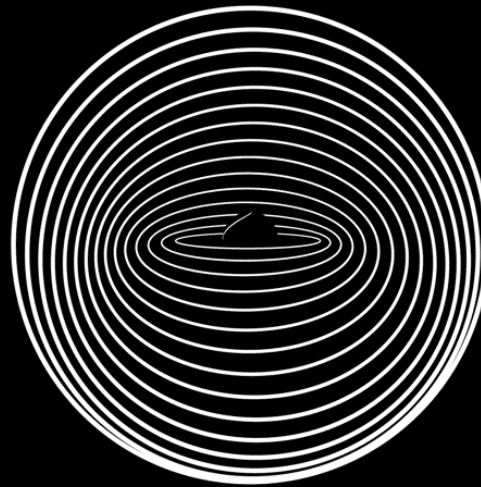
Bibliography

- Román Scoccimarro,
    Cosmological Perturbations: Entering the Non-Linear Regime

- F. Bernardeau, S. Colombi, E. Gazta˜naga, R. Scoccimarro,
    Large-Scale Structure of the Universe and Cosmological Perturbation Theory

- Diego Blas , Mathias Garny , Thomas Konstandin,
    On the non-linear scale of cosmological perturbation theory

Introduction

Contextualization

➢ First N-body simulation: P.J.E. Peebles
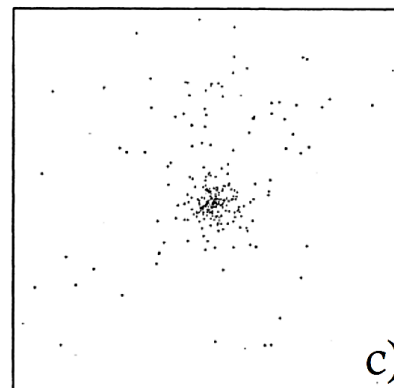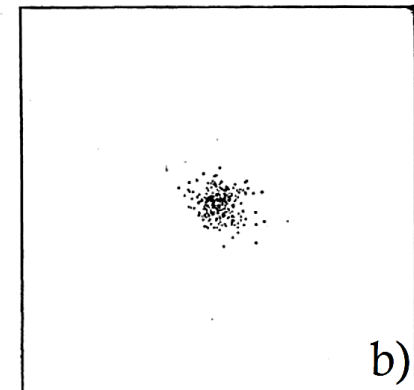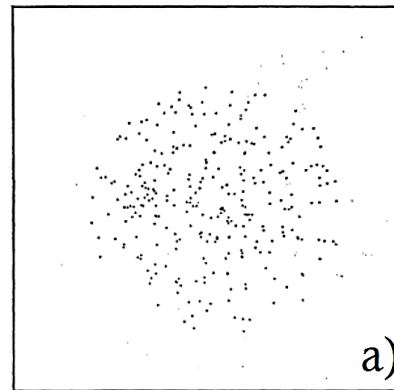
a) $t_0 \doteq 2.8$ b.y.

b) $t_1 = 5.6$ b.y.

c) $t_2 = 8.4$ b.y.

Image taken from the original paper

Introduction

Contextualization

➢ Klypin and Shandarin already using 3D Particle-Mesh simulating with 32,768 particles.
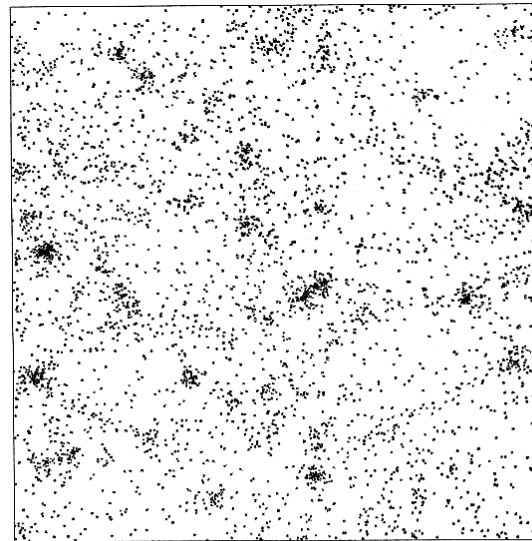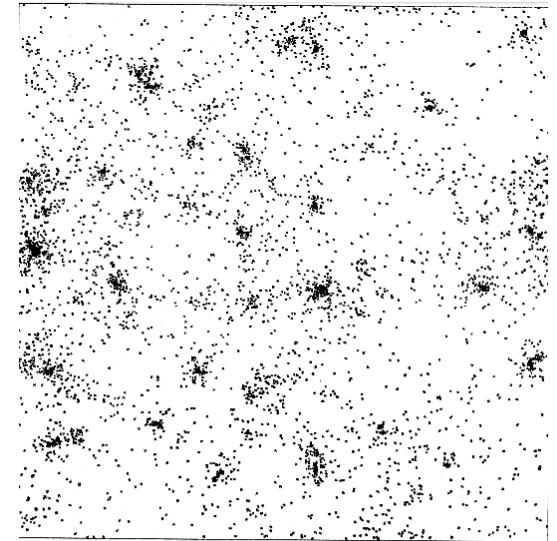
a)   b)

Images taken from the original paper

Introduction

Contextualization

➢ M. Davis et al. used the Particle–Particle–Particle–Mesh (P3M) code developed by Hockney and Eastwood to run 3^{23} particles with high (at that time) resolution simulates both galaxies and dark matter flux
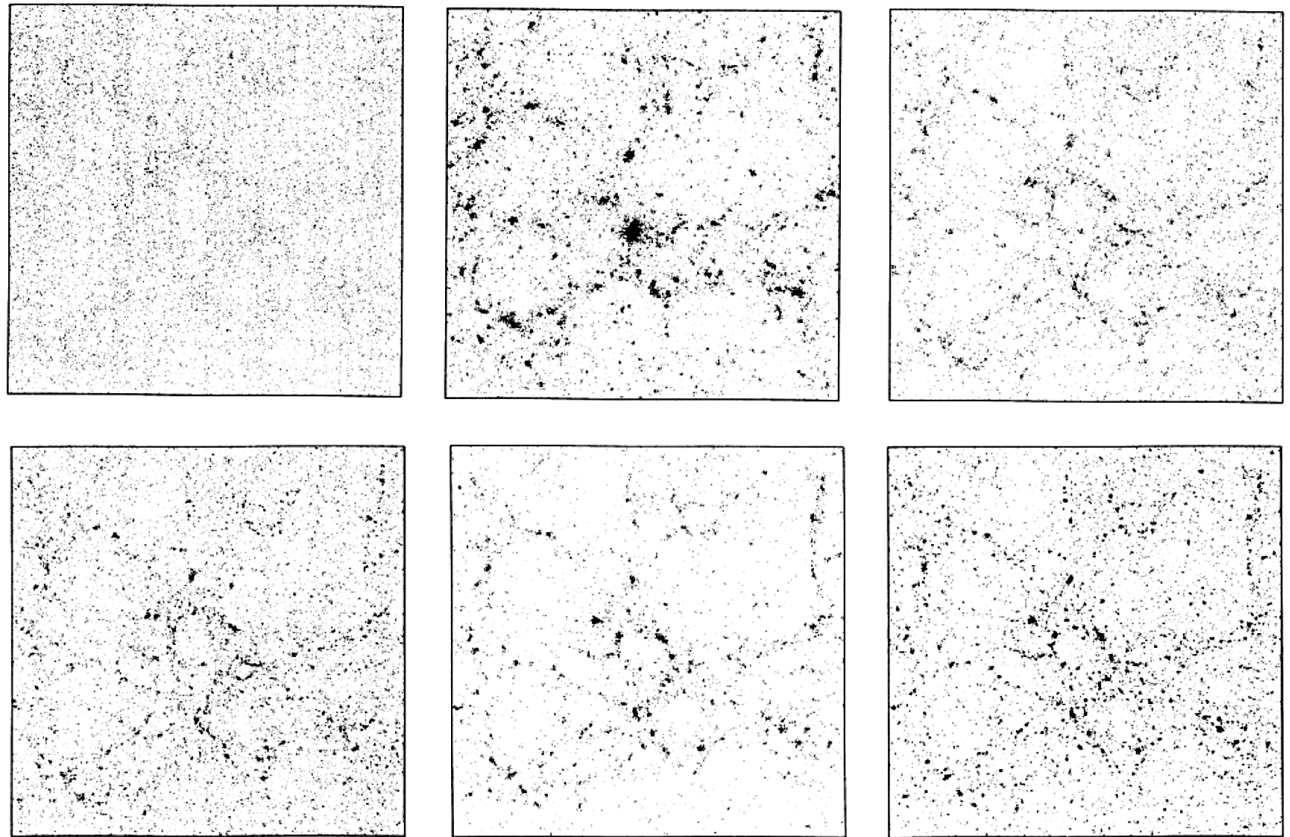
Image taken from the original paper

Introduction

Contextualization

➢ Nowadays…

There are 2 techniques that prevail:

- The Adaptive Mesh Refinement (AMR)
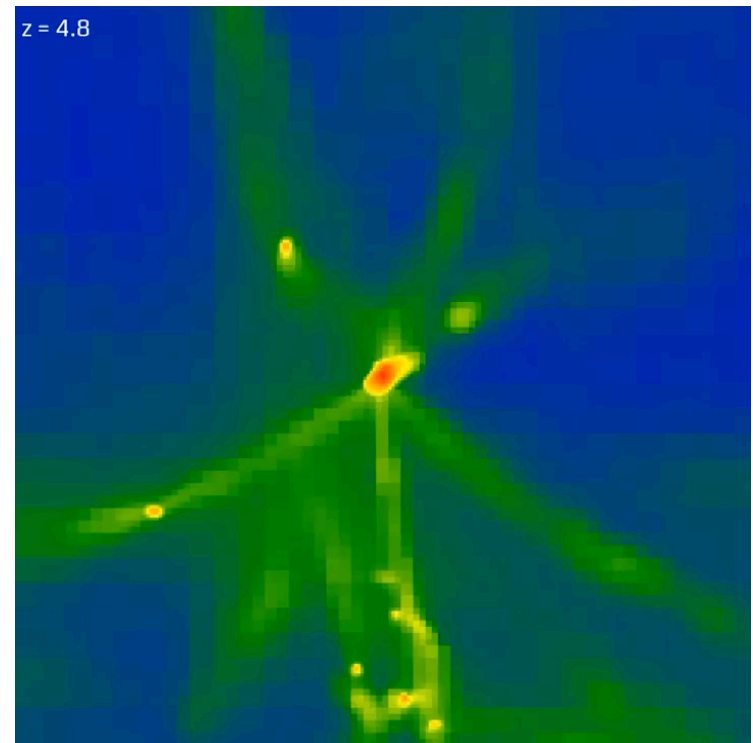
https://www.youtube.com/watch?v=g2JaOBsGumk&ab_channel=BradGibsonBradGibson

Introduction

Contextualization

➢ Nowadays...

There are 2 techniques that prevail:

- PM + Tree Codes
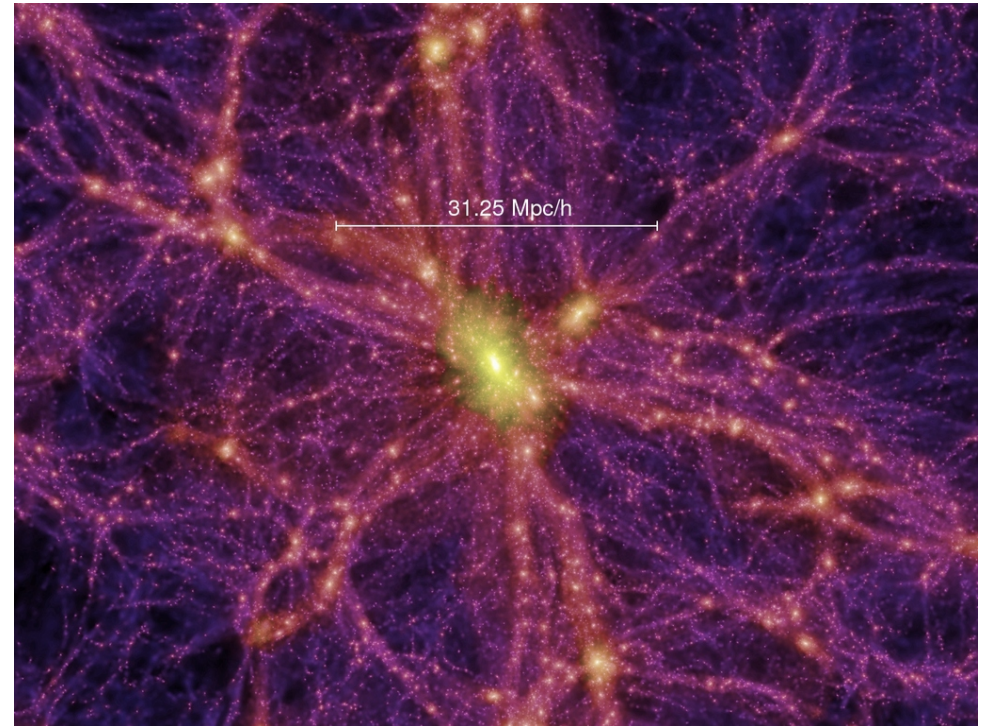
How can we build an N-body simulation?

We start by understanding the essence of the problem.

For given coordinates $\vec{r}_{init}$ and velocities $\vec{v}_{init}$ of N massive particles at moment $t = t_{init}$, find their velocities $\vec{v}$ and coordinates $\vec{r}$ at the next moment $t = t_{next}$ assuming that the particles interact only through the force of gravity.
The equations of motion are:

$$\frac{d^2\vec{r}_i}{dt^2} = -G \sum_{j=1,\ i \neq j}^{N} \frac{m_j(\vec{r}_i - \vec{r}_j)}{|\vec{r}_i - \vec{r}_j|^3}$$

But first we need to solve 2 problems before we think how can we translate this to an algorithm…

How can we build an N-body simulation?

We start by understanding the essence of the problem.

First, we need to introduce force softening: we make the force weaker ("softer") at small distances to avoid very large accelerations when two particles collide or come very close to each other.

$$\Delta \vec{r}_{ij} = |\vec{r}_i - \vec{r}_j| \rightarrow \Delta \vec{r}_{ij}' = (\Delta \vec{r}_{ij} + \varepsilon^2)^{1/2}$$

Second, we need to introduce new variables to avoid dealing with too large or too small physical units of a real problem.

$$r_i = \tilde{r}_i R$$

$$t_0 = (\frac{GM}{R^3})^{-1/2}$$

$$v_i = \tilde{v}_i \frac{R}{t_0} \qquad t = \tilde{t} \ t_0$$

$$m = m_i M$$

How can we build an N-body simulation?
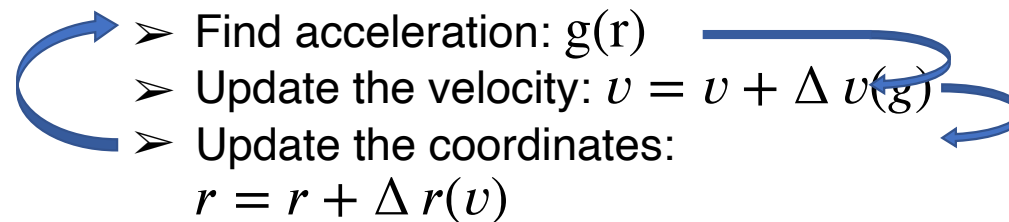
We start by understanding the essence of the problem.

We can now change the equation of motion to this coordinates, and we get:

$$\frac{d^2 \vec{r}_i}{dt^2} = g = -G \sum_{j=1,\, i \neq j}^{N} \frac{m_j(\vec{r}_i - \vec{r}_j)}{|\vec{r}_i - \vec{r}_j|^3} \quad \longrightarrow \quad \tilde{g}_i = -\sum_{j=1}^{N} \frac{\tilde{m}_j(\tilde{r}_i - \tilde{r}_j)}{(\Delta \vec{r}_{ij} + \varepsilon^2)^{3/2}}$$

How can we build an N-body simulation?

All numerical algorithms for solving these equations include three steps, which are repeated many times:

➤ Find acceleration: $g(r)$
➤ Update the velocity: $v = v + \Delta v(g)$
➤ Update the coordinates:
$r = r + \Delta r(v)$

Although this variations are usually treated as integrals to get a higher precision.

How can we build an N-body simulation?

So, we usually treat the variation of positions or velocity's as:

$$v_1 = v_0 + \int_{t_0}^{t_1} g(t)\, dt$$

And to solve it, we expand the integral into a Taylor series around t_0. If the aproximation is only in the first order, we get:

$$x_1 = x_0 + v_0\, \Delta t \qquad\qquad v_1 = v_0 + g_0\, \Delta t \qquad \text{(Euler)}$$

$$x_1 = x_0 + \int_{t_0}^{t_1} v(t)\, dt$$
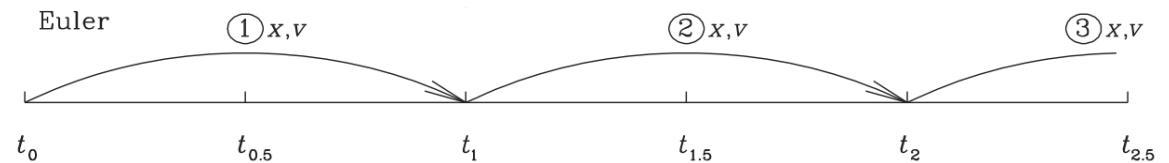
How can we build an N-body simulation?

Not going into much detail on how the more advanced time-stepping algorithms work, we can see that both Leap Frog and Kick-Drift-Kick methods will accomplish a more precise position of the particles (and its velocity) at each step made.
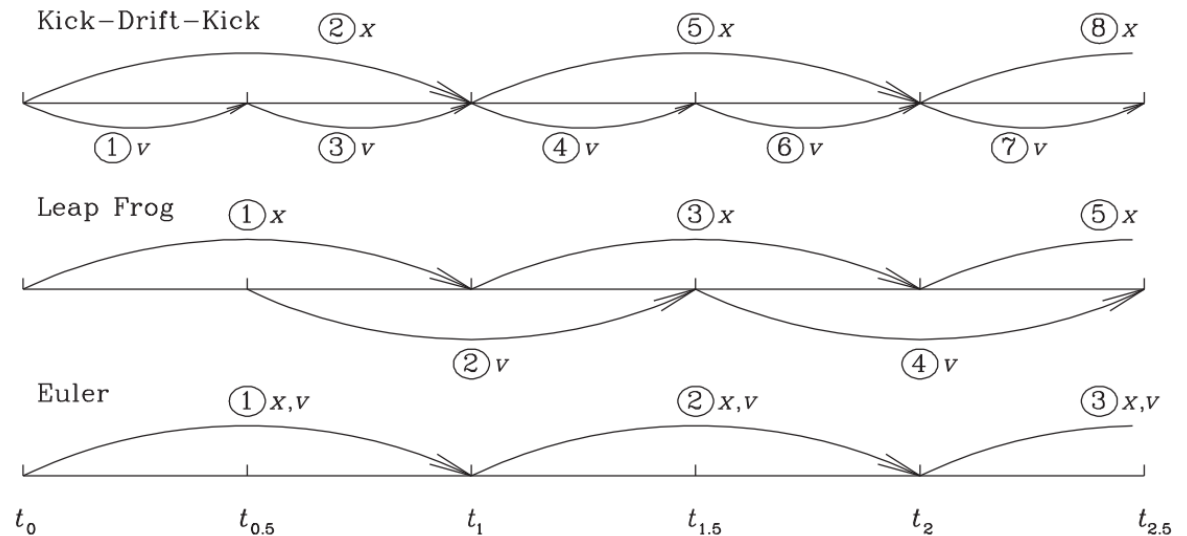
Brief discussion on the different methods

The different methods of approach and their main differences:

PM codes (fastest) :

Solves using a regularly spaced 3D mesh that covers the cubic
domain of a simulation. The gravitational potential is differentiated
to produce acceleration and particles are advanced by one time step.
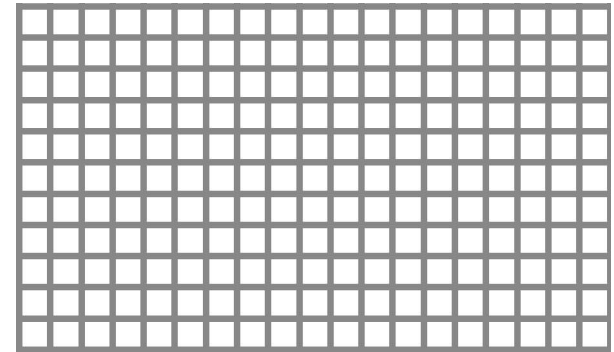
AMR code:

increased resolution only where it is needed: by placing additional
small-size elements — cubic cells — only in regions where there are
many particles and where the resolution should be larger.
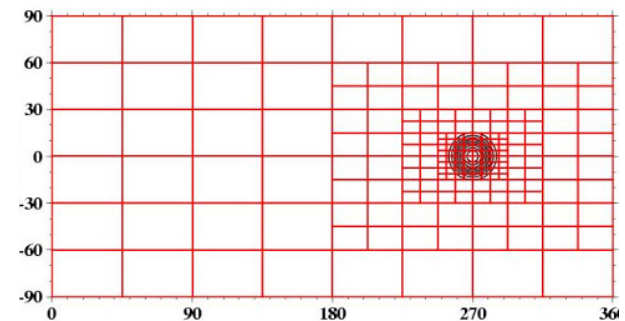
Brief discussion on the different methods

The different methods of approach and they're main differences:

Tree and Tree-PM code :
Instead of solving the Poisson equation on a mesh as PM and AMR codes do, the Tree codes split particles into groups of different sizes and replace the force from individual particles in the group with a single multipole force of the whole group. The larger the distance from a particle, the bigger the allowed size of the particle group.

Modern variants of the Tree algorithm are typically hybrid codes with the long-range force treated by a PM algorithm and the short range handled by a Tree code.
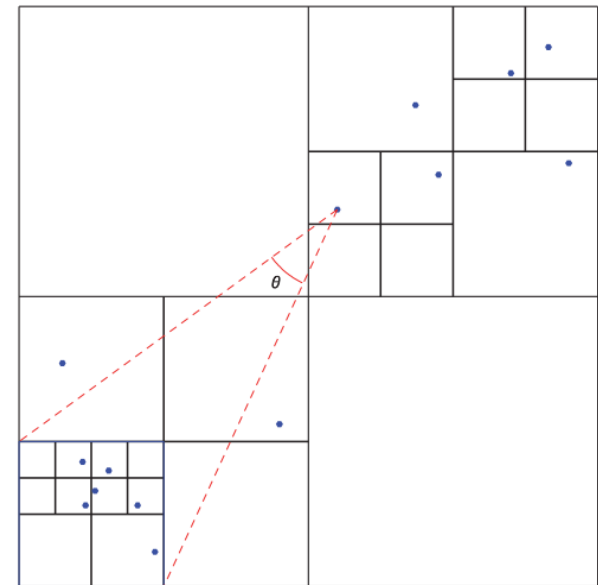
Relevant results that N-body Simulations provided

Dark matter density distribution function:

We start with the evolution of the probability density function (PDF), that will have two regimes:

➢ The Linear

$$D_L(\rho) = \frac{1}{\sqrt{2\pi\sigma^2}}\exp\left(-\frac{\delta^2}{2\sigma^2}\right)$$

➢ The Nonlinear

$$D_{NL}(\rho) = \frac{1}{\sqrt{2\pi\sigma^2}}\left(\frac{\rho}{\rho_m}\right)^{-1}\exp\left(-\frac{\left[\ln\left(\frac{\rho}{\rho_m}\right) + \sigma^2/2\right]^2}{2\sigma^2}\right)$$
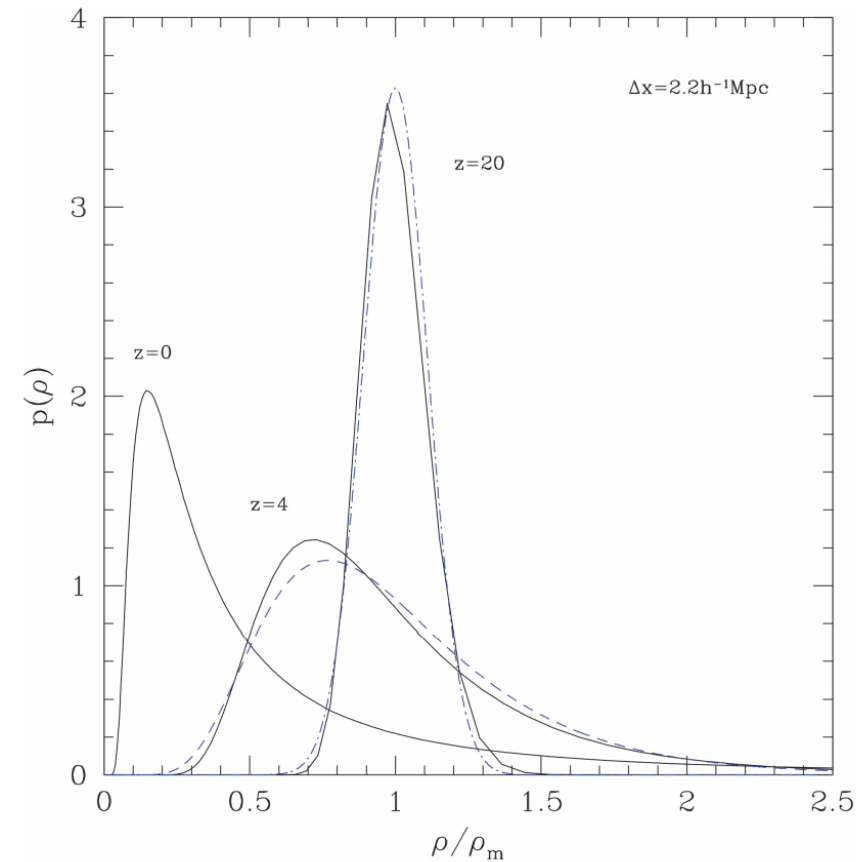
Relevant results that N-body Simulations provided

Dark matter density distribution function:

➤ When the fluctuations become strongly nonlinear, the PDF develops a very long tail at large densities while its maximum shifts to even lower densities

➤ At at a stronger nonlinear regime, the distribution function develops a nearly power-law shape with an exponential decline:

$$D_{SNL}(\rho) = \rho^{-2}\exp(-\alpha\rho^{3/4})$$

$$\rho > 10\,\rho_m$$
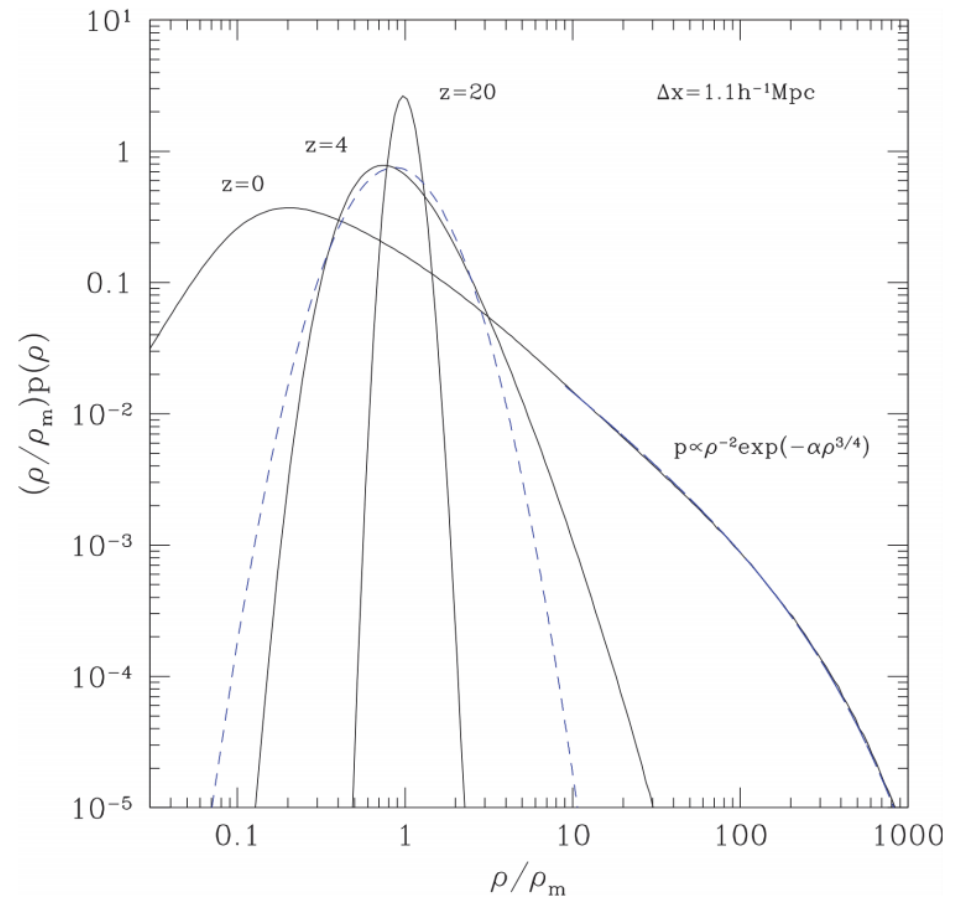
Relevant results that N-body Simulations provided

Dark matter power spectrum:

Calculating the power spectrum, we observe that exist 3 distinte regimes:

I. linear growth on very long waves (small k≈0.1 h⁻¹Mpc).

II. the weakly nonlinear regime where fluctuations grow much faster than predictions of the linear theory.

III. strongly nonlinear evolution at k > 1 h⁻¹Mpc. In this regime, the power spectrum gradually approaches power law $P(k) \propto k^{-2}$ shown as the dashed line in the plot.
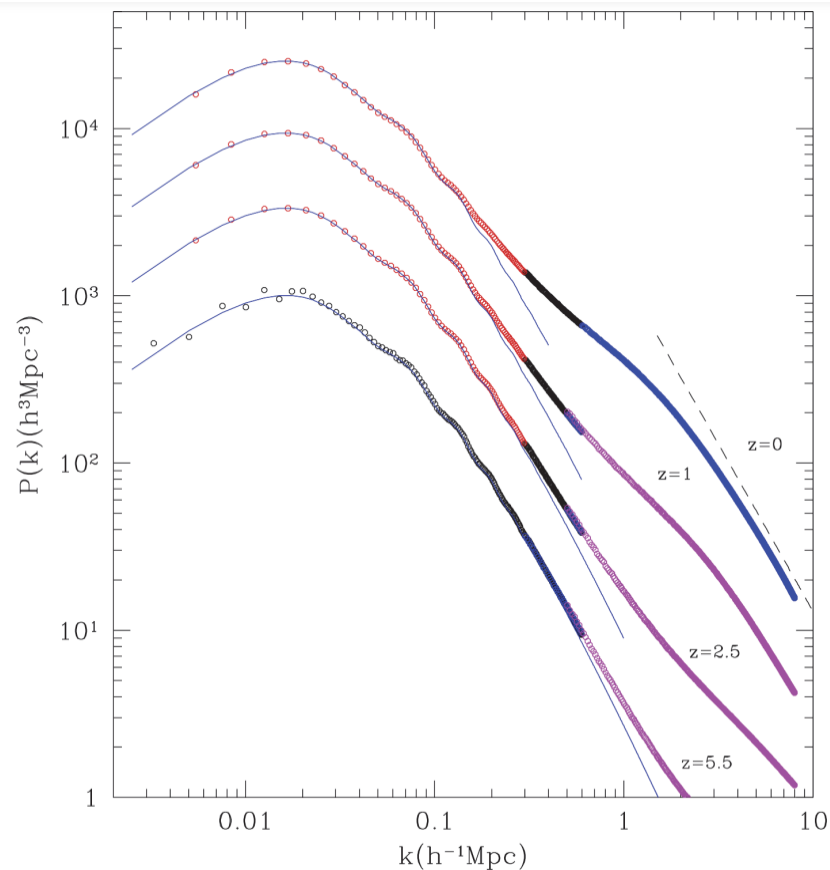
Relevant results that N-body Simulations provided

Dark matter power spectrum:

Bias:

Measures how linear the power spectrum is:

$$b^2(k, z) = \frac{P(k, z)}{P_{lin}(k, z)}$$
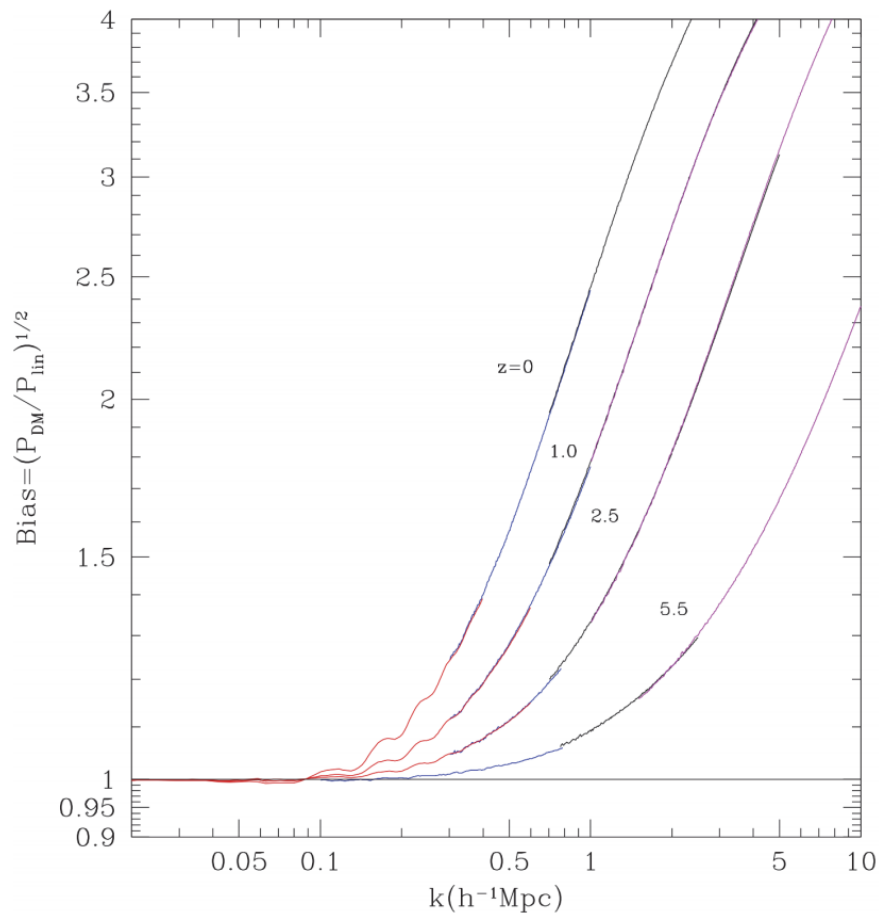
Physical Cosmology

Topic 16 : Weak lensing theory

Iu Chi Tou, fc55199
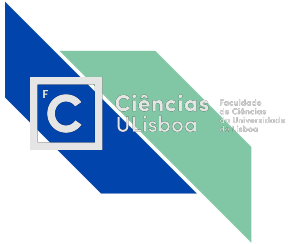
Overview

1) Introduction of Gravitational lensing (focus on weak lensing)

2) The lens equation

3) Propagation equation for the transverse separation between the light rays

4) Amplification matrix (cosmic shear and cosmic convergence)

5) Relation between the shear power spectrum(Cosmological probes) and the matter power spectrum

6) Summary

Introduction: Gravitational lensing

Gravitational lensing is the effect of deflection of light caused by gravity

Image: multiple image , image distortion , flux enhancement enables galaxies to be seen down to fainter intrinsic magnitudes
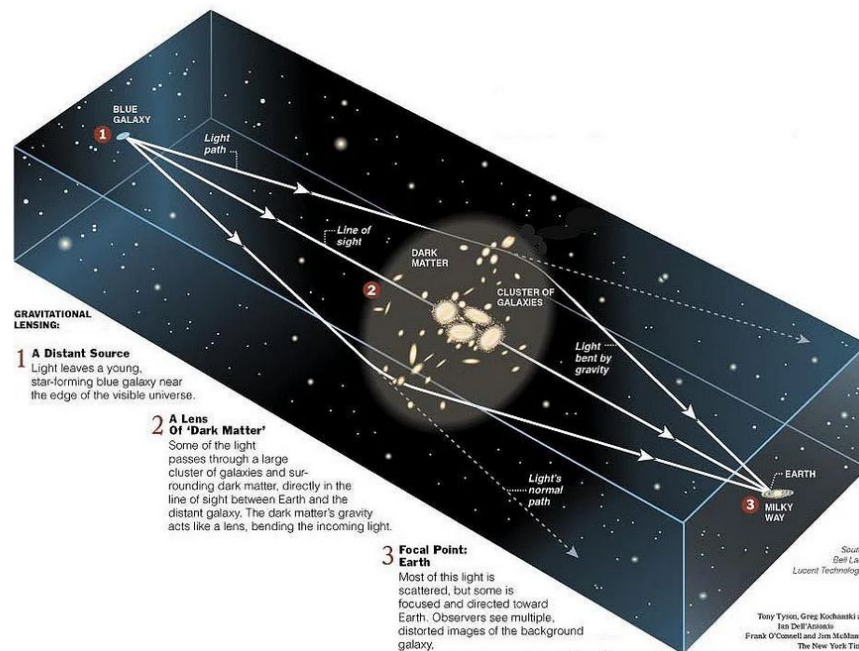
Gravitational Lensing

Two general type of lensing: weak lensing and strong lensing

Occur in regions of the image plane where the values of the convergence and shear fields are small (weak lensing) or large (strong lensing).
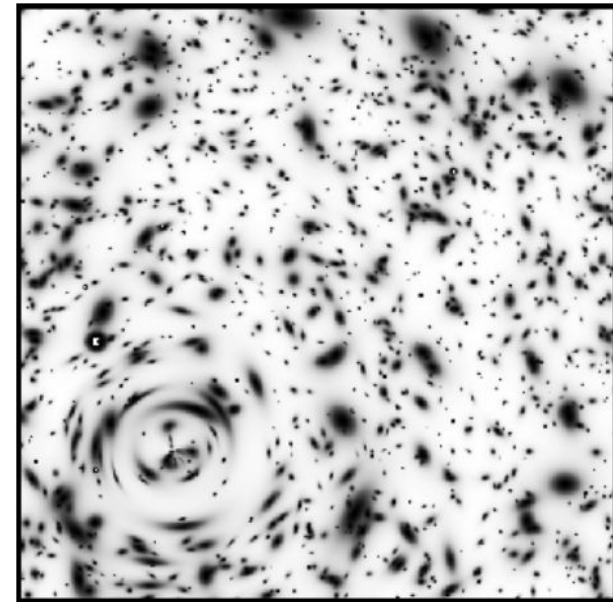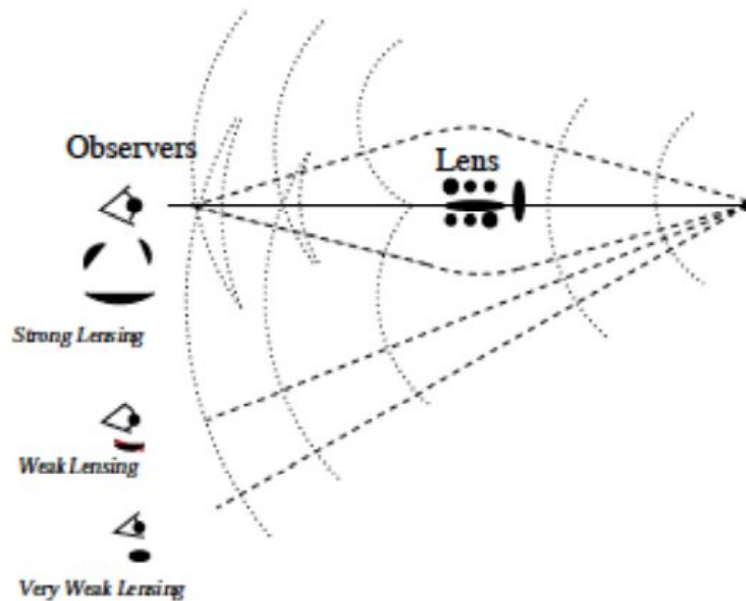
Weak Lensing

Weak Lensing occurs further from the line of alignment of source-lens-observer, or with lenses of lower density contrast

Effects: small increase of ellipticity of the source galaxy (shear),
slight alignment of images

Difficulty: The shear is so small that it cannot be detected in individual galaxies

Solved by : Measurement on the correlation of ellipticities from large amount of galaxies sources

Use Weak lensing as a cosmological probe of the large-scale structure distribution like dark matter
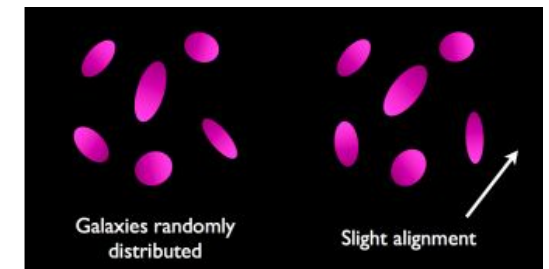
The lens equation

Suppose a galaxy cluster place between Observer and source galaxy
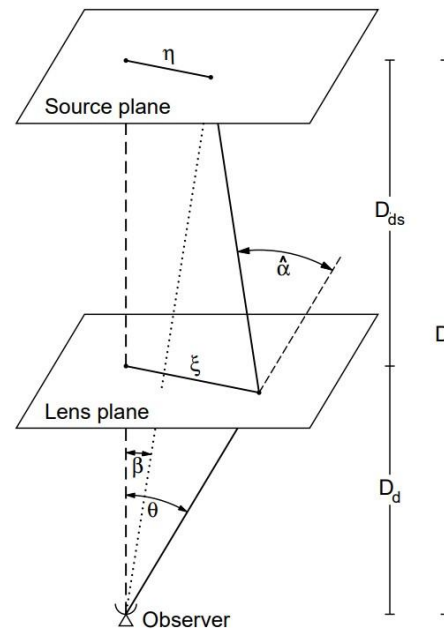
→ galaxy cluster act as a lens

→ produces a deflection of α for a light ray emitted from source from a distance Ds

$\vec{\eta}$ denote the two-dimensional position of the source on the source plane

Source position in the source plane

Len Equation

$$D_s\vec{\theta} = D_s\vec{\beta} + 2D_{ds}\frac{\hat{\vec{\alpha}}}{2}$$

Deflection angle: Vector alpha

Impact parameter in the lens plane :
Angular diameter distance Ds ,Dd , Dds

Optical axis

Image position in the image plane

Fig. 11. Sketch of a typical gravitational lens system.

Robertson-Walker metric with a small inhomogeneity

Light propagation from source to observer in the Universe described by the Robertson-Walker metric with a small inhomogeneity(lensing potential):

$$ds^2 = -\left(1 + \frac{2\Phi}{c^2}\right)c^2 dt^2 + \left(1 - \frac{2\Phi}{c^2}\right)\left[dx_1^2 + dx_2^2 + dx_3^2\right]$$

Light follows null geodesics(path of extremal time), and setting ds^2 = 0
Speed of light change when travelling in the gravitational field of the lens, it act as a change of medium.

$$c' = \frac{|d\vec{x}|}{dt} = c\sqrt{\frac{1 + \frac{2\Phi}{c^2}}{1 - \frac{2\Phi}{c^2}}} \approx c\left(1 + \frac{2\Phi}{c^2}\right)$$

Rearrange the terms we have the effective index of refraction:

$$n = c/c' = \frac{1}{1 + \frac{2\Phi}{c^2}} \approx 1 - \frac{2\Phi}{c^2}$$

Euler-Lagrange equations

Finding the lagrangian of the system.
Find the path of extremal time, by setting a small changes in the configuration equal
zero. Since refraction index is dt/dx

$$\int_A^B n[\vec{x}(l)]\mathrm{d}l \longrightarrow \delta \int_A^B n[\vec{x}(l)]\mathrm{d}l = 0 \qquad \text{x(l): light path crossing the medium}$$

$$\delta \int_A^B n(\vec{x})dx = 0 = \delta \int_{\lambda_A}^{\lambda_B} n(\vec{x}(\lambda))\frac{dx}{d\lambda}d\lambda = \delta \int_{\lambda_A}^{\lambda_B} n(\vec{x}(\lambda))|\dot{\vec{x}}|d\lambda = \delta \int_{\lambda_A}^{\lambda_B} L(x,\dot{x};\lambda)d\lambda,$$

We have found the Euler Lagrange equations.
Describe the light path using the Euler-Lagrange equations:

$$\frac{\mathrm{d}}{\mathrm{d}\lambda}\frac{\partial L}{\partial \dot{\vec{x}}} - \frac{\partial L}{\partial \vec{x}} = 0 \qquad \boxed{n(\vec{x}(\lambda))|\dot{\vec{x}}| = L(x,\dot{x};\lambda)}$$

We obtain: $\dfrac{\partial L}{\partial \dot{\vec{x}}} = n\dfrac{\dot{\vec{x}}}{|\dot{\vec{x}}|}$ and $\dfrac{\partial L}{\partial \vec{x}} = |\dot{\vec{x}}|\dfrac{\partial n}{\partial \vec{x}} = (\vec{\nabla}n)|\dot{\vec{x}}|$

Total deflection

Substitute the previous equation and rearrange the term,

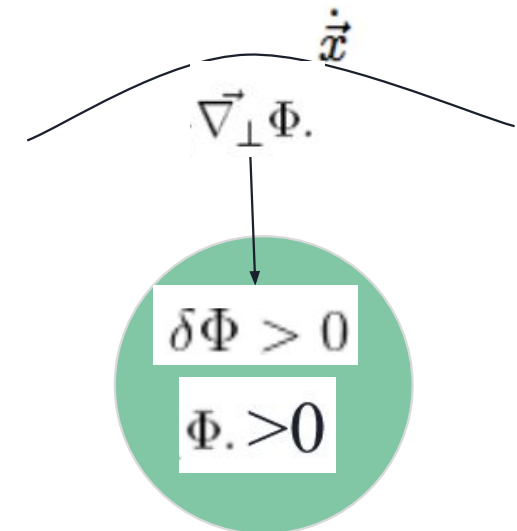The light path is described by Euler-Lagrange equation:(change in velocity)

$$\dot{\vec{u}}_x = \frac{d^2\vec{x}}{d\lambda^2} = \frac{1}{n(\vec{x})}\left(\vec{\nabla}n - (\vec{\nabla}n.\vec{u}_x)\vec{u}_x\right) = \frac{1}{n(\vec{x})}\vec{\nabla}_\perp n(\vec{x}) = (1 + \frac{2\Phi}{c^2})(-\frac{2}{c^2}\vec{\nabla}_\perp\Phi) \approx -\frac{2}{c^2}\vec{\nabla}_\perp\Phi.$$

where $\dot{\vec{x}}$ is the velocity vector tangent to the light path

derivative of the acceleration vector $\dot{\vec{u}}_x$ is define as the deflection

Total deflection:

$$\vec{\alpha} = -\frac{2}{c^2}\int_{\lambda_A}^{\lambda_B}\dot{\vec{u}}_x\,d\lambda = \frac{2}{c^2}\int_{\lambda_A}^{\lambda_B}\vec{\nabla}_\perp\Phi\,d\lambda,$$

$\dot{\vec{x}}$

$\vec{\nabla}_\perp\Phi.$

$\delta\Phi > 0$

$\Phi. > 0$

Evolution of the comoving transverse separation:

Define the separation x between two light rays when travelling through the homogeneous

universe (without deflection)

$$x_i = \theta_i \, f_K(w)$$

fK(w):comoving diameter angular distance
(Trigonometric, linear, or hyperbolic function of w)

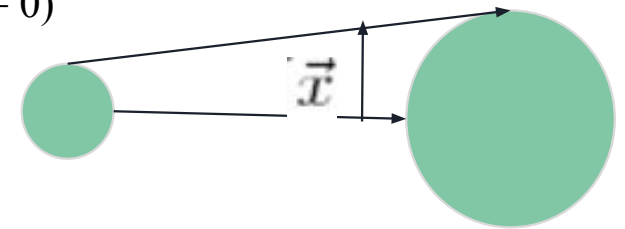The differential equation for the evolution of the comoving transverse separation:

If K = 0 , nocurvature ,the lightray travel straight to observer

$$\frac{d^2 x_i}{dw^2} + K x_i = 0.$$

Add the local deflection to the equation of comoving transverse separation:

defined with respect to a reference light ray at separation vector x = 0)

$$\frac{d^2 \vec{x}}{dw^2} + K\vec{x} = -\frac{2}{c^2} \left[\vec{\nabla}_\perp \Phi(\vec{x}(\vec{\theta}, w), w) - \vec{\nabla}_\perp \Phi(0, w) \right]$$

Amplification matrix

Gravitational lensing refers to extended sources. Neighbouring points from the source experience slightly different deflections in the lens plane,
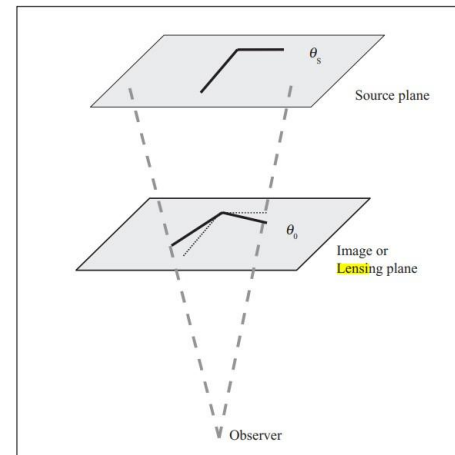result in a image distortion:

The lens equation is a mapping from image positions to source positions

$$\vec{\beta}(\theta) = \vec{\theta} - \vec{\alpha}$$

A is the amplification matrix describes the lensing linear transformation between source and image planes.

Aij is a 2D matrix, since β (position in the source plane) and θ (position in the lens plane) are 2D vectors

$$A_{ij}(\theta) = \frac{\partial \beta_i}{\partial \theta_j} = \left(\delta_{ij} - \frac{\partial \alpha_i}{\partial \theta_j} \right)$$
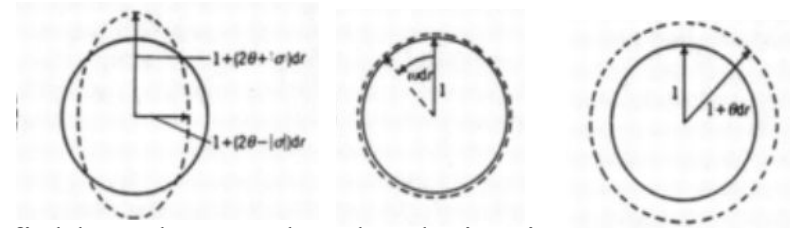
Amplification matrix

Seperate amplification matrix can be decomposed in 3 parts:

$$A_{ij}(\theta) = \frac{\partial \beta_i}{\partial \theta_j} = \left(\delta_{ij} - \frac{\partial \alpha_i}{\partial \theta_j} \right)$$

We can seperate the amplification matrix into:
(traceless) symmetric + (traceless) antisymmetric + diagonal
γ shear+ω rotation + k convergence.

$$\begin{bmatrix} \gamma_1 & \gamma_2 \\ \gamma_2 & -\gamma_1 \end{bmatrix} + \begin{bmatrix} 0 & \omega \\ -\omega & 0 \end{bmatrix} + \begin{bmatrix} k & 0 \\ 0 & k \end{bmatrix}$$

Shear and convergence are derivatives of the deflection field, and second-order derivatives of the potential. And

shear $\gamma_1 = \frac{1}{2}(\psi_{,11} - \psi_{,22})$, $\gamma_2 = \psi_{,12}$

convergence $\kappa = \frac{1}{2}(\psi_{,11} + \psi_{,22})$

Amplification matrix

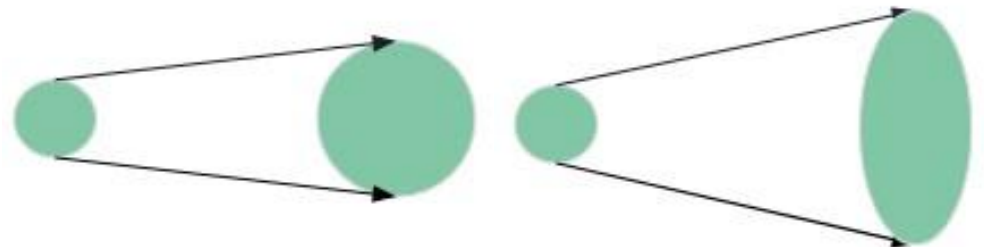Amplification matrix :(Lensing distortion does not produces rotations)

$$A = \begin{pmatrix} 1 - \kappa - \gamma_1 & -\gamma_2 \\ -\gamma_2 & 1 - \kappa + \gamma_1 \end{pmatrix}$$

$$A_{ij}(\theta) = \frac{\partial \beta_i}{\partial \theta_j} = \left(\delta_{ij} - \frac{\partial \alpha_i}{\partial \theta_j} \right)$$

The determinant of the amplification matrix defines the magnification
detA = 0 (infinity magnification), different combination of shear and convergence may give same magnification

$$\mu = \frac{1}{det\, A} = \frac{1}{(1 - \kappa)^2 - \gamma^2}$$

Solving the comoving transverse separation equation by Green Function

$$\frac{d^2\vec{x}}{dw^2} + K\vec{x} = -\frac{2}{c^2}\left[\vec{\nabla}_\perp \Phi(\vec{x}(\vec{\theta}, w), w) - \vec{\nabla}_\perp \Phi(0, w)\right]$$

Solving the inhomogeneous differential equation using green function

Solution = homogeneous solution + convolution of the equation Green's function with the inhomogeneous term.

$$f(x) = f^{(0)}(x) + \int dx'\, g(x')\, G(x, x')$$

The solution is the form of

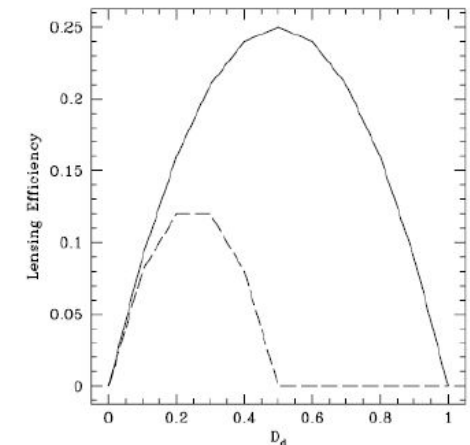$$\vec{\beta}(\theta) = \vec{\theta} - \vec{\alpha}$$

Lensing efficiency factor:

$$\vec{x}(\vec{\theta}, w) = f_K(w)\vec{\theta} - \frac{2}{c^2}\int_0^w dw'\, f_K(w - w')\left[\vec{\nabla}_\perp \Phi(\vec{x}(\vec{\theta}, w'), w') - \vec{\nabla}_\perp \Phi(0, w')\right]$$

$$\Leftrightarrow \beta_i(\vec{\theta}, w) = \theta_i - \frac{2}{c^2}\int_0^w dw' \frac{f_K(w - w')}{f_K(w)} f_K(w')\left[\Phi_{,i}(\vec{x}(\vec{\theta}, w'), w') - \Phi_{,i}(0, w')\right].$$

$$\frac{D_{ds} D_d}{D_s}$$

$$p(z) \propto \left(\frac{z}{z_0}\right)^\alpha \exp\left[-\left(\frac{z}{z_0}\right)^\beta\right]$$

Born approximation:

Since the seperation vector x is a Recursive solution:

Separation x depends on the potential at the position x.

$$\vec{x}(\vec{\theta}, w) = f_K(w)\vec{\theta} - \frac{2}{c^2} \int_0^w dw' \, f_K(w - w') \left[\vec{\nabla}_\perp \Phi(\vec{x}(\vec{\theta}, w'), w') - \vec{\nabla}_\perp \Phi(0, w') \right]$$

Simplify the problem $\longrightarrow$ Taylor expand the potential around the unperturbed trajectory(x = fK θ))

$$\Phi_{,i}(x) = \Phi_{,i}(f_K\theta - f_K\alpha(x)) = \Phi_{,i}(f_K\theta) - f_K\alpha(x)\Phi_{,ik}(f_K\theta) + \mathcal{O}(\alpha^2)$$

$$\beta_i(\vec{\theta}, w) = \theta_i - \frac{2}{c^2} \int_0^w dw' \, \frac{f_K(w - w')}{f_K(w)} f_K(w') \Phi_{,i}(f_K\theta, w')$$

Now, we can related the physical gravitational potential to the amplification matrix

$$A_{ij}(\theta) = \frac{\partial \beta_i}{\partial \theta_j} = \left(\delta_{ij} - \frac{\partial \alpha_i}{\partial \theta_j} \right)$$

$$A_{ij}(\vec{\theta}, w) = \delta_{ij} - \frac{2}{c^2} \int_0^w dw' \, \frac{f_K(w - w')}{f_K(w)} f_K(w') \Phi_{,ij}(f_K\theta, w')$$

Amplification matrix

$$\nabla_p^2 \Phi = 4\pi G \rho$$

$$A_{ij}(\vec{\theta}, w) = \delta_{ij} - \frac{2}{c^2} \int_0^w dw' \, \frac{f_K(w - w')}{f_K(w)} f_K(w') \Phi_{,ij}\left(f_K\theta, w'\right)$$

$$\underbrace{\hspace{6cm}}_{\psi_{,ij}\left(\vec{\theta}, w\right)}$$

convergence $\qquad \kappa = \frac{1}{2}(\psi_{,11} + \psi_{,22})$.

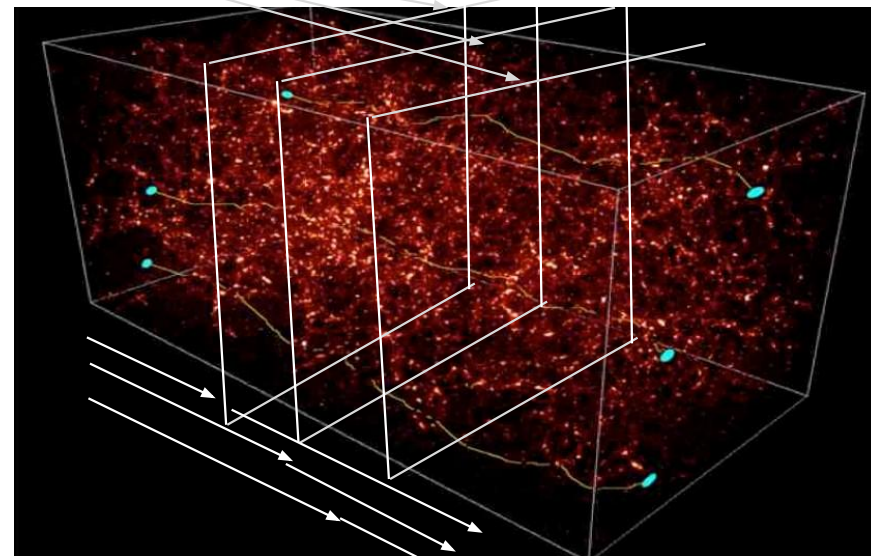shear $\qquad \gamma_1 = \frac{1}{2}(\psi_{,11} - \psi_{,22}) \quad , \quad \gamma_2 = \psi_{,12}$

Effective lensing potential:

Sum over all the lens respect to
is own Lensing efficiency factor

$$\psi(\vec{\theta}, w) = \frac{2}{c^2} \int_0^w dw' \, \frac{f_K(w - w')}{f_K(w)} f_K(w') \Phi(f_K\theta, w')$$

The second derivative of potential
in shear and convergence is
related to the matter density
through poisson equation

Lens exist between the
source and observer

Convergence field

Relate density contrast field to Amplification matrix through the Poisson equation.

This indicate the convergence power spectrum can be related to the dark matter power spectrum.

$$\nabla_p^2 \Phi = 4\pi G\rho = 4\pi G\bar{\rho}\delta \Leftrightarrow \nabla^2 \Phi = a^2\, 4\pi G\, \Omega_m \rho_c a^{-3}\, \delta = \frac{3H_0^2\, \Omega_m\, \delta}{2a}$$
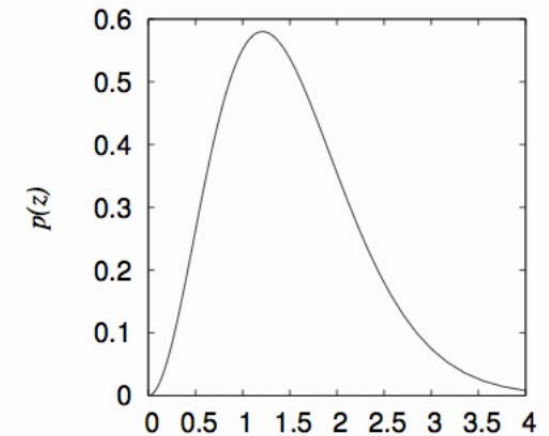
Convergence for one source at position theta and z experience multi-lens:

source redshift distribution

$$\kappa(\vec{\theta}, w) = \frac{3}{2}\left(\frac{H_0}{c}\right)^2 \Omega_m \int_0^w dw'\, \frac{f_K(w-w')f_K(w')}{f_K(w)\, a(w')}\, \delta\left(f_K(w')\vec{\theta}, w'\right)$$

Since weak lensing signal can only be detected statistically,

we need to measure over a large number of source galaxies.

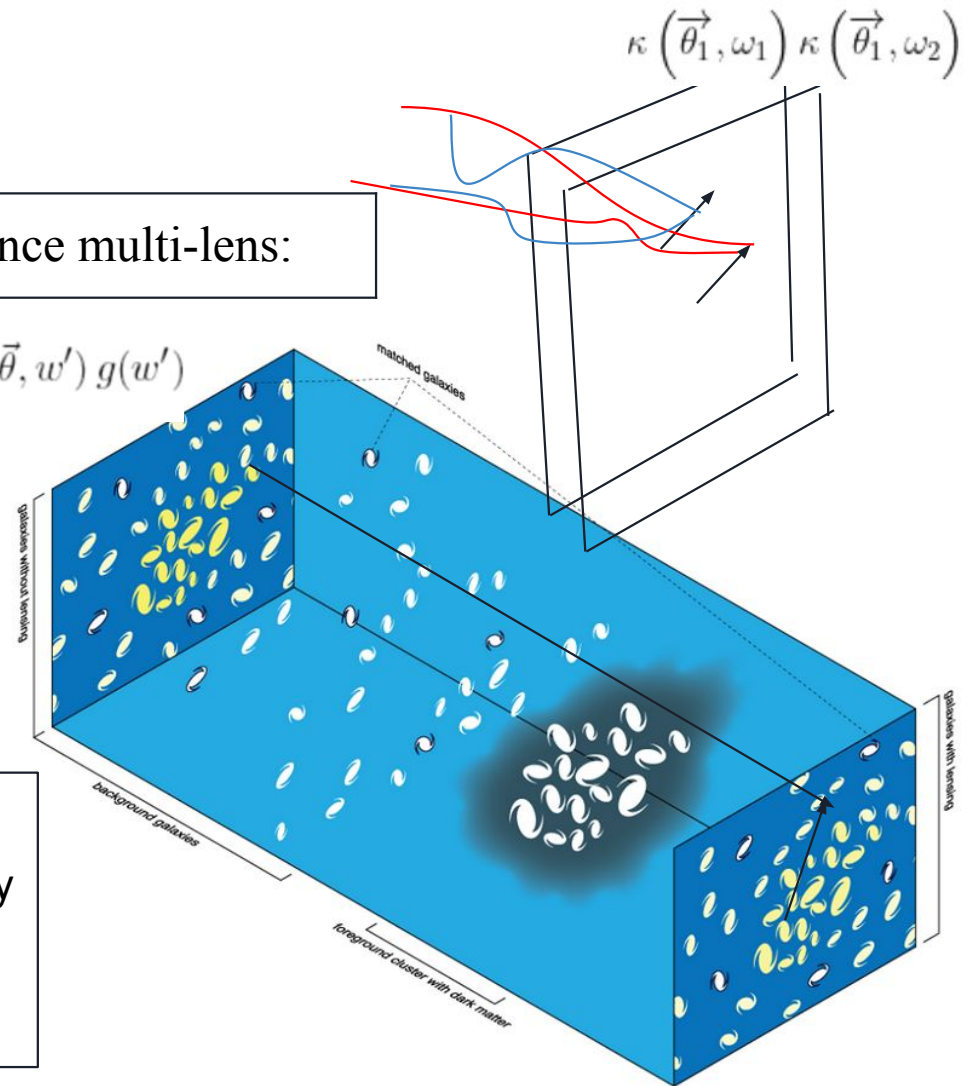$$\longrightarrow \quad \kappa(\vec{\theta}) = \int_0^{w_H} dw\, p(w)\, \kappa(\vec{\theta}, w)$$

Convergence field

For multi-sources along the path experience multi-lens:

$$\kappa(\vec{\theta}) = \frac{3}{2}\left(\frac{H_0}{c}\right)^2 \Omega_m \int_0^{w_H} dw' \frac{f_K(w')}{a(w')} \delta(f_K(w')\vec{\theta}, w') \, g(w')$$

$$g(w') = \int_w^{w_H} dw \, p(w) \frac{f_K(w - w')}{f_K(w)}$$

$$\kappa\left(\vec{\theta_1}, \omega_1\right) \kappa\left(\vec{\theta_1}, \omega_2\right)$$

Notice that the len with same position(theta) at different redshift, the convergence may contribution by different sets of light rays by background sources that why we need to integrate from w to wH of g(w')

Power spectrum of the convergence field

Power spectrum of the convergence is projected power spectrum which is a weighted line-of sight integral of the matter power spectrum

$$P_\kappa(\ell) = \frac{9}{4}\left(\frac{H_0}{c}\right)^4 \Omega_m^2 \int_0^{w_H} dw \, \frac{g^2(w)}{a^2(w)} P_\delta\left(\frac{\ell}{f_K(w)}, w\right)$$

Model dependent   redshift of the sources, diameter angular distances

Difficulty: Hard to obtain Convergence Power spectrum

Goal: 1) Measure shear power spectrum from the observed image

2) Obtain Convergence Power spectrum through the theoretical model

3) Obtain Power spectrum of matter density

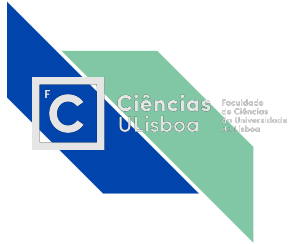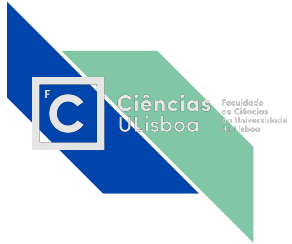| Shear and the convergence power spectra are identical.	$P_\gamma(\ell) = P_\kappa(\ell)$	shear	$\gamma_1 = \frac{1}{2}(\psi_{,11} - \psi_{,22})$, $\gamma_2 = \psi_{,12}$.
		convergence	$\kappa = \frac{1}{2}(\psi_{,11} + \psi_{,22})$.

Summary

- The observed shear gravitational lensing distortion is an unbiased tracer of δ_dm

- The theory allow us to obtain the propagation equation for the transverse separation between the light rays

- Obtain the amplification matrix from lensing equation.

- Combine the two equations and simplify it using mathematical techniques like Born approximation and Green function.
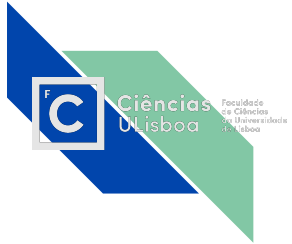
Summary

- We treat the large scale structure as lens at different redshift and we obtain the amplification matrix for the universe (specific model)

- Poisson equation provide us a way to link the matter density to the Shear Power spectrum

- Therefore by measuring the shear power spectrum through observation, we can obtain the matter density power spectrum indirectly

Thank you